

NRC Publications Archive Archives des publications du CNRC

Aerodynamic testing of drag reduction technologies for HDVs: progress toward the development of a flow treatment system (year 2) version for public release

McAuliffe, Brian R.; D'Auteuil, Annick; de Souza, Fenella

For the publisher's version, please access the DOI link below. / Pour consulter la version de l'éditeur, utilisez le lien DOI ci-dessous.

Publisher's version / Version de l'éditeur:

<https://doi.org/10.4224/23000643>

Laboratory Technical Report (National Research Council of Canada. Aerospace. Aerodynamics Laboratory); no. LTR-AL-2014-0014P, 2014-07-15

NRC Publications Archive Record / Notice des Archives des publications du CNRC :

<https://nrc-publications.canada.ca/eng/view/object/?id=ab507ed0-8973-4705-ae56-d6be89ca7bf0>

<https://publications-cnrc.canada.ca/fra/voir/objet/?id=ab507ed0-8973-4705-ae56-d6be89ca7bf0>

Access and use of this website and the material on it are subject to the Terms and Conditions set forth at

<https://nrc-publications.canada.ca/eng/copyright>

READ THESE TERMS AND CONDITIONS CAREFULLY BEFORE USING THIS WEBSITE.

L'accès à ce site Web et l'utilisation de son contenu sont assujettis aux conditions présentées dans le site

<https://publications-cnrc.canada.ca/fra/droits>

LISEZ CES CONDITIONS ATTENTIVEMENT AVANT D'UTILISER CE SITE WEB.

Questions? Contact the NRC Publications Archive team at

PublicationsArchive-ArchivesPublications@nrc-cnrc.gc.ca. If you wish to email the authors directly, please see the first page of the publication for their contact information.

Vous avez des questions? Nous pouvons vous aider. Pour communiquer directement avec un auteur, consultez la première page de la revue dans laquelle son article a été publié afin de trouver ses coordonnées. Si vous n'arrivez pas à les repérer, communiquez avec nous à PublicationsArchive-ArchivesPublications@nrc-cnrc.gc.ca.

***Aerodynamic Testing of Drag Reduction
Technologies for HDVs: Progress Toward
the Development of a Flow Treatment System
(Year 2) Version for Public Release***

Unclassified

Unlimited

LTR-AL-2014-0014P

July 15, 2014

Brian R. McAuliffe, Annick D'Auteuil, Fenella de Souza

Aerodynamic Testing of Drag Reduction Technologies for HDVs: Progress Toward the Development of a Flow Treatment System (Year 2) Version for Public Release

Report No.: LTR-AL-2014-0014P

Date: July 15, 2014

Authors: Brian R. McAuliffe, Annick D'Auteuil, Fenella de Souza

Classification:	Unclassified	Distribution:	Unlimited
For:	ecoTECHNOLOGY for Vehicles Stewardship and Sustainable Transportation Programs Transport Canada		
Project #:	A1-000740		
Submitted by:	Dr. Steven J. Zan, Director R&D Aerodynamics		
Approved by:	Jerzy Komorowski, General Manager, Aerospace Portfolio		

Pages:	100	Copy No:	
Figures:	60	Tables:	10

This report may not be published wholly or in part without the written consent of the National Research Council Canada

Disclaimer

This report reflects the views of the authors only and does not reflect the views or policies of Transport Canada.

Neither Transport Canada, nor its employees, makes any warranty, express or implied, or assumes any legal liability or responsibility for the accuracy or completeness of any information contained in this report, or process described herein, and assumes no responsibility for anyone's use of the information. Transport Canada is not responsible for errors or omissions in this report and makes no representations as to the accuracy or completeness of the information.

Transport Canada does not endorse products or companies. Reference in this report to any specific commercial products, process, or service by trade name, trademark, manufacturer, or otherwise, does not constitute or imply its endorsement, recommendation, or favoring by Transport Canada and shall not be used for advertising or service endorsement purposes. Trade or company names appear in this report only because they are essential to the objectives of the report.

References and hyperlinks to external web sites do not constitute endorsement by Transport Canada of the linked web sites, or the information, products or services contained therein. Transport Canada does not exercise any editorial control over the information you may find at these locations.

Abstract

Through its ecoTECHNOLOGY for Vehicle II program, Transport Canada has commissioned a project to investigate the aerodynamic improvements possible with current and emerging drag reduction technologies for heavy-duty vehicles (HDVs), with the intent of guiding future implementation of such technologies for Canada's transportation industry. The project will consist of wind-tunnel testing of a scale-model HDV with various drag reduction technologies.

Progress towards the development of a Flow Treatment System (FTS) for generating winds experienced by HDVs on the road is presented (Phase 1 - Stream A). This includes the results and analysis of 1) the on-road tests to measure the winds experienced by road vehicles, 2) the small-scale wind tunnel tests to evaluate concepts for simulating the measured winds, 3) the small-scale wind tunnel tests to investigate the sensitivity of HDV drag to turbulence, 4) the intermediate-scale demonstration of the selected concept, and 5) the selection of an appropriate blockage correction method for HDVs in turbulent flow. The project progress to date is described and the required next steps are defined.

This report forms a redacted version of the original LTR-AL-2014-0014 for public dissemination.

Table of Contents

Abstract	vii
List of Figures	xi
List of Tables	xiv
Nomenclature	xv
1. Introduction	1
1.1 Background	1
1.2 Project Objectives and Outcomes	2
1.3 Project Requirements and Outline	4
2. On-Road Turbulence Measurements	9
2.1 Problem Description	9
2.2 Data Processing Procedures	9
2.3 Classification of the On-Road Wind Measurements	12
2.3.1 Procedures for Classification	12
2.3.2 Terrain Roughness	12
2.3.3 Traffic Density	14
2.3.4 Wind Strength	16
2.3.5 Categorization of Wind Measurements	16
2.4 Analysis of On-Road Wind Measurements	17
2.4.1 Turbulence Intensities and Length Scales	17
2.4.2 Wind Spectra	23
2.4.3 Spatial Correlations of Turbulence	26
2.4.4 Comparison to Previous Work	30
2.4.5 Preliminary Target for FTS	31
2.4.6 Summary	31

3. Concept Design for Flow Treatment System	35
3.1 Problem Description	35
3.2 Measurements and Analysis Procedures	36
3.3 Analysis of Small-Scale FTS Measurements	39
3.3.1 Flow Uniformity	39
3.3.2 Influence of Settling-Chamber-Mounted Spire Shape	42
3.3.3 Influence of Test-Section-Mounted Turbulence Configurations	42
3.3.4 Influence of Changes in Large Spire Configuration	45
3.3.5 Influence of Changes in Small Spire Configuration	47
3.3.6 Comparison of Small Scale FTS Configurations	47
3.4 Selection of Candidate Concept and Comparison to Target Conditions	50
3.5 Summary	56
4. Sensitivity of HDV Drag to Turbulence	57
4.1 Problem Description	57
4.2 Wind Tunnel Setup and Measurement Procedures	58
4.3 Wind Loads	63
4.4 Surface Pressures	67
4.5 Summary	73
5. Intermediate Scale Verification of the Flow Treatment System Concept	75
5.1 Problem Description	75
5.2 Approach	76
5.3 Design	77
5.4 Results	78
5.5 Summary	85
6. Design of the Full-Scale Flow Treatment System	87
7. Blockage Corrections for HDVs	89
7.1 Problem Description	89
7.2 Setup	90

7.3	Results	91
7.4	Summary	96
8.	Conclusions and Future Work	97
	References	99

List of Figures

1.1	Relative merits of wind-tunnel versus track measurements for ground vehicles	2
1.2	Project overview	3
1.3	SUV with support rig for on-road turbulence measurements	5
1.4	Passive techniques examined to for turbulence generation in the NRC NRC 1.0 m × 0.8 m Pilot Wind Tunnel	5
1.5	HDV models and FTS concepts in NRC NRC 1.0 m × 0.8 m Pilot Wind Tunnel .	6
2.1	Sample Cobra-probe and GPS time-series measurements for Run 38 with seg- mentation based on classification method identified	13
2.2	Examples of terrain roughness experienced during the on-road measurements .	14
2.3	Examples of traffic density experienced during the on-road measurements . . .	15
2.4	Turbulence intensity measurements from on-road measurement campaign at 1.5 m from the ground	19
2.5	Turbulence length scale measurements from on-road measurement campaign at 1.5 m from the ground	20
2.6	Variations in turbulence intensities and length scales with height for M-L-L, M- M-M, R-D-S and M-W-M conditions (grey lines represent measured min/max of respective conditions)	22
2.7	Wind spectra from on-road measurement campaign (1.5 m from the ground) .	24
2.8	Variation of wind spectra with height from on-road measurement campaign (Moderate Terrain, Moderate Traffic, Moderate Winds))	25
2.9	Vertical turbulence correlation distributions from on-road measurements, refer- enced to a location 0.5 m from the ground.	28
2.10	Horizontal turbulence correlation distributions from on-road measurements, measured at 1.5 m from the ground.	29

 Drag Reduction for HDVs - Progress Toward a Flow Treatment System - Year 2

3.1	Cobra probe holders mounted to positioning arm of 3-axis traverse system . . .	36
3.2	Flow-field survey for C6Q spire configuration	39
3.3	Influence of FTS concepts on the mean flow in the test section	41
3.4	Influence of settling-chamber-spire shape on the vertical turbulence profiles . .	43
3.5	Influence of settling-chamber-spire shape on the wind spectra at $z = 0.06$ m . .	43
3.6	Influence of test-section-mounted configurations on the vertical turbulence profiles	44
3.7	Influence of test-section-mounted configurations on the wind spectra at $z = 0.06$ m	44
3.8	Influence of varying the C3 spire configuration on the vertical turbulence profiles	46
3.9	Influence of varying the C3 spire configuration on the wind spectra at $z = 0.06$ m	46
3.10	Influence of varying the C6 spire configuration on vertical turbulence profiles .	48
3.11	Influence of varying the C6 spire configuration on wind spectra at $z = 0.06$ m .	48
3.12	Comparison of the vertical turbulence profiles for concepts selected to evaluate HDV drag sensitivity	49
3.13	Comparison of the wind spectra at $z = 0.06$ m for concepts selected to evaluate HDV drag sensitivity	49
3.14	Comparison of candidate FTS concept (C6Q) with on-road wind spectra measurements	51
3.15	Comparison of candidate FTS concept (C6Q) with on-road vertical correlation measurements	52
3.16	Comparison of candidate FTS concept (C6Q) with on-road horizontal correlation measurements	53
3.17	C6Q turbulence characteristics at different longitudinal locations	55
3.18	C6Q vertical correlation measurements at different longitudinal locations . . .	55
3.19	C6Q horizontal correlation measurements at different longitudinal locations . .	55
4.1	Simplified HDV models for drag-sensitivity measurements (left - lightweight foam model, right - Renshape pressure model)	58
4.2	Pressure tap locations and groupings on HDV model	61
4.3	Influence of turbulence and Reynolds number on the mean drag coefficient . .	63
4.4	Influence of turbulence and wind angle on the mean drag coefficient	64
4.5	Influence of turbulence and wind angle on the drag coefficient for 44 m/s yaw-sweep cases (VB case at 34 m/s)	65

4.6	Influence of turbulence on the wind-averaged drag coefficient for a range of vehicle ground speeds	66
4.7	Influence of wind angle on HDV pressure distribution in smooth-flow conditions	68
4.8	Influence of turbulence HDV pressure distribution at 0° wind angle	70
4.9	Influence of turbulence HDV pressure distribution at -10° wind angle	71
4.10	Surface-pressure spectra at four locations, for 0° and -10° wind angles, under the smooth-flow, C6Q, VB and C3W conditions	72
5.1	Dimensions of the settling chamber and test section with the contraction ratio for three NRC Wind Tunnels	75
5.2	Left: View from upstream of the vertical traverse for measurements at the centre of the test section with the 4 Cobra probes mounted on a horizontal bar and spaced by 15 cm. Right: Side view of the vertical traverse during wind on measurements	77
5.3	Sketch of the top view of the test section with the 12 lateral positions and the 3 longitudinal positions where wind measurements were performed using Cobra probes	77
5.4	Left: Cobra probes mounted on the bar for the horizontal spatial correlation. Right: Cobra probes mounted on the bar for the vertical spatial correlation . . .	78
5.5	Spectrum of the longitudinal, lateral and vertical wind components for configurations tested in the NRC 2 m × 3 m Wind Tunnel (ISFTS) compared with results from NRC 1.0 m × 0.8 m Pilot Wind Tunnel (SSFTS) and on-road measurements	79
5.6	Mean wind-speed ratio, turbulence intensity and turbulence length scales for the longitudinal, lateral and vertical wind components for the configuration using 6 spires	80
5.7	Mean wind-speed ratio, turbulence intensity and turbulence length scales for the longitudinal, lateral and vertical wind components for the configuration using 5 spires	81
5.8	Mean values of the 12 lateral positions for the mean wind-speed ratio, turbulence intensity and turbulence length scales to characterize the 6-spire configuration	82
5.9	Lateral distributions of flow, ISFTS Measurements	83
5.10	Vertical spatial correlation as measured at the centre of the test section for the 3-wind components	84
5.11	Horizontal spatial correlation as measured at the centre of the test section for the 3-wind components	84

7.1	Simplified HDV models for the blockage-correction study	91
7.2	Comparison of blockage-corrections: body axis (open markers) and wind-tunnel axis (solid markers) drag coefficient distributions with wind angle for three turbulence levels (left column - 0.6%, middle column - 3.8%, right column - 4.6%) uncorrected (top row) and corrected with Maskell III method (middle row), and Thom-Herriot method (bottom row)	92
7.3	Comparison of blockage-corrections: body-axis drag coefficient distributions with model scale for three turbulence levels (left column - 0.6%, middle column - 3.8%, right column - 4.6%) and three wind angles (-1° - top row, -5° - middle row, -10° - bottom row)	94
7.4	Comparison of blockage-corrections: centreline pressure coefficient distributions for two conditions (0.6% turbulence at 0° wind angle - left column, and 4.6% turbulence at -10° wind angle - right column) uncorrected (top row) and corrected with Maskell III method (middle row), and Thom-Herriot method (bottom row)	95
7.5	Comparison of blockage-corrections: dynamic pressure and wake-increment drag-coefficient corrections for the Maskell III and Thom-Herriot methods (0.6% turbulence at -5° wind angle)	96

List of Tables

2.1	Categorization of the 215 vertical-rake on-road wind measurement segments .	17
2.2	Categorization of the 77 horizontal-rake on-road wind measurement segments	17
2.3	Breakdown of classification categories experienced in the on-road measurements	17
2.4	Target turbulence intensities and length scales for FTS development representing the Moderate Terrain, Moderate Traffic, Moderate Winds (M-M-M) condition, at 1.5 m from ground	32
3.1	Spire shapes for settling chamber (REDACTED, quantities replaced with relative qualifiers)	37
3.2	Small-scale FTS concepts tested (REDACTED)	38
3.3	Comparison of C6Q turbulence characteristics to the target on-road condition (M-M-M: Moderate Terrain, Moderate Traffic, Moderate Winds)	54
4.1	Turbulence intensities and length scales of configurations used to evaluate sensitivity of HDV drag to turbulence, measured 0.09 m from the ground	62

5.1	Mean lateral values of the 3-component of turbulence intensity and length scales at 20 cm from the floor for the cases with 6 spires and 5 spires	84
5.2	Comparison of SSFTS and ISFTS turbulence characteristics with the target on-road condition (M-M-M: Moderate Terrain, Moderate Traffic, Moderate Winds)	85

Nomenclature

Symbols:

A	area [m ²]
C_D	drag-force coefficient $\left(= \frac{F_D}{1/2\rho U_{ref}^2 A} \right)$ []
C_{WAD}	wind-averaged drag coefficient []
C_P	pressure coefficient $\left(= \frac{P - P_{ref}}{1/2\rho U_{ref}^2 A} \right)$ []
f	frequency [Hz]
f_r	reduced frequency []
F_D	drag force [N]
L	length [m]
L_u^x	longitudinally-correlated length scale of u -turbulence component [m]
L_v^x	longitudinally-correlated length scale of v -turbulence component [m]
L_w^x	longitudinally-correlated length scale of w -turbulence component [m]
R_{ii}	spatial cross-correlation function []
S_P	mean-square spectral distribution []
U	wind speed [m/s]
u	wind speed component in x direction [m/s]
v	wind speed component in y direction [m/s]
w	wind speed component in z direction [m/s], trailer width [m]
x, X	longitudinal coordinate [m]
y, Y	lateral coordinate [m]
z, Z	vertical coordinate [m]
θ	terrestrial wind angle [°]
η	vehicle-referenced wind angle [°]

ρ	air density [kg/m ³]
ϕ	wind pitch angle [°]
ψ	wind yaw angle [°]

Acronyms:

EC	Environment Canada
EPA	Environmental Protection Agency
eTV	ecoTECHNOLOGY for Vehicles
FTS	flow treatment system
GESS	Ground Effects Simulation System
GHG	greenhouse gas
GPS	global positioning system
HDV	heavy duty vehicle
NRC	National Research Council
NRCan	Natural Resources Canada
PSD	power spectral density
SAE	Society of Automotive Engineers
SUV	sport utility vehicle
TC	Transport Canada

1. Introduction

1.1 Background

Transport Canada, through its ecoTECHNOLOGY for Vehicles II (eTV II) program, undertakes testing and evaluation of current and emerging vehicle technologies. The program helps inform various stake-holders that are engaged in the development of regulations, codes, standards, and products for the next generation of advanced light and heavy-duty vehicles.

In a report prepared for Transport Canada in 2012 (Patten *et al.*, 2012), NRC identified that aerodynamic drag (resistance to motion due to movement through air) is the greatest component of resistance to motion for heavy vehicles operating under highway conditions, and is thus a prime contributor to greenhouse gas emissions and fuel consumption. In cold and windy Canadian climates, aerodynamic drag can be an even more significant contributor to these issues. Drag is also a dissipative loss that cannot be recovered by any means. Many drag-reduction technologies are currently on the market and many are being proposed for improving fuel efficiency and reducing emissions. Some evidence has shown that fuel savings on the order of 10%-20% from such technologies are achievable for long-haul dry-van-trailer combinations (National Academy of Sciences, 2010). However, the evaluation of such technologies is difficult and error prone, thus making many manufacturer's claims suspect.

Transport Canada, through its eTV II program, is interested in investigating aerodynamic performance of current and emerging drag reduction technologies for heavy vehicles, and in particular for tractor-trailer combinations. Through several decades of working in the fields of ground-vehicle aerodynamics and wind engineering, NRC has the capabilities and expertise to evaluate properly the aerodynamic performance of drag reduction technologies for ground vehicles and report on their aerodynamic benefits, ease of use, and potential fuel savings. As such, Transport Canada commissioned NRC to undertake a multi-year project to evaluate the performance of current and emerging drag reduction technologies to guide Transport Canada and its stakeholders in reducing greenhouse-gas emissions and fuel consumption from heavy vehicles.

The use of scale-model testing in a wind tunnel provides the benefit of testing in a systematically-controlled and representative environment including relative vehicle/ground/wind motions and the turbulent winds near the ground. Figure 1.1 shows the relationship between wind-tunnel and track testing, and identifies the benefits of each. Although aerodynamic experiments on a test track provide realistic wind conditions, current experimental techniques and procedures are not conducive to repeatable or accurate aerodynamic performance assessments. This shortcoming is being addressed in a separate project under the eTV II program that will provide enhanced techniques for track testing and thus complementing the current

proposed work. The wind-tunnel technologies NRC will implement in the current project will provide a significantly improved simulation of the environment in which heavy vehicles operate, therefore improving the realism and accuracy of the wind-tunnel measurements and providing confidence in the final recommendations of the project. NRC is confident these technologies will provide the most accurate wind-tunnel simulation of drag reduction technologies for HDVs in the world, and will allow an accurate measure of the differences between these technologies.

test method	wind conditions	drag measurements
wind tunnel	approximate (simulation)	reliable (excellent repeatability)
track	accurate (reality)	approximate (poor repeatability)

Figure 1.1: Relative merits of wind-tunnel versus track measurements for ground vehicles

The project consists of two phases. Phase 1, initiated in the first year of work (2012-2013) has two parallel streams of work that focus on the design and development aspects of the project. Phase 2, to follow in subsequent years of the project (2014+), will consist of the test and evaluation part of the project. Figure 1.2 shows an overview of the project structure, including the two phases of the project, their streams, and their major project elements.

This report describes the progress made in the second year of the project towards Phase 1, Stream A. A companion report (McAuliffe, 2014b) documents the progress made towards Phase 1 Stream 2.

1.2 Project Objectives and Outcomes

The primary objective of the project is to provide recommendations to HDV regulators, including Transport Canada (TC), Environment Canada (EC), Natural Resources Canada (NR-Can), and the U.S. Environmental Protection Agency (EPA), on the most efficient means to reduce greenhouse gas emissions and fuel consumption of HDVs through aerodynamic drag-reduction technologies. The inconsistency of typical drag-reduction evaluations, combined with the inaccuracy associated with many of those techniques, requires a common objective basis upon which such evaluations must be performed. NRC is planning a wind-tunnel test campaign that will provide the consistency and realism required to ensure the most reliable predictions of drag reduction possible. To do so, it is important to simulate the effects of relative motion between the vehicle, the ground and the wind, and to simulate the turbulent wind characteristics near the ground encountered by heavy vehicles on the road. The performance of modern and emerging drag-reduction technologies will be evaluated using scale models of various heavy-vehicle combinations, including long-combination vehicles. These evaluations will be done in a manner that eliminates the largest uncertainties generally associated

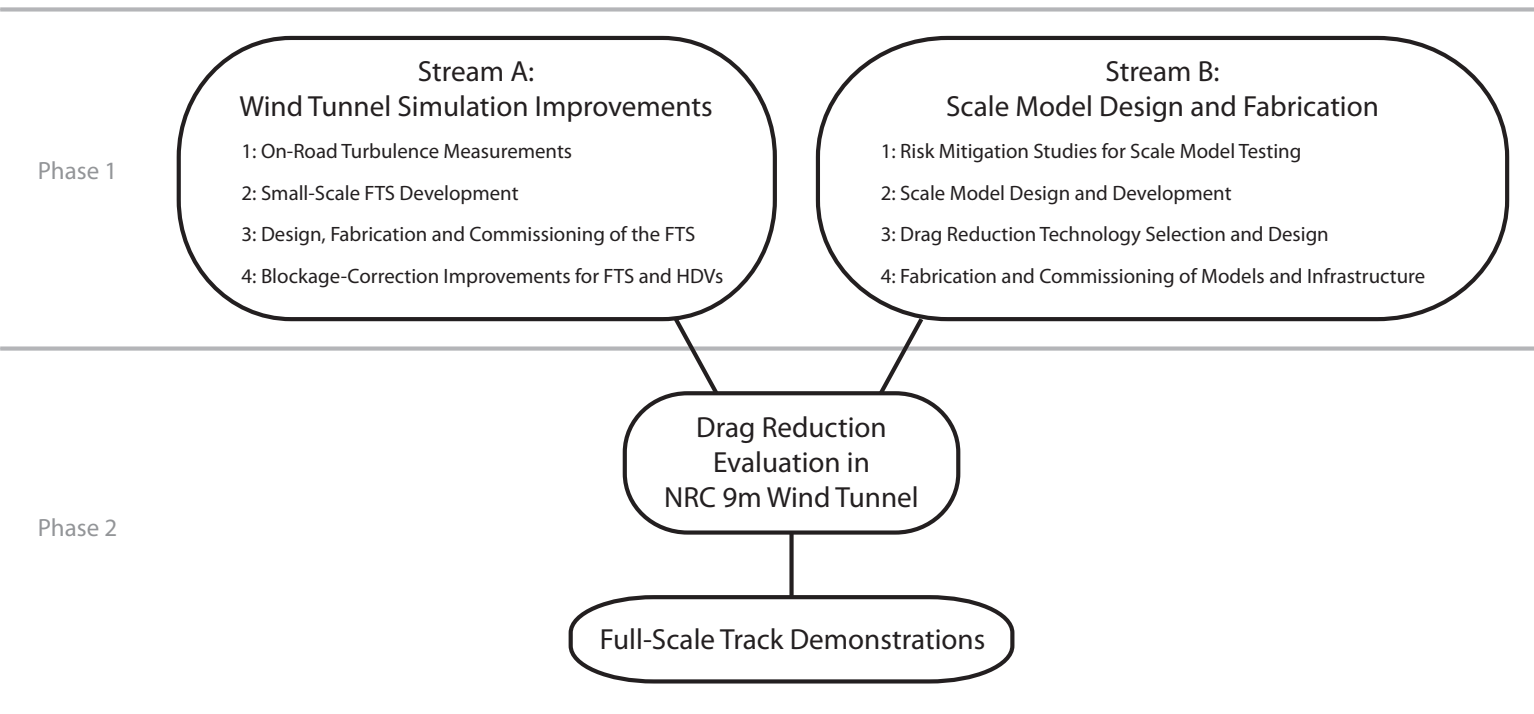


Figure 1.2: Project overview

with wind-tunnel testing; those being the simulation of natural winds and the simulation of relative motions between the vehicle, the ground and the wind.

This project will support the following three eTV II program outcomes:

- Provide data to help support the development of future environmental (emissions) regulations: by providing test results on the efficiency gains offered by various HDV aerodynamic modifications/technologies.
- Provide data to help support the development of non-regulatory codes and standards: testing results will help industry optimize drag reduction technologies.
- Support energy efficiency programs: testing outcomes will help inform energy efficiency programs by providing data on various drag reduction technologies (for example, the Canadian Smartway Program).

1.3 Project Requirements and Outline

The requirements set forth for the development of a Flow Treatment System (FTS) to provide a representative wind profile and turbulence levels in the NRC 9 m Wind Tunnel are as follows:

- Provide wind characteristics in the test section representative of what HDVs experience on Canadian roads;
- Use passive technology (no energy input) to avoid an expensive and complex system to build and maintain; and
- Develop a system that can be deployed or removed in a time period no longer than five hours (half a test day), to avoid excessive costs during a test program.

A survey of pertinent literature that led to the development of the current approach for generating appropriate turbulence in the NRC 9 m Wind Tunnel was provided in Section 1.3 of the year 1 progress report (McAuliffe *et al.*, 2013a).

To achieve the requirements noted above, a seven-step approach is being taken, outlined as follows:

1. Measure the winds that HDVs experience on Canadian roads. This has been accomplished by mounting an array of fast-response pressure probes to a vehicle to measure vertical and horizontal variations in the unsteady winds experienced by HDVs (see Figure 1.3), and measurements have been performed on Canadian roads in a variety of wind, traffic and terrain conditions. An SUV was used to provide a strong enough support structure while minimizing its influence on the winds measured by the probes.
2. Examine various passive techniques in a small wind tunnel that may provide the important wind characteristics identified from the on-road measurements. This has been performed in the NRC 1.0 m × 0.8 m Pilot Wind Tunnel which is approximately 1/10 the scale of the NRC 9 m Wind Tunnel (see Figure 1.4). The techniques examined include:



Figure 1.3: SUV with support rig for on-road turbulence measurements (left - side view, right - front view)



Figure 1.4: Passive techniques examined to for turbulence generation in the NRC 1.0 m \times 0.8 m Pilot Wind Tunnel: vertical bars + screen (top left), moving spires (top right), short and narrow settling-chamber spires (bottom left), tall and staggered settling-chamber spires (bottom right)

Drag Reduction for HDVs - Progress Toward a Flow Treatment System - Year 2

- A vertical-bar turbulence grid at the inlet of the test section;
 - A screen at the inlet of the test section;
 - A set of moving spires designed to move under the actions of the wind at a natural frequency that will provide scales of flow fluctuations greater than the scale of a 1/10-scale HDV model; and
 - Wooden obstacles mounted in the settling chamber.
3. Examine the sensitivity of HDV drag to various unsteady wind characteristics. This has been accomplished by building two small simple HDV models to test in the NRC 1.0 m \times 0.8 m Pilot Wind Tunnel in the various turbulence environments developed in 2 above (see Figure 1.5). One model is a lightweight model that provides the dynamic response of the vehicle drag to the wind fluctuations. The second model has identical geometry to the first but is instrumented with 64 pressure taps, calibrated for the pressure-tubing frequency response, that was used to examine where on the HDV model differences in drag-producing forces occur due to turbulence.
 4. Use the results of items 1, 2 and 3 above to select an appropriate turbulence environment that will provide drag characteristics for an HDV representative of what would be experienced on the road.
 5. Use the results of item 4 above to design an intermediate-scale FTS concept, for testing in the NRC 2 m \times 3 m Wind Tunnel which has a circular settling chamber arrangement similar to the NRC 9 m Wind Tunnel, unlike the rectangular settling chamber of the NRC 1.0 m \times 0.8 m Pilot Wind Tunnel.
 6. Scale-up the selected FTS concept for installation in the NRC 9 m Wind Tunnel, to be commissioned in year 3 of the project prior to the drag-reduction-technology evaluation (Phase 2).
 7. Evaluate the influence of turbulent winds on the most appropriate manner in which to correct for wall-interference and blockage effects in the NRC 9 m Wind Tunnel test



Figure 1.5: HDV models and FTS concepts in NRC NRC 1.0 m \times 0.8 m Pilot Wind Tunnel (left - pressure model with short spires, right - lightweight model with tall spires)

program of Phase 2.

The year 1 progress report (McAuliffe *et al.*, 2013a) documented the setup, test procedures, and preliminary results for items 1, 2, and 3 above. This report describes the analysis of data collected from those tasks, in Sections 2, 3, and 4, respectively, with the results of task 4 included in those sections. Tasks 5, 6, and 7 above are presented in Sections 5, 6 and 7, respectively. This report excludes the commissioning of the full-scale FTS (part of item 6) that will be accomplished in the third year of work.

2. On-Road Turbulence Measurements

2.1 Problem Description

To provide representative conditions in a wind tunnel, the characteristics of the winds experienced by moving vehicles on the road must be known, and such wind characteristics have not been well studied. The winds near the ground (0.1 to 4 m) are highly dependent on the local terrain (urban, rural, road-side obstacles, etc.). Although some recent on-road measurements have been performed by a research group at Monash University in Australia (Wordley and Saunders, 2009), they concluded that more measurements are required to assess adequately the winds to be simulated in a wind tunnel. Their study also considered only a few types of local terrain and did not consider some of the terrain environments prevalent on Canadian roads. As a first step towards developing the Flow Treatment System (FTS) for the NRC 9 m Wind Tunnel, NRC has performed on-road measurements over highways in Eastern Ontario and Western Quebec to measure the winds experienced by HDVs.

In the progress report for the first year of the project (McAuliffe *et al.*, 2013a), a description of the test vehicle, the measurement system, the measurement procedures, the preliminary analysis procedures, the test program, and a sample of the wind measurements were provided. In the following sections, the detailed results and analysis of the test data are provided.

2.2 Data Processing Procedures

The preliminary data processing procedures were described in detail in the progress report for the first year of the project (McAuliffe *et al.*, 2013a). The processed data, which consisted of the time series of velocity and pressures as measured from the Cobra probes, have been further processed to yield a data set useful for identifying typical wind characteristics experienced by vehicles on the road. The additional processing steps are described as follows:

1. A classification system was devised for categorizing and comparing the on-road measurements. This classification system is described in Section 2.3.
2. Each measurement run was subdivided into segments, each of which representing a time period of constant ground speed for which the wind conditions could be categorized according to the classification system.
3. The Cobra probe measurements were corrected for alignment offsets in the flow angles, based on a combination of known conditions including some on-road measurements and the tests performed in the NRC 9 m Wind Tunnel.

4. For each data segment, the following parameters were calculated from the GPS data and Cobra probe time series:
 - Reference speed defined by the mean ground speed of the vehicle (U_{ref}),
 - Mean velocities (U, u, v, w), flow angles (ϕ, ψ) and static pressure (P),
 - Mean velocity ratios ($U/U_{ref}, u/U_{ref}, v/U_{ref}, w/U_{ref}$),
 - RMS velocities ($U_{rms}, u_{rms}, v_{rms}, w_{rms}$), flow angles (ϕ_{rms}, ψ_{rms}) and static pressure (P_{rms}),
 - Turbulence intensities ($U_{rms}/U_{ref}, u_{rms}/U_{ref}, v_{rms}/U_{ref}, w_{rms}/U_{ref}$),
 - Turbulence length scales (L_u^x, L_v^x, L_w^x),
 - The wind spectrum, defined by the power-spectral-density (PSD) distributions, of each wind component.
5. Low-frequency variations in the wind measurements arose due to some non-stationarity of the conditions encountered on the road. This likely results from translation of the vehicle through a non-homogeneous environment, combined with long-period cycles of the vehicle cruise control system. As a result, the low-frequency range of the calculated spectra (<0.25 Hz) did not compare well for similar conditions, despite agreement in the high frequency range. To eliminate any bias in the turbulence intensities as a result of such non-stationary variations, the turbulence intensities quantified in this report represent those calculated from an integration of the appropriate spectra for which the energy levels below 0.25 Hz were limited to a value defined by the average energy between 0.2 Hz and 0.3 Hz. This process provided a better representation of the low-frequency content expected for atmospheric turbulence, as compared to high-pass filtering of the data which eliminates these low-frequency fluctuations altogether. In addition, the turbulence length scales were also calculated using a best-fit von-Karman distribution to the modified spectra (as defined above), according to the generic von-Karman spectra defined by ESDU (2001).
6. For each set of conditions defined by the classification system, the spectra from the associated segments were averaged to provide a wind spectrum representative of that condition. To account for differences in vehicle speed, and to provide a means to compare the on-road data to subsequent wind-tunnel measurements, the wind spectra were normalized. The appropriate frequency scaling is the reduced frequency, defined as:

$$f_r = \frac{f \cdot L_{ref}}{U_{ref}}. \quad (2.1)$$

For the on-road data, the reference length scale (L_{ref}) is taken as 1 m. The reference speed (U_{ref}) is taken as the vehicle ground speed. The PSD is normalized as:

$$PSD(f_r) = \frac{PSD(f)}{L_{ref} \cdot U_{ref}} \quad (2.2)$$

which ensures that the energy level of the normalized spectra is appropriately scaled for the reduced frequency definition. This normalization was performed prior to averaging

of the wind spectra for a given set of conditions. For each condition, the maximum and minimum of the normalized wind spectra were also identified to provide the bounds within which the turbulence energy for the condition were limited. Different spectra showed different levels of scatter in the spectral distributions due to differences in the length of the time series used for each. This results from a greater number of spectral averages from the longer time series, and hence smoother spectral distributions. Therefore, the mean, maximum, and minimum spectra were subsequently smoothed to provide negligible scatter and allow ease of visual comparison to other conditions.

7. Spatial cross-correlations between each of the probes were calculated for each data segment. A correlation value for each probe pair was calculated for the u , v , and w components. With four probes, six pairs (1-2, 1-3, 1-4, 2-3, 2-4, 3-4) and hence six correlation values were calculated. The vertical correlation distributions presented in this report only make use of probe pairs 1-2, 1-3, and 1-4 (where probe 1 is lowest and probe 4 is the highest) providing correlations reference to a location 0.5 m from the ground. This was done because the correlation values between probe pairs was observed to increase with height, due most likely to the change in wind speed and turbulence characteristics with height, and therefore caused incorrect inferences of the shape of the correlation distributions if compared to those referenced to probe 1 at 0.5 m from the ground. All six pairs are presented for the horizontal probe configuration because the winds near the ground show a much greater level of lateral uniformity than vertical uniformity. To avoid the low-frequency non-stationarity of the on-road measurements, described in item 5 above, the time series were high-pass filtered with a cut-off frequency of 0.25 Hz prior to the correlation calculations. The spatial cross-correlation for a given spacing ($\Delta x, \Delta y, \Delta z$) is defined as:

$$R_{ii}(\Delta x, \Delta y, \Delta z) = \frac{\langle u_i(x + \Delta x, y + \Delta y, z + \Delta z, t) u_i(x, y, z, t) \rangle}{\sigma(x + \Delta x, y + \Delta y, z + \Delta z, t) \sigma(x, y, z)} \quad (2.3)$$

where i refers to the velocity component (u, v, w), σ is the standard deviation of the specific component over the full length of the time series, and $\langle \rangle$ represents a time average.

8. As described in the progress report for the first year of the project (McAuliffe *et al.*, 2013a), to allow correction of the wind measurements for offsets in the physical probe angles, due to alignment uncertainty during installation, as well as to characterize the influence of the vehicle on the winds at the measurement locations, the test vehicle was installed over the Ground Effect Simulation System (GESS) of the NRC NRC 9 m Wind Tunnel. This provided a known uniform flow in which to perform yaw sweep measurements with the vehicle measurement system. By comparing probe measurements to the known wind condition as measured by the wind-tunnel data acquisition system, the angle offsets and vehicle influence effects were quantified. Under zero yaw conditions, the probes measured wind speeds of 78%, 86%, 95% and 98% of the blockage-corrected wind-tunnel speed, from lowest to highest, respectively. The probe measurements also showed sensitivity to wind angle, with a decrease in sensed wind speed at 15° yaw of approximately 5% from the zero-yaw values. The lowest probe showed the greatest sensitivity of the sensed wind angle to yaw, with a 5° increase in wind-angle at a yaw angle of 15° (measured 20°). The three higher probes showed an increase in wind angle over this

range no greater than 2° . To simplify the analysis, only corrections for probe-angle misalignments were performed in the data processing procedures. Turbulence intensities are based on vehicle ground speed, rather than the measured mean wind speed at each probe location, and therefore correction for the vehicle influence on the mean wind speed is not necessary. Furthermore, the influence of the vehicle body on the turbulence spectrum is discussed in Section 2.4.2. Measurements of the wind angle and lateral-velocity components for the lowest probe have a greater uncertainty than the three higher probes due to the vehicle influence effect noted above.

2.3 Classification of the On-Road Wind Measurements

2.3.1 Procedures for Classification

The video and Cobra-probe data for each set of on-road wind-measurement data were analyzed and subdivided into segments representing what appeared to be a constant set of conditions. Each of these segments, which varied in length typically between 30 seconds and 10 minutes, were subsequently processed and categorized based on three different criteria:

- Terrain Roughness;
- Traffic Density; and
- Wind Strength.

A sample of a time series, with notes identifying different traffic conditions experienced, is shown in Figure 2.1. The following sections describe the reasoning behind the categorization for each of these criteria.

2.3.2 Terrain Roughness

In standard wind-engineering practice, the characteristics of the winds are categorized by the terrain type over which the winds prevail. The wind characteristics, including variations with height and turbulence levels, are highly correlated with the terrain roughness. It was anticipated that the turbulent wind characteristics experienced by road vehicles will therefore also be correlated with terrain roughness.

For each of the segments extracted from the on-road wind measurements, a relative measure of the local terrain roughness was assigned based on observations from the video data combined with examining topographical maps of the route travelled. The terrain roughness was classified into four categories, for which a sample video frame is shown for each in Figure 2.2. The four categories are:

- Flat: Regions with little or no infrastructure and obstacles. Predominantly vast stretches of farmland. Such regions were primarily found in the Eastern Townships of Ontario. (sample image in Figure 2.2(a))

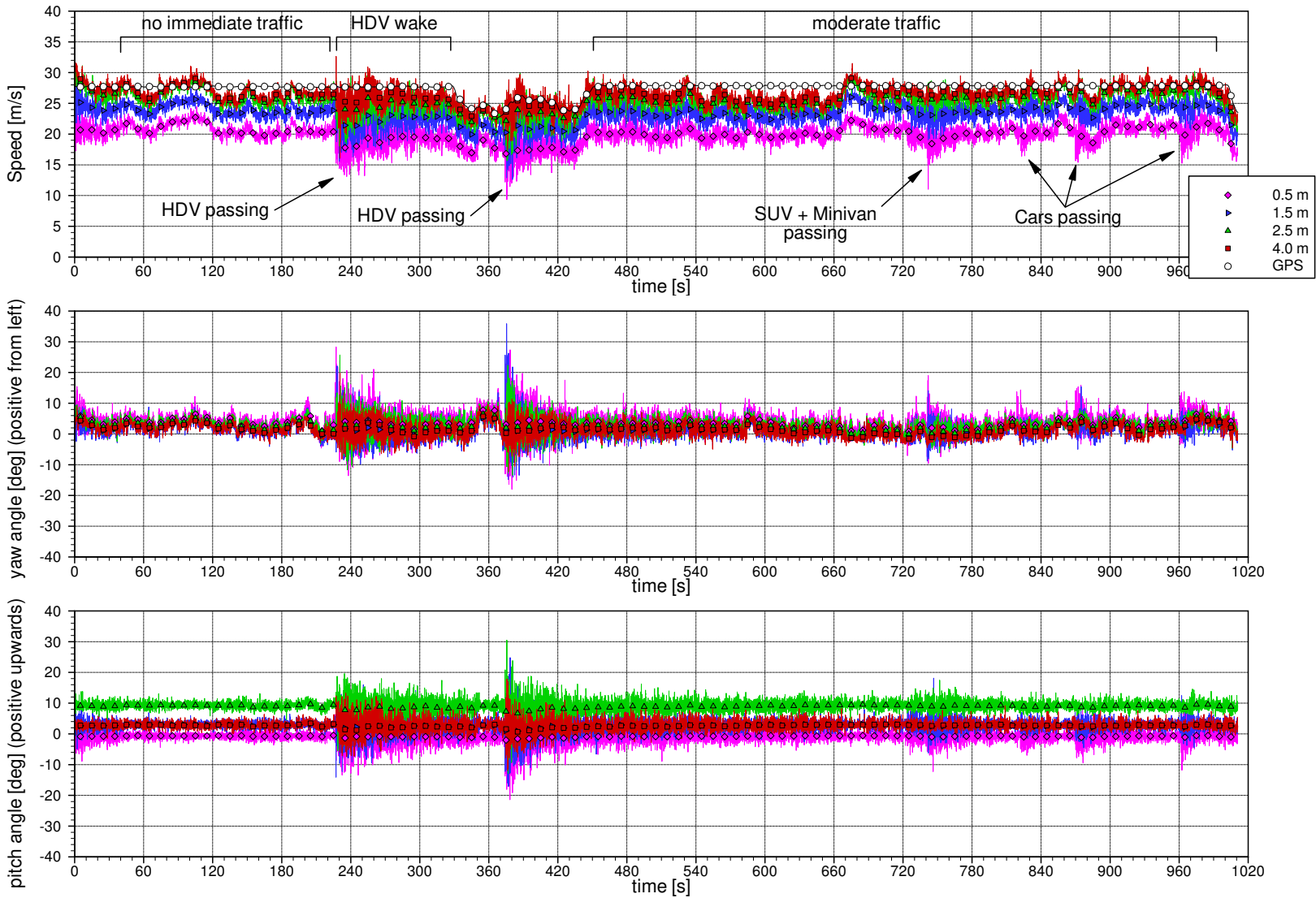


Figure 2.1: Sample Cobra-probe and GPS time-series measurements for Run 38 with segmentation based on classification method identified

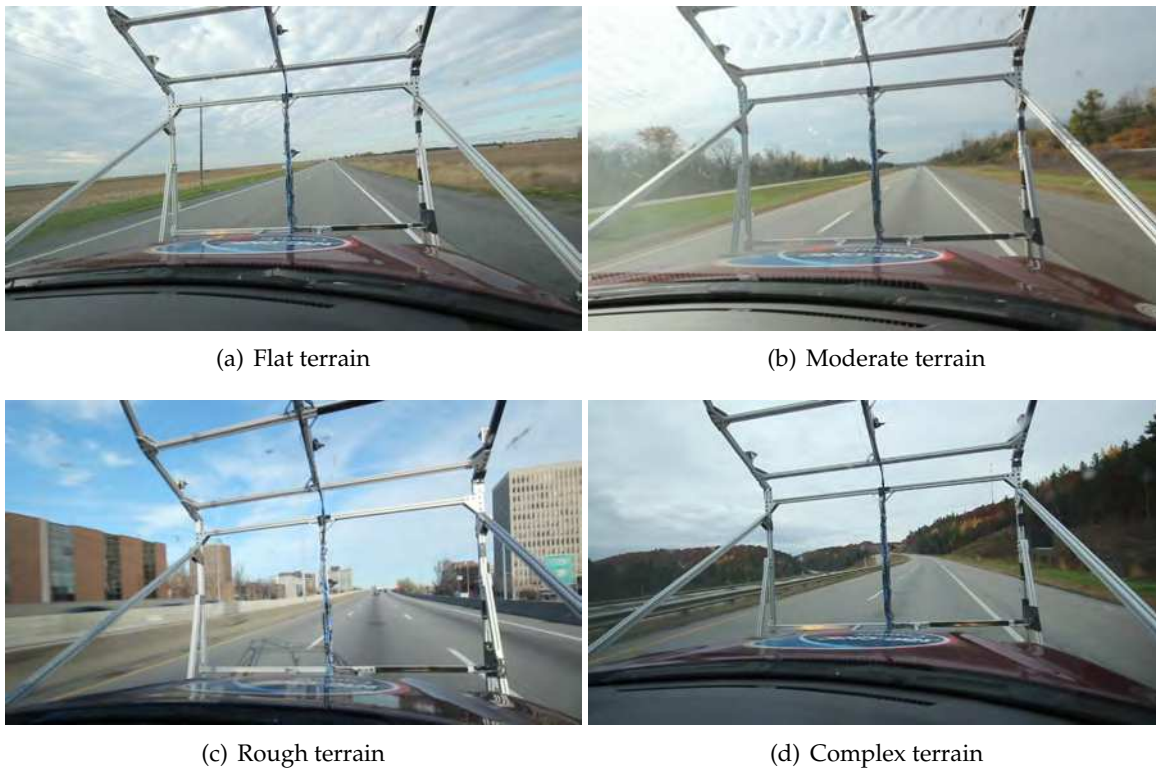


Figure 2.2: Examples of terrain roughness experienced during the on-road measurements

- Moderate: Regions with vegetation such as forests or mixed farmland-and-forests. (sample image in Figure 2.2(b))
- Rough: Urban infrastructure. Such regions were found in the greater Ottawa area along Highway 417. (sample image in Figure 2.2(c))
- Complex: Forested Regions with large hills. Such regions were predominantly found in the Gatineau Hills of Quebec. (sample image in Figure 2.2(d))

2.3.3 Traffic Density

The wake of a road vehicle is highly unsteady and affects the wind characteristics experienced by trailing vehicles on the road. The high turbulence in the wake also decays with distance from its source vehicle, such that the strength of the turbulence experienced by following vehicle is dependent on the spacing between the vehicles. It is therefore anticipated that traffic density will have an impact on the turbulent wind characteristics experienced by HDVs on the road, with higher turbulence levels experienced in dense traffic conditions.

For each of the segments extracted from the on-road wind measurements, a relative measure of the traffic density was assigned based on observations from the video data combined with examination of the measured wind fluctuations. The traffic density was classified into four cat-

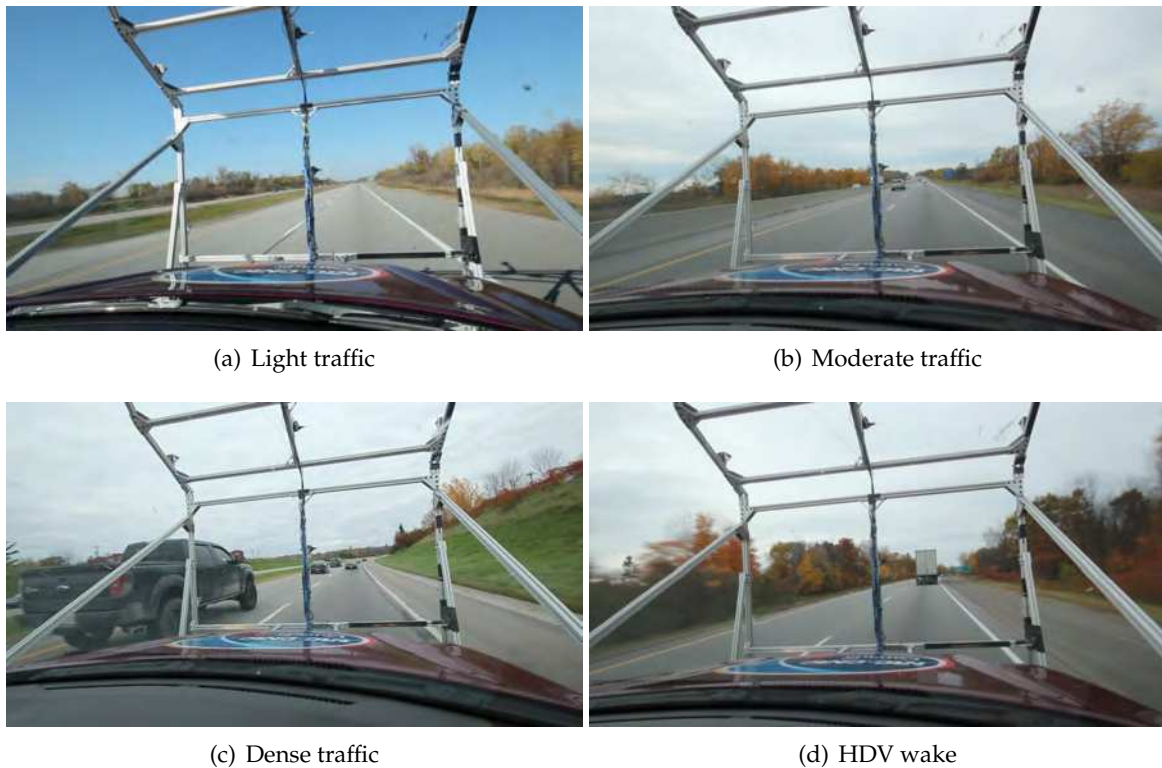


Figure 2.3: Examples of traffic density experienced during the on-road measurements

egories, for which a sample video frame for each are shown in Figure 2.3. The four categories are:

- Light - Very little traffic with no vehicles immediately ahead. Long stretches between vehicle passings. (sample image in Figure 2.3(a))
- Moderate - Increased number of vehicles with inter-vehicle distances greater than about 20 m. Wind data shows signatures of ambient terrain and wind conditions for part of the time (30-70%), and signatures of vehicle wakes for remainder of the time. An example of typical vehicle wake signatures are found in Figure 2.1. (sample image in Figure 2.3(b))
- Dense - Many vehicles in multiple lanes in which measured winds are dominated by vehicle wakes. (sample image in Figure 2.3(c))
- HDV Wake - When traveling in the wake of an HDV, the wind fluctuations are often dominating by a vortex-shedding phenomena that causes high fluctuations at a frequency on the order of 2 Hz (see McAuliffe, 2013c for description of phenomena). Under these situations, the wind fluctuations are dominated by the effect of the HDV. (sample image in Figure 2.3(d))

2.3.4 Wind Strength

As the strength of the atmospheric winds increases, so do the wind fluctuations and gust strengths which constitute the turbulence experienced by vehicles on the road. To categorize the wind strength for the on-road measurements, meteorological data was compiled from the weather stations across Eastern Ontario and Western Quebec and used as a reference. For each data segment, for which its location and time were known from the GPS data, corresponding weather data from the nearest weather station (10 m height) was used to identify a wind strength representative of the conditions under which the measurements were acquired. The inferred wind strengths were categorized as follows:

- Light - Meteorological-station wind measurement lower than 10 km/h.
- Moderate - Meteorological-station wind measurement between 10 km/h and 20 km/h.
- Strong - Meteorological-station wind measurement higher than 20 km/h.

The stability of the atmospheric boundary layer is one factor that has not been considered in the current classification system. For the current measurements performed close to the ground (up to 4 m from the ground), it is not expected that atmospheric stability will play a significant role in the turbulence characteristics very near the ground. If any effect is present it will likely be on the low-frequency/large-scale turbulence motions.

2.3.5 Categorization of Wind Measurements

After classification of the terrain roughness, traffic density, and wind strength for each data segment, the classifications were compiled to identify the most prevalent conditions encountered. Tables 2.1 and 2.2 show the numbers of data segments for each combination of terrain, traffic, and wind categories extracted from the vertical-rake and horizontal-rake configurations, respectively. It is evident from both tables that moderate terrain conditions were encountered most often, which was expected based on the terrain and vegetation conditions in Eastern Ontario. A total of 215 vertical-rake data segments have been produced, and 77 horizontal-rake data segments.

The analysis of wind conditions experienced by road vehicles described in the next section is based predominantly on the vertical-rake data set as it has the greatest number of measurements from which to evaluate the differences in wind conditions. The horizontal-rake has been used primarily for the spatial-correlation analysis.

For much of the subsequent discussions and data presentation, the Moderate Terrain, Moderate Traffic, and Moderate Winds condition will be the baseline against which the rest of the data will be compared. This specific condition is representative of 20% of all the run segments analyzed. To further identify the “Moderate” categories as the dominant conditions experienced on the road, Table 2.3 presents the proportion, based on number of run segments, of each category within each classification. These numbers further emphasizes the Moderate Terrain, Moderate Traffic, and Moderate Winds case as a representative target condition for developing the Flow Treatment System (FTS), although it represents only the test conditions

Table 2.1: Categorization of the 215 vertical-rake on-road wind measurement segments

Traffic		Low			Moderate			Dense			HDV Wake		
Winds		Low	Mod	Str	Low	Mod	Str	Low	Mod	Str	Low	Mod	Str
Terrain	Flat	0	1	1	0	7	0	0	0	0	0	0	0
	Moderate	8	25	21	16	49	5	0	12	2	3	12	5
	Rough	0	3	3	0	9	1	0	7	11	0	1	0
	Complex	0	5	1	0	6	0	0	0	0	0	1	0

Table 2.2: Categorization of the 77 horizontal-rake on-road wind measurement segments

Traffic		Low			Moderate			Dense			HDV Wake		
Winds		Low	Mod	Str	Low	Mod	Str	Low	Mod	Str	Low	Mod	Str
Terrain	Flat	0	4	0	0	1	0	0	0	0	0	0	0
	Moderate	8	19	0	13	8	2	0	0	0	0	6	0
	Rough	0	4	0	1	5	0	0	5	0	0	1	0
	Complex	0	0	0	0	0	0	0	0	0	0	0	0

Table 2.3: Breakdown of classification categories experienced in the on-road measurements

Terrain Roughness		Traffic Density		Wind Strength	
Flat	5%	Light	35%	Light	17%
<i>Moderate</i>	<i>73%</i>	<i>Moderate</i>	<i>42%</i>	<i>Moderate</i>	<i>65%</i>
Rough	17%	Dense	13%	Strong	18%
Complex	5%	HDV Wake	10%		

encountered during the measurement campaign. In addition, a large proportion of the heavy-vehicle highway traffic in Canada occurs along the Montreal-Toronto corridor, of which the conditions encountered in the current study are representative.

In the discussions of the various conditions, acronyms for the specific conditions are noted based on the identification of the Terrain Roughness (F-Flat, M-Moderate, R-Rough, C-Complex), the Traffic Density (L-Light, M-Moderate, D-Dense, W-HDV Wake), and the Wind Strength (L-Light, M-Moderate, S-Strong). For example, the data set for (R)ough Terrain, (M)oderate Traffic, and (L)ight Winds will be R-M-L.

2.4 Analysis of On-Road Wind Measurements

2.4.1 Turbulence Intensities and Length Scales

The simplest manner in which the characteristics of turbulence can be quantified and compared is through the turbulence intensity, which represents the magnitude of turbulent fluc-

tuations, and the turbulence length scale, which represents the size of the dominant energy-containing turbulent eddies in the wind. It is well known that, for bluff bodies, both of these characteristics should be replicated well in any simulation of the true wind environment, whether it is experimental or computational. For each of the conditions presented in Table 2.1 for the vertical-rake probe configuration, the turbulence intensities and length scales for each wind component (u -longitudinal, v -lateral, and w -vertical) were averaged over the total number of data segments in the category to yield a representative set of turbulence characteristics. Figures 2.4 and 2.5 show these averaged measurements at 1.5 m from the ground, along with the respective minimum and maximum values for each condition. All heights showed similar relative differences in turbulence conditions, and therefore 1.5 m was chosen as it is close to the mid-height of an HDV. These figures are plotted in a format to identify trends in the turbulence characteristics due to changes in terrain roughness, traffic density, and wind strength. The upper rows show the longitudinal turbulence component, with the middle and lower rows showing the lateral and vertical components, respectively. The left columns show the measurements for light winds, with the middle and right columns showing the measurements for moderate and strong winds, respectively. Within each plot, the turbulence characteristics are compared for the different categories of terrain roughness and traffic density, and represented by a coloured circle for which the colour and size represent the magnitude of the value. Additional inner and outer grey circles represent the minimum and maximum values measured.

The turbulence intensity measurements in Figure 2.4 show some distinct trends. In general, the longitudinal and lateral turbulence intensities (I_u and I_v) are the highest, with the longitudinal component most often but not always greater than the lateral component, and the intensity of the vertical component (I_w) is lowest. For example, the Moderate Terrain, Moderate Traffic, Moderate Winds (M-M-M) measurements have average turbulence intensities of the longitudinal (I_u), lateral (I_v), and vertical (I_w) components of 4.0%, 3.5% and 3.1%, respectively. A smaller magnitude for the lower vertical component has also been noted by Wordley and Saunders (2009) in their study of on-road turbulence and is considered an effect due to damping of the turbulence by the proximity of the ground. Despite this, all three components show the same trends with respect to the terrain roughness, traffic density, and wind strength. The most distinct observation regarding these environmental factors is the increase in turbulence intensity with traffic density, which is evident for all three turbulence components at all wind strengths and terrain roughnesses. As an example, for Moderate Terrain and Moderate Winds, the longitudinal turbulence intensity (I_u) increases from 3.1% under light traffic density to 4.0% under moderate traffic, to 5.3% under dense traffic, to 7.4% in the wakes of HDVs on the road. This effect is due to the turbulence generated in the wakes of other vehicles, which is superimposed on turbulence of the local terrain and wind conditions. Although wake turbulence decays with time, increased traffic density means a higher number of wakes are experienced before they decay, providing the higher levels of turbulence. In the wakes of HDVs on the road, the lateral turbulence intensity (I_v) is consistently greater than the longitudinal component (I_u) due to the vortex-shedding phenomenon that causes a large-scale side-to-side motion of the HDV wake.

It is also evident from the data in Figure 2.4 that the turbulence intensity increases with wind strength, however the sensitivity is not as strong as that for traffic density. Under Moderate

Drag Reduction for HDVs - Progress Toward a Flow Treatment System - Year 2

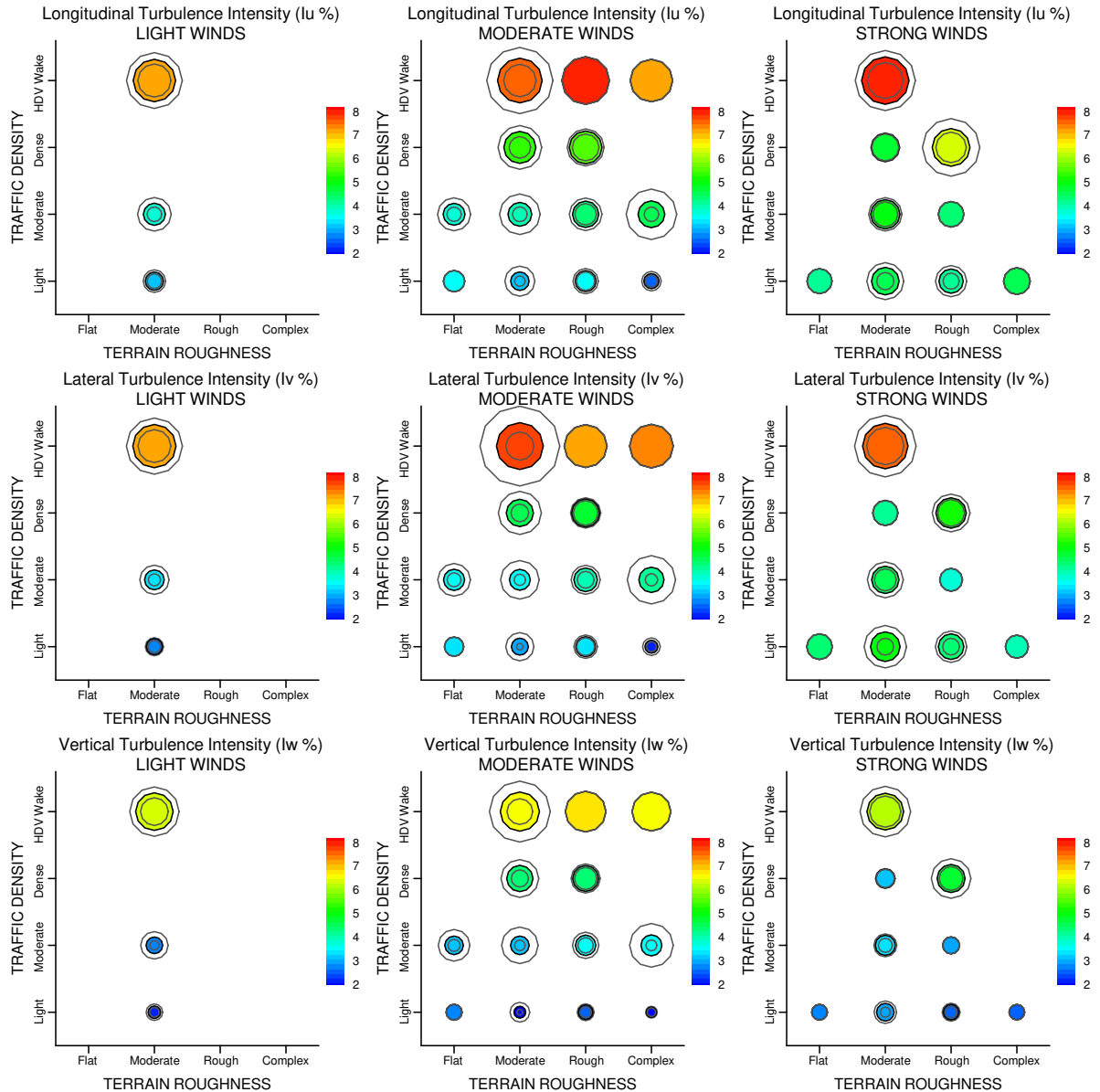


Figure 2.4: Turbulence intensity measurements from on-road measurement campaign at 1.5 m from the ground (circle size proportional to turbulence intensity and multiple circles for a condition show the minimum, mean, and maximum values from all data segments)

Drag Reduction for HDVs - Progress Toward a Flow Treatment System - Year 2

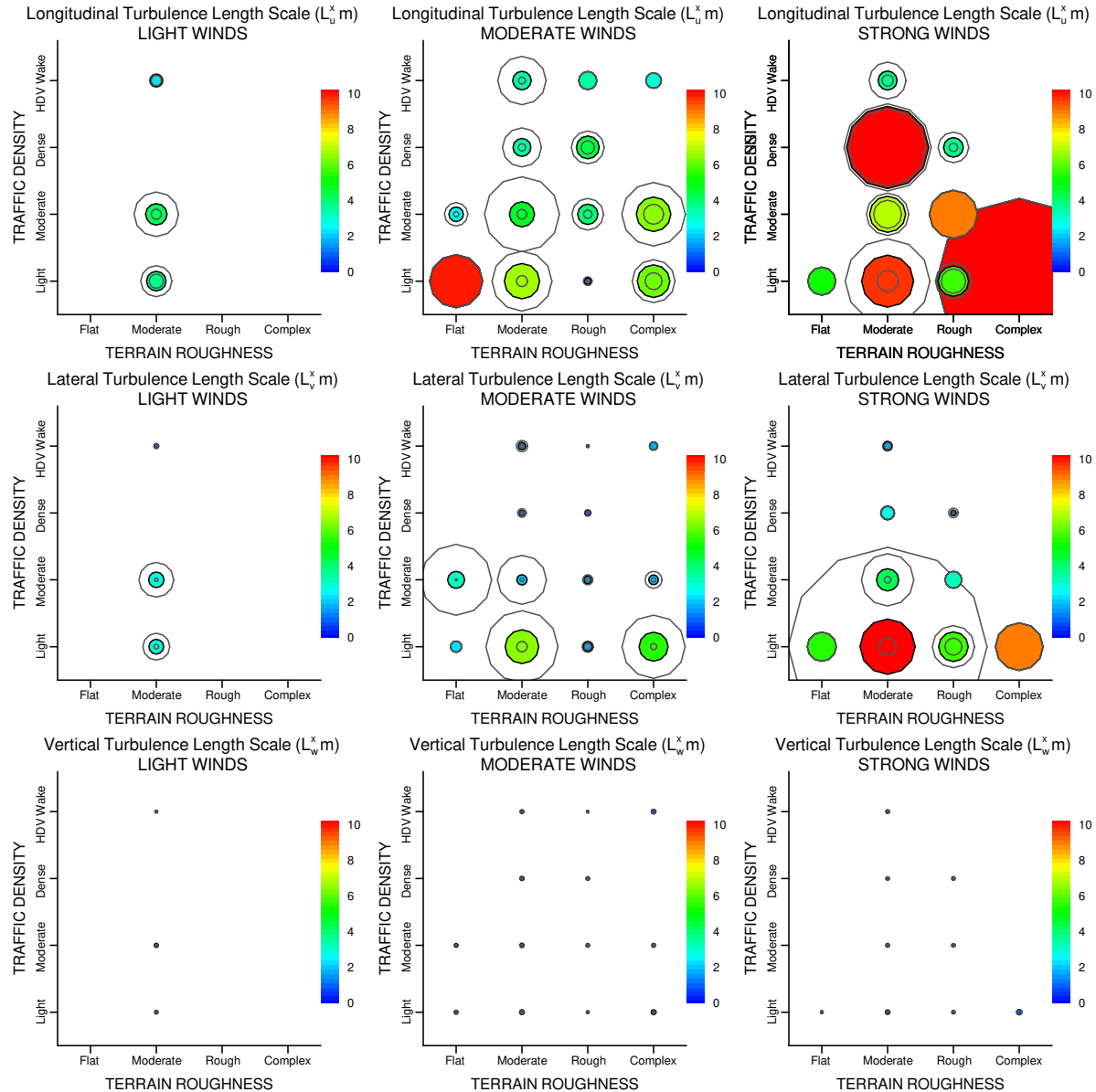


Figure 2.5: Turbulence length scale measurements from on-road measurement campaign at 1.5 m from the ground (circle size proportional to length scale and multiple circles for a condition show the minimum, mean, and maximum values from all data segments)

Terrain and Moderate traffic conditions, the longitudinal turbulence intensity increases from 3.7% in light winds, to 4.0% in moderate winds, to 4.9% in strong winds. For a stationary measurement of the turbulence at a given geographic location under neutral atmospheric conditions, the turbulence intensity based on the wind strength is typically constant (more so at higher wind speeds) which implies that the level of turbulence is proportional to the wind speed. For a vehicle travelling through this turbulence at a much higher speed than the terrestrial wind speed, the turbulence relative to the vehicle speed will show increased intensity with larger wind strength as reflected in the on-road observations.

There is no apparent trend in Figure 2.4 for the effect of terrain roughness on turbulence intensity, despite the fact that near-ground turbulence is generally expected to increase with the roughness of the local terrain. Such a trend may be masked by a stronger sensitivity to traffic density and wind strength and therefore is not apparent over the spread of the current data set. For example, under light traffic and moderate wind conditions, the longitudinal turbulence intensities for flat, moderate, rough, and complex terrain conditions are 3.5%, 3.1%, 3.5% and 2.5%, respectively, which show no particular trend.

Some of the same trends noted for the effects of terrain roughness, traffic density, and wind strength for the turbulence intensity measurements are also reflected in the turbulence length scale measurements of Figure 2.5. In particular, the vertical turbulence length scale (L_w^x) is distinctly smaller than the longitudinal and lateral components (L_u^x and L_v^x) as a result of the damping effect of the ground. However, unlike the turbulence intensities, there is a distinct difference between the longitudinal and lateral components, with the longitudinal length scales often much larger than the lateral length scales. For example, the Moderate Terrain, Moderate Traffic, Moderate Winds (M-M-M) measurements have average turbulence length scale of the longitudinal (L_u^x), lateral (L_v^x), and vertical (L_w^x) components of 4.7 m, 1.9 m and 0.6 m, respectively. The higher longitudinal component may result from the non-stationarity of some of the data segments when travelling through the non-homogeneous environment. Although the spectra were filtered to remove such effects, the selection of a single cut-off frequency for the analysis may not be appropriate for all conditions encountered.

In Figure 2.5, there is also a general trend of increasing length scales with increasing wind strength, although not all terrain and traffic combinations show this trend. Most distinct is an apparent trend for smaller length scales with greater traffic density. As an example, for Moderate Terrain and Moderate Winds, the lateral turbulence length scale (L_v^x) decreases from 10.3 m under light traffic density to 4.2 m under moderate traffic, to 2.5 m under dense traffic, to 1.6 m in the wakes of HDVs on the road. With higher traffic density, the small-scale turbulence structures from the wakes of other vehicles dominate the wind measurements. The highest length scale observed in Figure 2.5 is approximately 30 m for the longitudinal component in Complex Terrain with Light Traffic and Strong Winds. Complex, or hilly, terrain changes significantly with time as observed by a moving vehicle and therefore, particularly under strong wind conditions, will experience low-frequency/large-length-scale variations in the turbulence properties.

The measurements presented in Figures 2.4 and 2.5 are based on data measured at a location 1.5 m from the ground. Similar trends for terrain, traffic, and wind effects were observed in the measured turbulence intensities and length scales at the other heights of 0.5 m, 2.5 m and

Drag Reduction for HDVs - Progress Toward a Flow Treatment System - Year 2

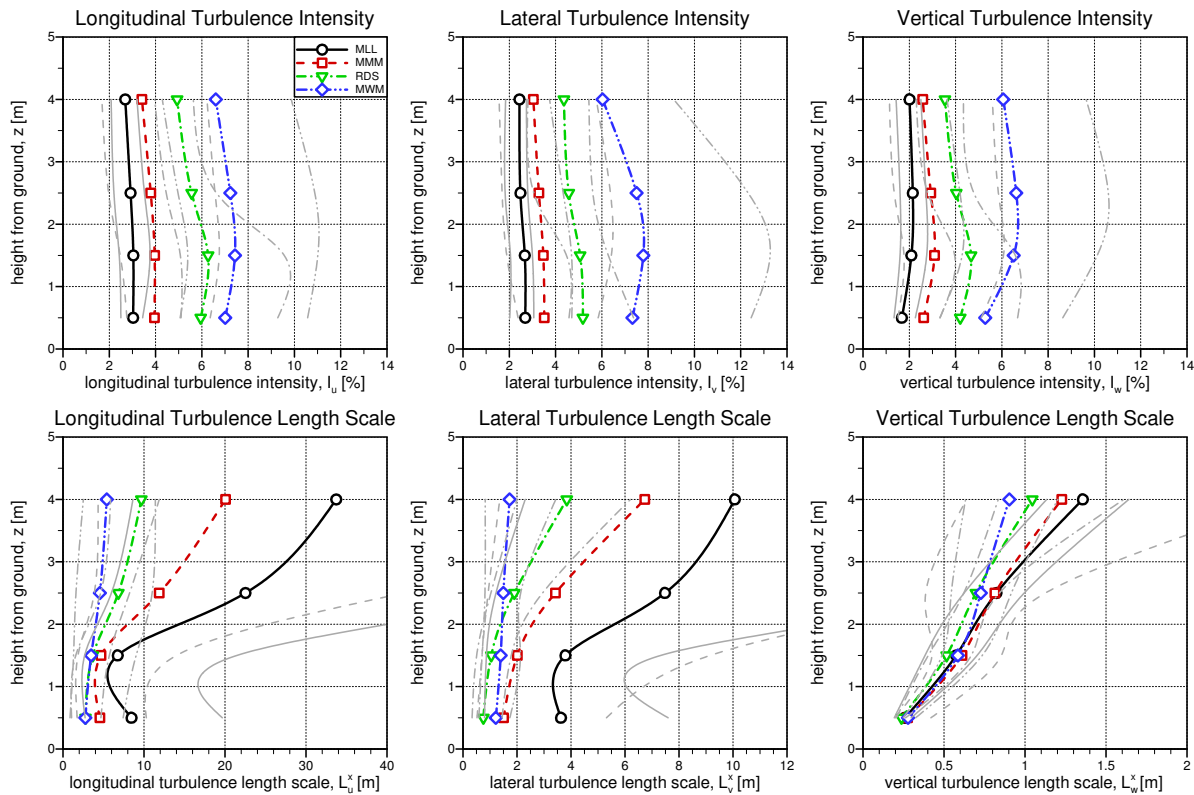


Figure 2.6: Variations in turbulence intensities and length scales with height for M-L-L, M-M-M, R-D-S and M-W-M conditions (grey lines represent measured min/max of respective conditions)

4.0 m, but there are vertical gradients associated with these characteristics. Figure 2.6 shows the change with height of the turbulence intensities and length scales for four conditions that reasonably represent the range of conditions observed.

Although only four conditions are shown in Figure 2.6, the trends inferred below are reflective of the larger data set. In general, the change in turbulence characteristics with height shows approximately the same trends for the different conditions, with higher overall intensity and smaller length scales when terrain toughness, traffic density, or wind strength is increased. In addition, the lower-turbulence cases in Figure 2.6 (represented by the M-L-L and M-M-M conditions) show slightly higher I_u and I_v components adjacent to the ground at 0.5 m, whereas the high turbulence conditions show a peak in turbulence intensity in the range 1 m to 2 m from the ground. Despite these subtle changes, the gradients in turbulence intensity with height are relatively small. The length scales, on the other hand, show much greater sensitivity to height. The cause for this sensitivity of the length scales to height is described in the next section.

2.4.2 Wind Spectra

Although the turbulence intensity and length scale are a basic quantitative measure of the turbulence characteristics of the winds experienced on the road, they are generalizations resulting from a typical wind spectrum. A wind spectrum, which identifies the distribution of turbulent energy across a range of frequencies, provides a detailed characterization of the turbulence and is an important consideration when attempting to simulate turbulent winds in a wind tunnel. For the current project the goal is to match, in a wind tunnel, a target set of wind spectra as measured on the road.

Figure 2.7 shows a set of the averaged wind spectra for some of the conditions experienced on the road. These measurements are from the probe at 1.5 m from the ground with each column showing the sensitivity of the wind spectra to one of the classification parameters. The Moderate Terrain, Moderate Traffic, Moderate Winds (M-M-M) condition is the baseline condition against which each of the classification parameters are varied in each plot. As with the turbulence intensity and length scale measurements presented earlier, the longitudinal, lateral and vertical components are shown in the upper, middle, and lower rows, respectively. The coloured lines in each plot represent the averaged spectra, with the minimum and maximum extent of the measurements shown as gray lines with the corresponding line style. The spectra are normalized in such a way that a higher the curve in relation to the ordinate (y-axis) has a higher the turbulence intensity level for the condition. Evident from Figure 2.7, as was noted earlier with respect to the turbulence intensity measurements, the wind spectra show the strongest sensitivity to traffic density for which the differences are distinct at the higher-frequency range of the spectra, resulting from the greater level of small-scale/high-frequency turbulent motions in the wakes of other vehicles. This is contrary to the wind-strength sensitivity that shows its differences primarily at the low-frequency end of the spectra. The terrain roughness plots show slight increase in the overall spectra with increasing roughness, but with a sensitivity much less than that for the traffic or winds.

In the middle plot (traffic-density sensitivity for lateral component of turbulence), the HDV wake spectra shows a peak at a reduced frequency of approximately 0.08-0.09 associated with the vortex shedding phenomena from the upwind vehicles. This reduced frequency, if normalized with a reference length scale of 2.6 m (typical width of an HDV) becomes approximately 0.2 which is similar to the vortex shedding frequency associated with circular cylinders. Vortex shedding from an HDV in this reduced frequency range was also noted in regards to wind tunnel measurements of an HDV model in a sister project under the eTV II program (McAuliffe, 2013c).

As noted in regards to the turbulence intensity and length scales, variations with height have been observed in the turbulence characteristics. These trends are also evident in the wind spectra, shown for a single case (M-M-M) in Figure 2.8. For the longitudinal and lateral components (u and v) there is no significant difference in the measured spectra at low frequencies. The differences are predominantly at the higher frequencies where a distinct trend towards decreased turbulence energy with height is observed. This is evident for all three components at the higher frequencies. The vertical component shows significant damping of the low-frequency turbulence at 0.5 m from the ground, compared to the higher locations. This is

Drag Reduction for HDVs - Progress Toward a Flow Treatment System - Year 2

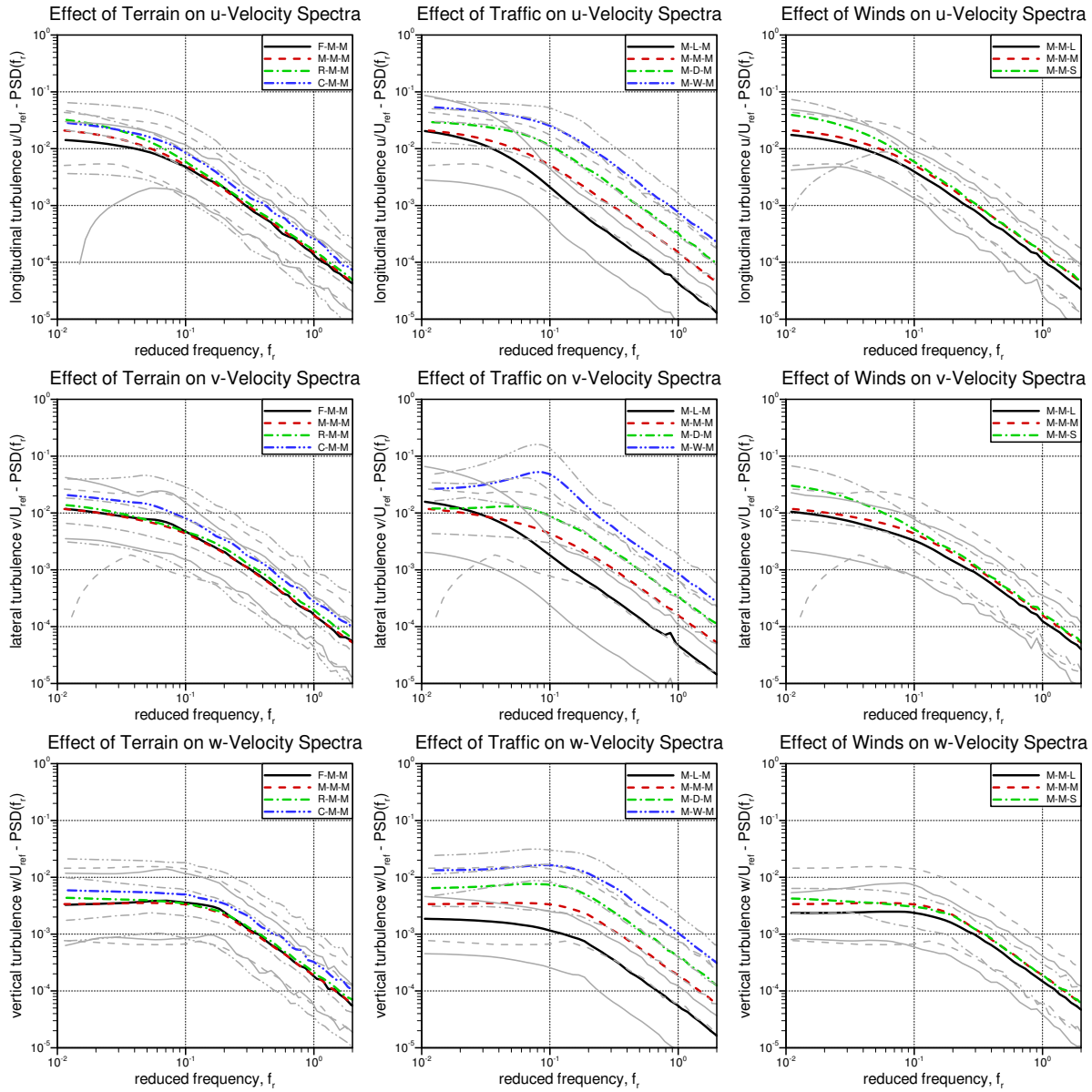


Figure 2.7: Wind spectra from on-road measurement campaign (1.5 m from the ground)

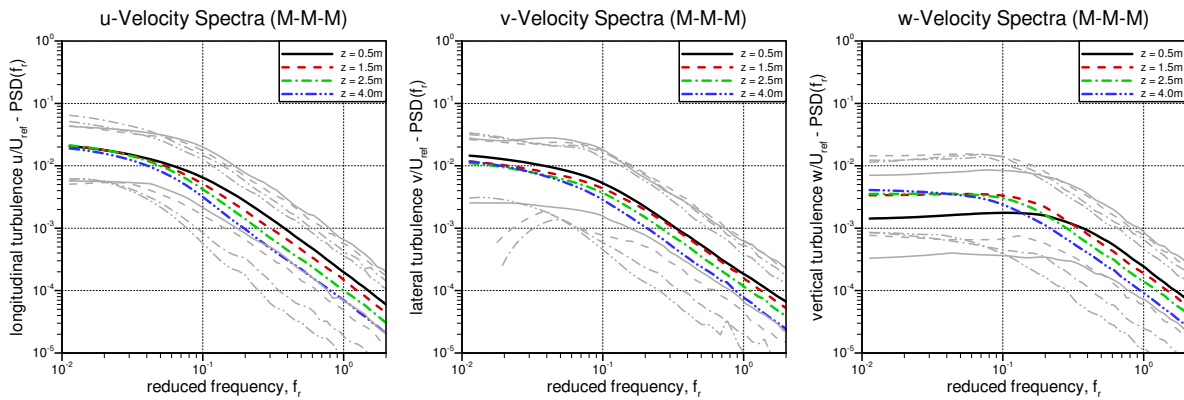


Figure 2.8: Variation of wind spectra with height from on-road measurement campaign (Moderate Terrain, Moderate Traffic, Moderate Winds))

a result of the presence of the ground which blocks the vertical motions associated with larger (low-frequency) fluctuations in the wind. Some of this damping at 0.5 m might be due to the influence of the test vehicle. Bearman and Morel (1983) showed that as the stagnation point of a bluff body is approached, the spectrum of turbulence is affected. They showed an amplification in the turbulence energy at high frequencies and a damping in the low frequency energy, resulting from the induced strain rate in the flow from the presence of the body. Bearman and Morel's measurements were performed much closer to the body, relative to the body size, than the distance of the 0.5 m probe from the front of the vehicle. For the current on-road measurements, the lack of damping at low-frequencies for the longitudinal and lateral components, relative to the higher locations, indicates that the damping of the vertical component is predominantly influenced by the presence of the ground and not the vehicle proximity.

The variation in wind spectra with height shown in Figure 2.8 also provides evidence to understand the strong variation with height of the turbulence length scales, identified previously in regards to Figure 2.6. The turbulence length scale is defined as a measure of the dominant energy containing eddies in the wind, and a visual metric for identifying relative differences in length scales is to identify where in a wind spectrum the distribution changes from a relatively flat energy content at low frequencies to the exponential decay at higher frequencies (linear decay on the logarithmic plots shown here). For the longitudinal turbulence component (u) in Figure 2.8, the leftward shift in this location with increasing height is inferred as an increase in the length scale of the turbulence. However, the size of the eddies in the wind don't actually change with height. What changes is the strength of the higher-frequency (smaller-scale) turbulence. Here, we have stronger fluctuations near the ground associated with the higher-frequency/smaller-scale eddies in the wind, but the lower-frequency/larger-scale fluctuations shows nearly the same energy content with height. Therefore, for the on-road measurements presented herein, the increase with height of the turbulence length scales should be inferred as a reduction of small-scale turbulence with height rather than an actual change in the scales of the turbulence. This leads to a warning that any near-ground measurement of length scales should be considered highly sensitive to distance from the ground and therefore have higher uncertainty when comparing one data set to another.

The variation in wind spectra with height shown in Figure 2.8 also provides evidence to understand the strong variation with height of the turbulence length scales, identified previously in regards to Figure 2.6. The turbulence length scale is defined as a measure of the dominant energy containing eddies in the wind, and a visual metric for identifying relative differences in length scales is to identify where in a wind spectrum the distribution changes from a relatively flat energy content at low frequencies to the exponential decay at higher frequencies (linear decay on the logarithmic plots shown here). For the longitudinal turbulence component (u) in Figure 2.8, the shift to lower frequencies in this location with increasing height is inferred as an increase in the length scale of the turbulence. However, the size of the eddies in the wind don't actually change with height. What changes is the strength of the higher-frequency (smaller-scale) turbulence. Here, we have stronger fluctuations near the ground associated with the higher-frequency/smaller-scale eddies in the wind, but the lower-frequency/larger-scale fluctuations shows nearly the same energy content with height. Therefore, for the on-road measurements presented herein, the increase with height of the turbulence length scales should be inferred as a reduction of small-scale turbulence with height rather than an actual change in the scales of the turbulence. This leads to a warning that any near-ground measurement of length scales should be considered highly sensitive to distance from the ground and therefore have higher uncertainty when comparing one data set to another.

The higher-energy/small-scale turbulence observed near the ground is a result of the roughness of the local terrain, and is influenced by the presence of other vehicles on the road whose wakes provide an increase in the level of small scale turbulence. Although not shown here, cases of low traffic density show smaller differences with height of the high-frequency energy content, providing further evidence to suggest that traffic density has a dominant influence on the turbulence characteristics experienced by vehicles on the road.

2.4.3 Spatial Correlations of Turbulence

The length scale measurements presented in the previous sections were calculated based on fitting a representative spectral distribution (the von Karman distribution) to the measured wind spectrum, for which the length scale is a parameter that defines the shape of the distribution. This method is also based on a "frozen turbulence" hypothesis that assumes the temporal fluctuations measured in the wind are a result of moving through this "frozen turbulence" field and hence there is a direct relationship between the measured frequencies of the turbulence to the spatial scales of the turbulence. In reality, the structure of the turbulence changes as it convects over a surface so this inference is not strictly true, however, the timescale over which the structural changes occur is generally lower than the wind speed and the "frozen turbulence" hypothesis is a reasonable approximation. Despite this, the length scales inferred from the wind spectra, and hence from the measured time series of wind fluctuations, only represents changes in the turbulence in the longitudinal direction as the vehicle moves through the wind.

The vertical and lateral sizes of the turbulence are also an important characteristics to identify and target for replicating the wind characteristics in a wind tunnel. Measurements of such characteristics were performed by acquiring data simultaneously from multiple spatially-separated probes. By looking at the similarity in these simultaneously-measured turbulence

signals, a measure of the lateral or vertical size of the turbulence structures can be inferred. This is done by performing a cross-correlation of the spatially-separated turbulence signals (defined earlier by equation 2.3). This procedure basically identifies what proportion of time the two signals appear identical, and when they are similar to what extent is the magnitude of the fluctuation level the same. The greater the correlation between two signals, the greater is the average size of turbulent structures relative to the spacing between the measurements.

To understand the physical meaning of the correlations to be presented, picture in your head two wind gusts that you might experience on a windy day. Picture one small gust similar to a jet of air issuing from a room fan or a large hair dryer. Picture the other gust as the kind that can blow you over on a windy day, associated with a wind front the size of a building. Now, imagine licking your index fingers and extending your arms to either side of you to feel the strength of the wind. For the small fan-driven gust, and depending on where you stand, you will likely only feel the wind on one finger. This dissimilarity between the wind experienced by both fingers implies the wind gust is small and not well correlated over the spacing of your fingers. If you then place your fingers in close proximity to each other, they will likely both feel a similar strength of the fan-driven wind gust and therefore the gust is correlated well for this finger spacing. Now picture the large building-sized gust. No matter how far apart you space your arms, you will feel similar wind strength at each finger due to the gust being much larger than your finger spacing. The similarity, or lack thereof, of the wind strength experienced by your two fingers can be used as a measure of the size of the wind gust, at least relative to the spacing between your fingers (much bigger or much smaller). If multiple sets of finger spacings are used, a refined measure of the size of the wind gust can be inferred. For the on-road measurements, by applying a cross-correlation calculation to the wind-fluctuation signals from two spatially-separated probes, the result, which is a value between 0 and 1, provides a relative measure of the size of the turbulence structures compared to the spacing between the probes. A small value close to 0 implies the turbulence scales are very small compared to the spacing, and a value near 1 implies the turbulence scales are very large compared to the spacing. With multiple probe spacings, and hence multiple correlation values, a distribution representing the typical spatial scales of the turbulence can be inferred.

Figures 2.9 and 2.10 show the vertical and horizontal correlation distributions, respectively, as measured for sets of similar conditions on the road. The layout of the subplots is the same as for the wind spectra, with the rows representing the different velocity components, and the columns representing different sensitivity studies to measured conditions. As with the wind spectrum measurements, the gray lines show the maximum and minimum extremes of the measurements.

The vertical correlation measurements in Figure 2.9 only show three correlation values, all of which are based on spacings between the 0.5 m probe height and the 1.5 m, 2.5 m and 4.0 m probe heights. Due to the spatially changing nature of the turbulence with height from proximity to the ground, a 1 m correlation inferred between the 0.5 m and 1.5 m probes is different than that between the 1.5 m and 2.5 m probes. Therefore, as a representation of the differences in various conditions, only the 0.5 m referenced correlation measurements are shown.

The majority of the correlation distributions, for different turbulence components and condi-

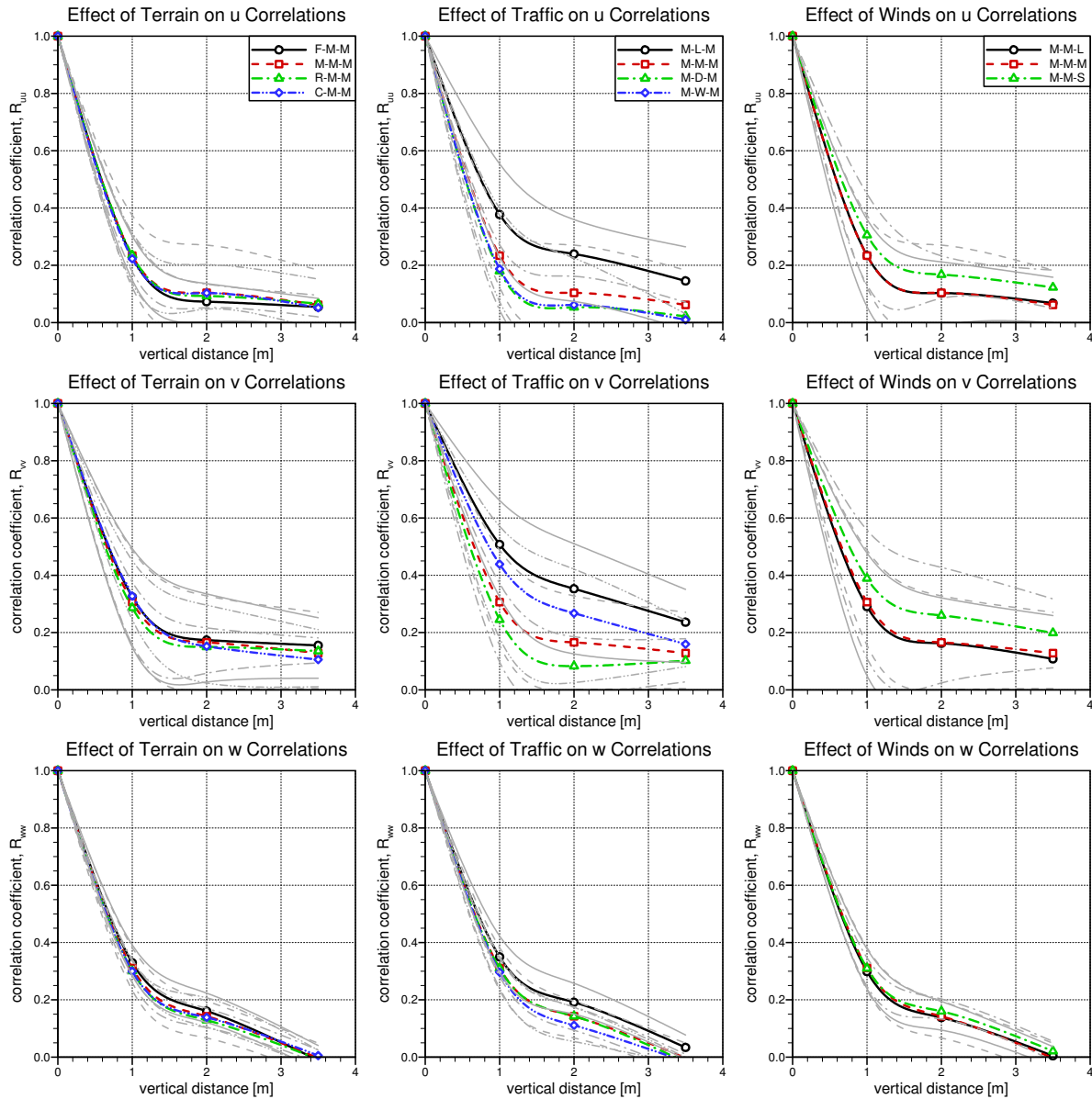


Figure 2.9: Vertical turbulence correlation distributions from on-road measurements, referenced to a location 0.5 m from the ground.

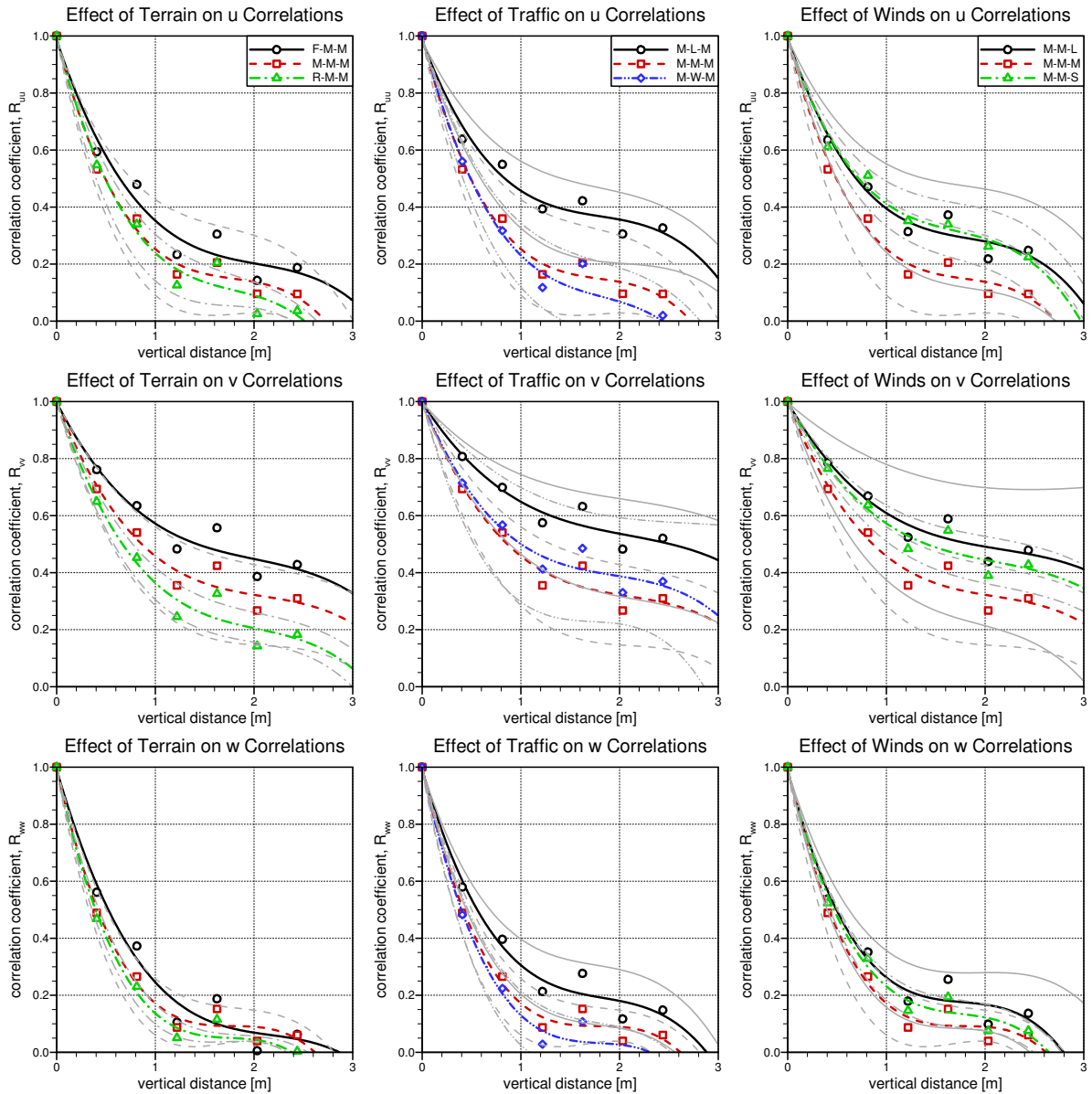


Figure 2.10: Horizontal turbulence correlation distributions from on-road measurements, measured at 1.5 m from the ground.

tions, shown in Figure 2.9 exhibit low correlation values above 1 m spacing. The correlation distributions show that the vertical scales of turbulence are predominantly sensitive to traffic density. The velocities are correlated to a greater extent when very little traffic is present. The smaller scales of turbulence generated in the wakes of other vehicles reduces the correlation values. Of interest is the lateral-velocity (v) correlation for conditions in the wake of HDVs. Unlike the longitudinal and vertical components, the lateral component is higher in this condition than for moderate or dense traffic conditions. This is caused by the distinct vortex shedding behind HDVs which provide a strong large-scale correlation from the strong side-to-side motion of the entire vehicle wake.

The horizontal correlation measurements, performed at 1.5 m from the ground, are shown in Figure 2.10. For this configuration the probes were spaced in closer proximity than for the vertical correlation measurements, and due to the lateral uniformity expected in the wind at a given height, all six correlation distances can be used from the rake arrangement of four probes.

In general, the horizontal distributions in Figure 2.10 show greater correlation than the vertical distributions, primarily due to the greater lateral uniformity of the winds. A general trend observed from the horizontal correlation measurements is that the length scales (inferred by the correlation magnitudes for a given spacing) are reduced when a mechanism for greater mechanical turbulence generation is introduced, whether through increased surface roughness, increased traffic density, or increased wind strength. The trends in the spatial correlation data also reflect the trends observed from the turbulence length-scale measurements presented earlier, providing further confidence that the single-value length-scale calculations provide a reasonable inference of the length scales encountered on the road.

2.4.4 Comparison to Previous Work

The most comprehensive road-turbulence data set published to date is that from Wordley and Saunders (2009). The current study confirms many of their findings, but with a test program that has been approached in a different manner. Wordley and Saunders targeted specific conditions and measured only under those conditions for short periods of time (20 to 40 seconds). In the current study, measurements were performed for long periods of time (up to 15 minute per measurement runs) which were subsequently segmented based (between 30 second to 10 minute segments) on a classification system selected to cover variations in terrain roughness, traffic density and wind strength. This current approach captures not only the characteristics under different conditions, but the relative proportion of time each is encountered, at least for the geographical region over which the measurements were performed. As such, the dominant conditions encountered over the course of the test campaign (Moderate Terrain, Moderate Traffic, Moderate Winds) will be used as a suitable target.

As with the current study, Wordley and Saunders provided measurements, for each of the three velocity components, of turbulence intensities, turbulence lengths scales, wind spectra, and spatial correlations. In general, the measurements provided herein compare well to those of Wordley and Saunders. The major differences result primarily from some different types of conditions experienced. Wordley and Saunders have a large data set associated with smooth

terrain for which there is very little vegetation and obstacles on the ground. Only a few locations east of Ottawa provided such conditions. However, those conditions were typically large stretches of farmland interspersed between forested areas. Under the smooth terrain conditions, Wordley and Saunders' data show smaller turbulence intensities and larger length scales than those observed in the current study for Flat Terrain conditions. They also noted greater levels of correlation at 1 m vertical and horizontal spacing for the smooth terrain measurements than has been observed in the current data set. Conversely, Wordley and Saunders did not provide measurements in complex terrain environments, nor did they provide measurements based on the lower 80 km/h road speeds also evaluated in the current study.

Wordley and Saunders provide a recommendation for turbulence conditions to target in the development of turbulence for wind tunnel simulation purposes. Their recommendation is based on what they believe is feasible in a wind tunnel while maintaining some of the important wind-spectra characteristics, consisting of matching the high-frequency/small-scale range while limiting the low-frequency/large-scale range under an assumption of quasi-static aerodynamic response of road vehicles at low frequencies. Wordley and Saunders' target is 3% intensity for the longitudinal and lateral components with associated 1 m length scales, and 2% intensity for the vertical component with an associated 0.5 m length scale. As shown in Figures 2.4 and 2.5, most of the conditions experienced in the test campaign have turbulence intensities and length scales exceeding these targets. In addition, the sensitivity of length scale to height as a result of the change in the shape of the wind spectra implies that the spectra themselves are more appropriate for direct comparison of wind tunnel conditions to road conditions.

2.4.5 Preliminary Target for FTS

Due to its predominance in the number of data segments it represents, and the high volume of heavy-vehicle traffic in the geographic region in which the measurements were performed, the Moderate Terrain, Moderate Traffic, Moderate Winds (M-M-M) condition has been chosen as the target against which the Flow Treatment System (FTS) will be designed. It represents approximately 20% of the specific conditions experienced on the road, and for each of the classification categories, represents the dominant condition (see Table 2.3). The wind spectra and correlation distributions for this condition, as shown in Figure 2.7, were used as the target for the small-scale development and intermediate-scale demonstration of the FTS, described in subsequent sections. Table 2.4 identifies the target turbulence intensities and length scales for this condition. As noted in the previous section, these are higher than the levels recommended by Wordley and Saunders due to the different environments encountered during the test program.

2.4.6 Summary

To measure the winds experienced on the road, a sport utility vehicle (SUV) was outfitted with an array of four fast-response pressure probes that could be arranged in vertical or horizontal rake configurations that provided measurements up to 4.0 m from the ground and span-

Table 2.4: Target turbulence intensities and length scales for FTS development representing the Moderate Terrain, Moderate Traffic, Moderate Winds (M-M-M) condition, at 1.5 m from ground

Component	Turbulence Intensity, I	Turbulence Length Scale, L^x
u	4.0 %	4.7 m
v	3.5 %	1.9 m
w	3.1 %	0.6 m

ning a width of 2.4 m. On-road measurements of the turbulence intensities, turbulence length scales, wind spectra, and spatial correlations were performed. Eight days of testing over a two month period in late 2012 were conducted over roads in Eastern Ontario and Western Quebec, Canada. Dates and test routes were selected to provide a variety of conditions. The time-series of on-road turbulence data were segmented and classified based on differences in the terrain roughness, traffic density, and wind strength experienced during the measurements, as inferred by topographical maps, on-board video, and weather-station data.

Typical wind spectra were developed based on an average of all spectra measured for each condition, from which the turbulence intensities (I_u, I_v, I_w) and turbulence length scales (L_u^x, L_v^x, L_w^x) were evaluated. The important conclusions regarding the on-road turbulence environment experienced by HDVs are:

- The wind spectra show changes with height predominantly at the high-frequency/small-scale end of the spectra, with greater high-frequency turbulence energy near the ground resulting in smaller turbulence length scales near the ground. Only the vertical w spectra showed significant change in the low-frequency/large-scale energy over the height of the measurements, due to the damping of the large-scale/low-frequency vertical motions of the wind near the ground.
- The vertical turbulence intensities (I_w) and length scales (L_w^x) are distinctly lower than their respective longitudinal (u) and lateral (v) components, resulting again from the damping of the large-scale/low-frequency vertical motions of the wind near the ground.
- In general, the turbulence length scales increase with height and show much greater variation with height than the turbulence intensities. This results from a larger magnitude of high-frequency/small-scale turbulence near the ground that does not contribute significantly to the turbulence intensity but causes a shift to smaller scales of the calculate length scales. Vertical profiles of turbulence intensity show slightly higher values below 2 m. The sensitivity with height of the length scales implies that a direct comparison between different data sets may not yield the same magnitudes of length scales, however trends with different conditions will likely not be influenced in a significant manner.
- All three components of turbulence intensity (I_u, I_v, I_w) show similar trends with terrain roughness, traffic density and wind strength. Some similarity in trends of the length scales (L_u^x, L_v^x, L_w^x) is apparent but not to the same magnitude as the turbulence intensities.

- Traffic density has the greatest influence on the turbulence environment experienced by vehicles on the road. In general, turbulence intensity increase and turbulence length scales decrease with increasing traffic density. These effects arise due to the increased levels of small-scale turbulence generated in the wake of other road vehicles. The location of maximum turbulence intensity moves upward with increasing traffic density, particularly in the wake of HDVs.
- The strength of the terrestrial winds also has a distinct influence on the turbulence experienced by vehicles on the road, whereby stronger winds amplify the large-scale/low-frequency turbulence leading to higher turbulence intensities and larger length scales.
- Terrain roughness did not show a significant influence on the turbulence experienced by vehicles on the road. Any differences were small in comparison to changes associated with traffic density and wind strength.

Based on the prevalence of the moderate classification for terrain roughness, traffic density, and wind strength, the M-M-M condition has been selected as a target condition for development of the FTS, for which the target turbulence characteristics were listed in Table 2.4.

3. Concept Design for Flow Treatment System

3.1 Problem Description

Generating turbulence in a wind tunnel to represent terrestrial winds is not a new concept. The field of wind engineering has been making use of such simulations for decades to design large structures such as buildings and bridges to withstand adequately the mean and dynamic wind forces acting on such structures. As noted in the report for the first year of the project (McAuliffe *et al.*, 2013a), typical wind-engineering turbulence-generating devices provide too high a turbulence intensity in the test section to be used for tests on full-scale or large-scale models. Obstacles in the upstream settling chamber are a good candidate technique instead of grids or spires for obtaining lower turbulence intensity levels typical of what are experienced on the road.

This component of the project has been performed to identify turbulence-generation techniques that may provide the turbulence characteristics encountered by vehicles on the road. Four types of passive turbulence-generating technique have been examined in the study:

- A vertical-bar turbulence grid at the inlet of the test section;
- A screen at the inlet of the test section;
- A set of moving spires designed to vibrate under the actions of the wind, tuned to amplify low-frequency turbulence;
- Wooden obstacles mounted in the settling chamber.

Preliminary results were presented in the report for the first year of the project (McAuliffe *et al.*, 2013a), in which it was identified that the moving spire concept provides an increase in turbulence over the full-range of turbulent frequencies, rather than just the low-frequencies intended to be amplified. Therefore, no additional consideration was given to the moving spire concept.

In the following, a description of additional measurements and analysis will be provided in brief, with a detailed analysis of the turbulence measurements for the various concepts evaluated.

3.2 Measurements and Analysis Procedures

Detailed descriptions of the NRC 1.0 m \times 0.8 m Pilot Wind Tunnel, its new test section, the test setup, and the test configurations were provided in the report for the first year of the project (McAuliffe *et al.*, 2013a). The basic test configuration for this study, consisting of three Cobra probes mounted to the 3-axis traverse system of the wind tunnel, is shown in Figure 3.1. Some additional measurements were performed this year, based on an analysis of the preliminary results presented in that report. A new settling-chamber spire concept has been evaluated, and additional Cobra probe measurements have been performed to evaluate the spatial correlations of turbulence in the wind tunnel.

To provide a concise list of all the test configurations evaluated, Tables 3.1 and 3.2 from the first-year progress report (McAuliffe *et al.*, 2013a) have been reproduced as Tables 3.1 and 3.2 here with the information for the configuration C7 added.

The basic measurement procedure was to perform a lateral-and-vertical flow survey to evaluate the turbulence properties over a plane near the front edge of the turntable. This location is also representative of the region of flow that will influence the leading edge of the 5% scale HDV model that will be discussed in Section 4. The measurement procedure was used for new C7 spire configuration, and was performed at different longitudinal locations in the test section for the selected FTS configuration (selected concept discussed later) to identify the decay rate in the turbulence with downstream distance. In addition to these flow surveys, vertical and horizontal spatial correlation measurements were performed at two longitudinal locations for the selected FTS concept to provide a measure of the change with downstream distance as well as to compare to the on-road turbulence measurements.



Figure 3.1: Cobra probe holders mounted to positioning arm of 3-axis traverse system

Table 3.1: Spire shapes for settling chamber (REDACTED, quantities replaced with relative qualifiers)

Name	Height [m]	Base Width [m]	Top Width [m]
C1	tall	medium	medium
C2	tall	wide	wide
C3	tall	narrow	narrow
C7	tall	narrower	narrower
C4	short	medium	medium
C5	short	wide	wide
C6	short	narrow	narrow

The Cobra probe data were processed in the same manner as for the on-road measurements, with the following parameters calculated:

- Reference speed defined by calibration of the wind-tunnel contraction for non-turbulent conditions (U_{ref}),
- Mean velocities (U, u, v, w), flow angles (ϕ, ψ) and static pressure (P),
- Mean velocity ratios ($U/U_{ref}, u/U_{ref}, v/U_{ref}, w/U_{ref}$),
- RMS velocities ($U_{rms}, u_{rms}, v_{rms}, w_{rms}$), flow angles (ϕ_{rms}, ψ_{rms}) and static pressure (P_{rms}),
- Turbulence intensities ($U_{rms}/U_{ref}, u_{rms}/U_{ref}, v_{rms}/U_{ref}, w_{rms}/U_{ref}$),
- Turbulence length scales (L_u^x, L_v^x, L_w^x),
- The wind spectrum, defined by the power-spectral-density (PSD) distributions, of each wind component.

To compare adequately the wind tunnel measurements to the full-scale on-road measurements, the wind speeds, length scales, frequencies, and PSDs must be scaled appropriately. This is done through the reference wind speed (U_{ref}) and a reference length scale (L_{ref}). The FTS configuration being developed here is intended to be scaled by a factor of 10 for the NRC 9 m Wind Tunnel, for which the model will be 30% of full scale. This provides an appropriate scaling factor for the current tests of 3% of full scale. Therefore, to represent full-scale on-road conditions for which the reference length was defined as 1 m, the reference length for the NRC 1.0 m \times 0.8 m Pilot Wind Tunnel measurements is 0.03 m. This length is used to normalize any length measurements (length scales or correlation distances). The reference wind speed (U_{ref}) and length (L_{ref}) are used in Equations 2.1 and 2.2 to provide data that can be compared directly to the on-road measurements.

Table 3.2: Small-scale FTS concepts tested (REDACTED)

Config. Name	Obstacle Location†	Obstacle Shape‡	Number of Obstacles	Obstacle Spacing [m]	Run Number	Description
FRM	none	-	-	-	197	settling-chamber frame only
C1	SC	C1	-	-	205	baseline configuration
C2	SC	C2	-	-	207	baseline configuration
C3	SC	C3	-	-	209	baseline configuration
C3Q	SC	C3	-	-	211	25% increase in spacing from baseline
C3H	SC	C3	-	-	213	50% increase in spacing from baseline
C3W	SC	C3	-	-	240	25% increase in spacing from baseline, wedge-shape
C3S7	SC	C3	-	-	245	25% increase in spacing from baseline, longitudinal stagger, spire at centre
C3S8	SC	C3	-	-	247	25% increase in spacing from baseline, longitudinal stagger, gap at centre
C4	SC	C4	-	-	199	baseline configuration
C5	SC	C5	-	-	194	baseline configuration
C6	SC	C6	-	-	201	baseline configuration
C6Q	SC	C6	-	-	215,387§	25% increase in spacing from baseline, spire at centre
C6H7	SC	C6	-	-	219	50% increase in spacing from baseline, spire at centre
C6H8	SC	C6	-	-	222	50% increase in spacing from baseline, gap at centre
C6VB	SC+TSI	C6+VB	-	-	225	C6H8 setup with vertical bar grid
C7H	SC	C7	-	-	381§	50% increase in spacing from baseline, spire at centre
C7F	SC	C7	-	-	385§	100% increase in spacing from baseline, spire at centre
VB	TSI	VB	-	-	228	baseline configuration
VBS	TSI	VB	-	-	232	baseline configuration with plastic screen
SCR	TSI	SCR	-	-	238	stainless steel screen

† SC - settling chamber, TSI - test section inlet

‡ Non-spire acronyms: VB - vertical bar grid, SCR - screen

§ - New test data for test number 2036, all others for test number 2034

3.3 Analysis of Small-Scale FTS Measurements

3.3.1 Flow Uniformity

An example of the flow survey measurements acquired for the C6Q configuration is shown in Figure 3.2. The upper row shows the distributions of the mean longitudinal wind speed magnitude on the left, the mean lateral wind angle in the middle, and the vertical wind angle on the right, all normalized by the reference wind speed. The bounding box for each plot represents the walls of the wind tunnel, and therefore gives a visual representation of the region of the tunnel surveyed. The middle row shows, from left to right, the distributions of longitudinal, lateral, and vertical turbulence intensities. The equivalent turbulence length scale distributions are shown in the bottom row.

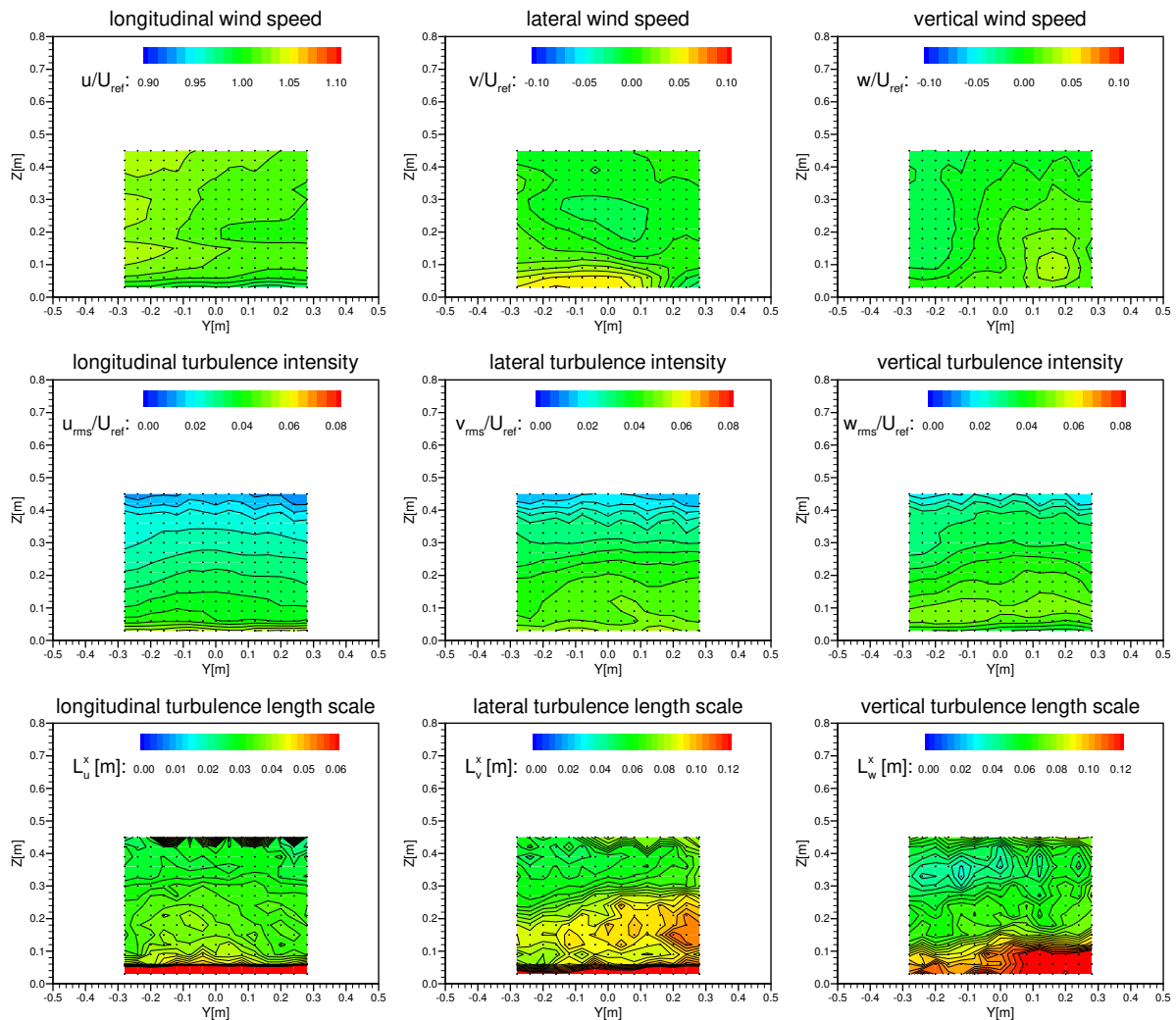


Figure 3.2: Flow-field survey for C6Q spire configuration

Vertical gradients in the turbulence characteristics, as observed in Figure 3.2, were anticipated due to the shape of the upwind spires (wide at the base, narrow at the top), and vertical variations were also observed in the on-road measurements presented in Section 2. Some lateral variations of the parameters are evident in Figure 3.2, however they are generally of smaller magnitude than the vertical gradients for the various configurations evaluated. For the comparison between different turbulence configurations, it has been assumed that the lateral variations are negligible and a single vertical distribution of the parameters can be used for comparative purposes. In subsequent figures of this section, the vertical distributions of the flow characteristics are shown by a thick line with symbols, representing lateral averages at each height. To identify the magnitude of any lateral variations, thinner lines of the same colour are shown and represent the lateral maxima and minima values. These maxima and minima provide a measure of the lateral uniformity of the mean flow characteristics.

Of note in Figure 3.2 is the appearance of wiggles in the turbulence intensity distributions near the top of the measurement window, above $z=0.35$ m. These wiggles represent the wakes of the settling chamber spires that have not fully mixed laterally near the top. This is a common observance in spire-generated turbulent flows and is not a concern as long as the model to be tested is contained well within the region of laterally-uniform turbulence, as would be the case here for a 3% HDV model that would have a height of 0.12 m. The 10% scale HDV model used for the blockage correction study of Section 7 sits 0.4 m high and is for the most part contained within the region of laterally-mixed turbulent flow for this particular configuration.

One of the concerns with using spires to generate turbulence for ground vehicles is the possibility of having a change with height of the mean wind speed. For stationary objects in the atmospheric boundary layer, a vertical gradient in the mean wind speed is commonly experienced and spires can be designed to provide the appropriate changes with height. For ground vehicles that may be travelling through the terrestrial winds, such gradients may be present but with differing behaviour depending on the direction of motion of the vehicle. For example, a head wind will provide a vertical gradient, relative to the vehicles, of increasing wind speed with height. Conversely, a tail wind will provide a condition, relative to the vehicle, where the wind speed is highest at the ground. In addition, side winds that change magnitude with height will also introduce a twist to the wind profile (change in lateral wind angle with height) as observed by a ground vehicle. To avoid complicating the issue regarding the effects of turbulence, a negligible vertical gradient and twist in wind vector is desired from the FTS.

Although spires generally provide the undesirable wind speed gradients in the vertical direction, when they are placed in the settling chamber the acceleration of the air through the wind-tunnel contraction counteracts this effect and reduces the vertical gradients of the mean wind speed in the test section. Figure 3.3 shows the vertical profiles of mean longitudinal wind speed (left plot) along with the mean lateral wind angle (middle plot) and the mean vertical wind angle (right plot). In the mean wind speed profiles of Figure 3.3, the first measurement location off the floor is submersed in the ground-plane boundary layer and shows a lower wind speed due to the frictional effects of the wall. This effect will be mitigated in the NRC 9 m Wind Tunnel by use of distributed suction (part of the GESS system) ahead of the turntable that removes this low-speed boundary layer. Neglecting this lowest point, the profiles show variations with height no greater than 2% of the reference wind speed. Some of this varia-

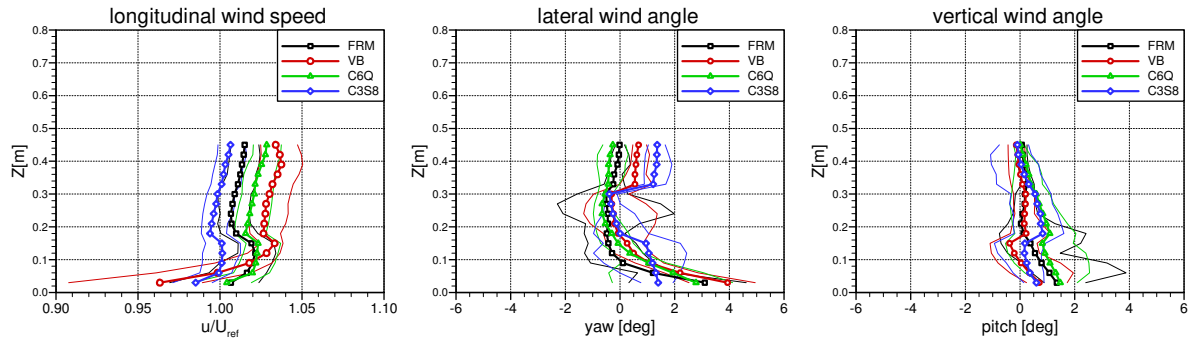


Figure 3.3: Influence of FTS concepts on the mean flow in the test section

tion is due to the influence effect of the vertical traverse rig on the flow at the measurement probe locations (see setup in Figure 3.1). This influence is the cause for the kink in the profiles between the 5th and 6th points from the ground which represents the interface between regions measured by the two lowest probes. The lateral wind angle, shown in the middle plot of Figure 3.3 shows a variation with height no greater than 2° for most of the profile with the exception of the points adjacent the ground. The higher positive wind angles near the ground are due to slight non-uniformities in the flow generated in the upstream settling chamber. The right plot of Figure 3.3 shows slightly higher vertical wind angles near the ground. This is a result of the growth of the ground-plane boundary layer that pushes the main flow upwards. This effect will also be mitigated in the NRC 9 m Wind Tunnel by the use of the GESS suction system. The variations in lateral and vertical wind angles are small and are not expected to provide any significant effects on the HDV model studies described in Section 4 and 7.

To select and optimize an appropriate concept for the FTS, it is important to evaluate the sensitivity of the turbulence characteristics to concept geometries and concept types. In the following, comparisons of similar configurations or types of configurations will be performed to identify appropriate design criteria for the FTS. As discussed with regards to the on-road turbulence measurements in Section 2, the turbulence intensities and length scales are quantities that provide a basic description of the wind spectra. Namely, the turbulence intensity represents the total turbulence energy content in the wind, and the turbulence length scale represents size of the dominant energy containing eddies in the wind and identified visually as the approximate frequency/wavelength at which the energy spectrum changes from a flat energy content to exponential decay (linear decay on the logarithmic plots here). In addition to the vertical changes in turbulence intensities and length scales, comparison of the wind spectra for the different FTS concepts are considered in the following which provide additional information to select a suitable concept for scaling to the NRC 9 m Wind Tunnel. For the comparisons, each spectrum presented will consist of a lateral average of all the spectra measured at a given height of 0.06 m from the floor. This same measurement location will be used for comparison to the on-road measurements in a subsequent section, as it represents a 2 m full-scale location from the ground relative to a 3% model.

3.3.2 Influence of Settling-Chamber-Mounted Spire Shape

The influence of spire shape and size on the vertical profiles of turbulence intensities and length scales can be inferred by the data shown Figure 3.4, and their influence on the turbulence spectra in Figure 3.5. Here, the measurements for the seven spire shapes are compared and the general observations regarding the effect of shape and size are given as follows:

- An increase in base width amplifies the turbulence energy near the ground over the full range of frequencies. This results in higher turbulence intensity with increasing base width. The change in the shape of the wind spectra in Figure 3.5 shows increased u and v length scales with base width.
- The vertical gradients of the turbulence characteristics are dependent on the rate of taper of the spire. Spires with higher effective peaks show lower vertical gradients.
- The v and w turbulence intensities are greater than the u turbulence intensity in the test section due to the effect of the strain rate on the flow structures as they accelerate through the contraction.
- The w turbulence intensity is damped near the ground due to the influence of the ground on the vertical wind fluctuation. This was also seen in the on-road measurements. In this wind-tunnel, the low frequencies are damped more so than the higher frequencies which leads to an effective decrease in w turbulence length scale with increasing base width.
- Large u and v turbulence length scales are observed close to the ground that are associated with the boundary-layer flow that develops on the walls of the wind tunnel contraction and test section.
- The largest-width spires show a peak in turbulence energy, predominantly observed for the v component, in the 0.08 to 0.3 reduced frequency range.

3.3.3 Influence of Test-Section-Mounted Turbulence Configurations

Several test-section-mounted concepts, similar to what has often been used in the NRC wind tunnels for generating turbulence appropriate for wind engineering studies, have been evaluated. The vertical profiles of turbulence intensity and length scale for these configurations are presented in Figure 3.6, with the associated wind spectra in Figure 3.7. Here, the measurements for the four configurations are compared and the general observations are given as follows:

- The fine-meshed screen (SCR) shows only a small influence on the vertical profiles and on the spectra relative to the smooth-flow conditions (smooth flow results not shown here). The turbulence intensity is below 1% and the length scales are likely influenced more by the background turbulence in the wind tunnel than the screen itself. The non-uniform variation with height for the SCR case is due to the presence of the upwind frame for mounting spires in the settling chamber.
- The vertical bar grid (VB) shows very little variation with height of the turbulence char-

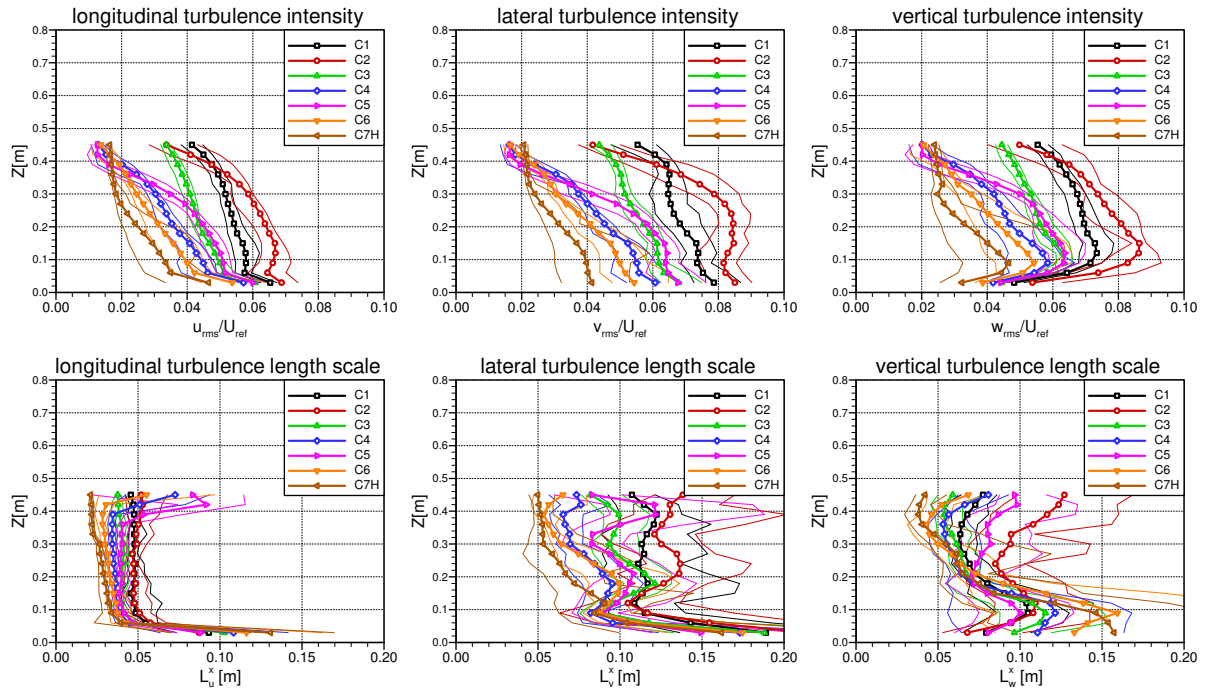


Figure 3.4: Influence of settling-chamber-spire shape on the vertical turbulence profiles

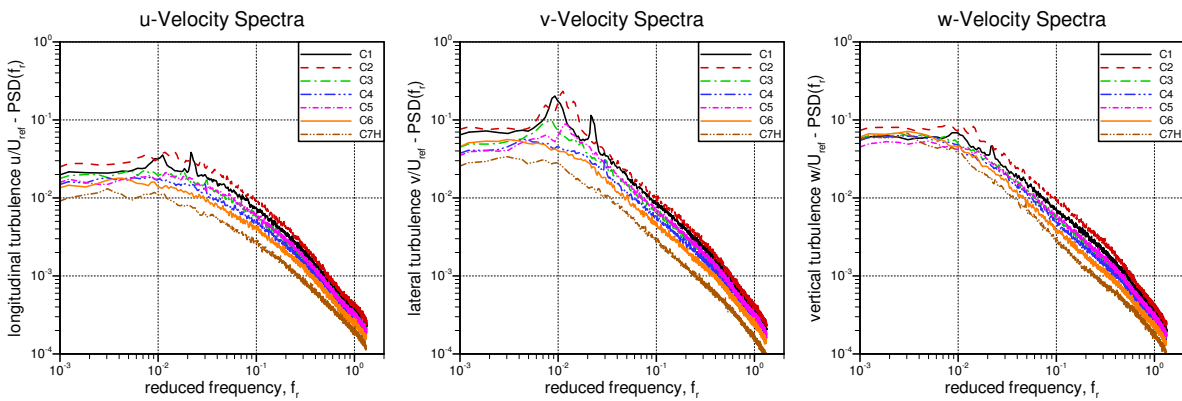


Figure 3.5: Influence of settling-chamber-spire shape on the wind spectra at $z = 0.06$ m

Drag Reduction for HDVs - Progress Toward a Flow Treatment System - Year 2

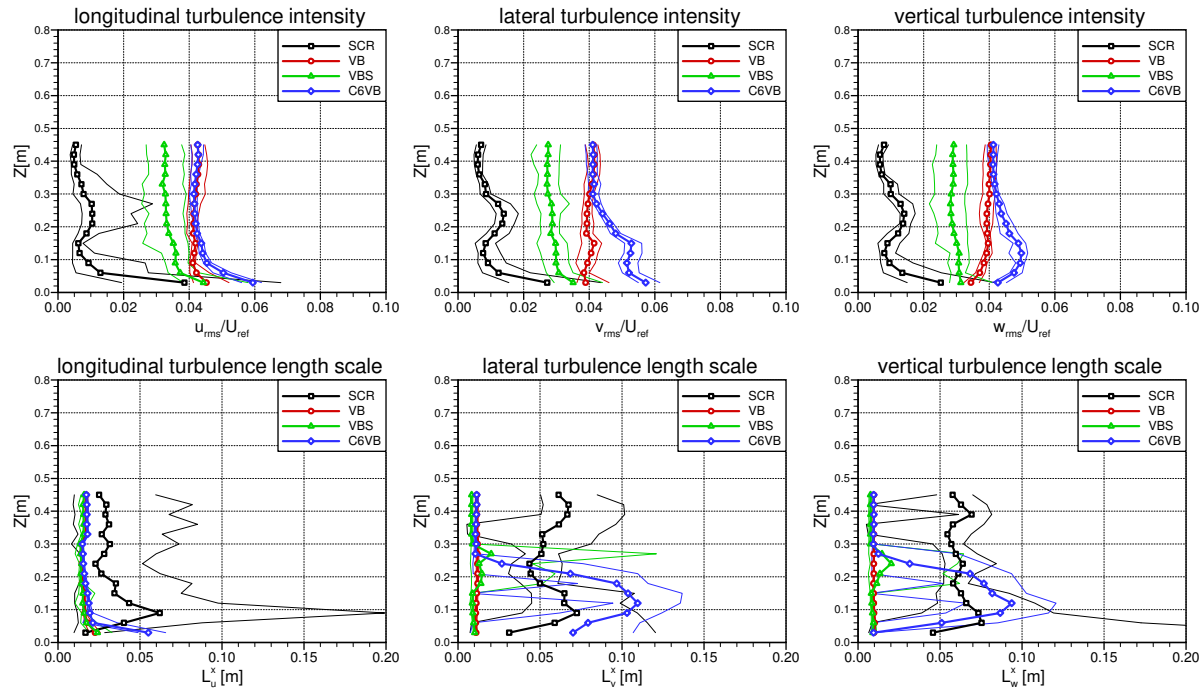


Figure 3.6: Influence of test-section-mounted configurations on the vertical turbulence profiles

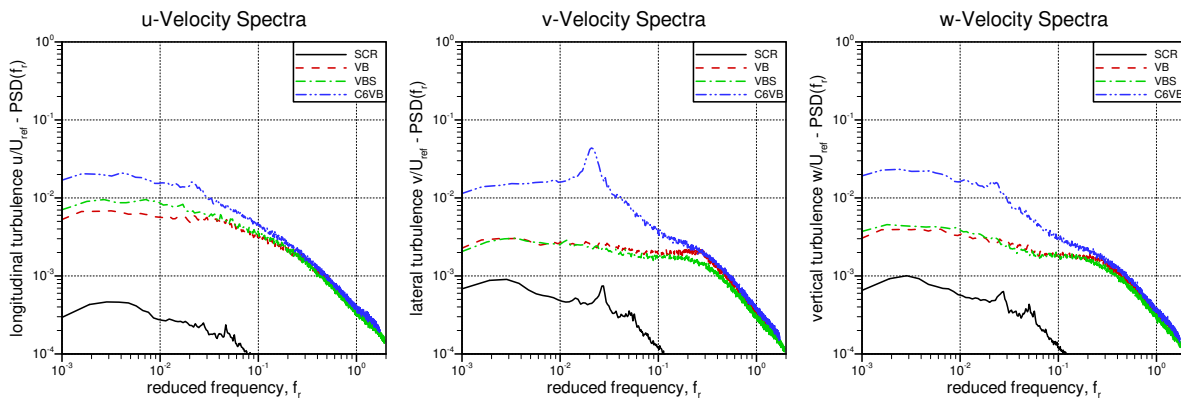


Figure 3.7: Influence of test-section-mounted configurations on the wind spectra at $z = 0.06$ m

acteristics, as is generally the case for such grids.

- Adding a screen to the vertical bar grid configuration decreases the turbulence intensities but has very little effect on the turbulence length scales. The decrease in turbulence intensity is predominantly associated with a decrease in the turbulence energy at high frequencies.
- The high-frequency turbulence generated by the vertical bars shifts the turbulence length scale to smaller values compared to the screen and background turbulence conditions.
- The addition of spires in the settling chamber with the vertical bar grid influences mainly the lower region of the flow, below 0.3 m, where increases in turbulence intensities and length scales are observed. The increased turbulence energy is produced in the low-frequencies range.

One of the drawbacks to test-section mounted turbulence generating devices is that they operate in a high wind speed environment and there must be built to withstand greater wind loads and will also generate greater pressure losses in the wind tunnel circuit potentially decreasing the maximum attainable wind speed. In the current study, the vertical bar configuration produced a strong whistling noise at high speeds that limited the maximum test speed.

3.3.4 Influence of Changes in Large Spire Configuration

For a given spire shape in the settling chamber, additional permutations in the setup were done to evaluate effects of spacing and spire planform shape. Figures 3.8 and 3.9 compare the vertical turbulence profiles and the wind spectra, respectively, for the various permutations of the C3 spire geometry. The general observations are given as follows:

- Increasing the spacing of the spires increases the turbulence intensities and length scales. The spectra show that increasing the spacing influences the low-frequency turbulence energy (lower energy with increased spacing), however an increase is observed at the high-frequencies.
- Using the wedge-shaped spire profile (V shape from above with tip point into the wind), with the same projected frontal shape as the flat spire, the turbulence intensities and length scales were reduced. In addition, vertical gradients in the v and w length scales were reduced.
- Staggering the spires longitudinally has the greatest effect on the v and w components of turbulence that show increasing values of intensities and length scales near the ground. This effect is greatest on the v component, for which its spectra show much greater energy at low-frequencies, including a strong peak in the energy near a reduced frequency of 0.01.
- No significant influence was observed for the number of spires of the staggered-spire arrangement, indicating that any effects near the side walls do not influence the flow of interest near the centre, at least for the spacings evaluated here.

Drag Reduction for HDVs - Progress Toward a Flow Treatment System - Year 2

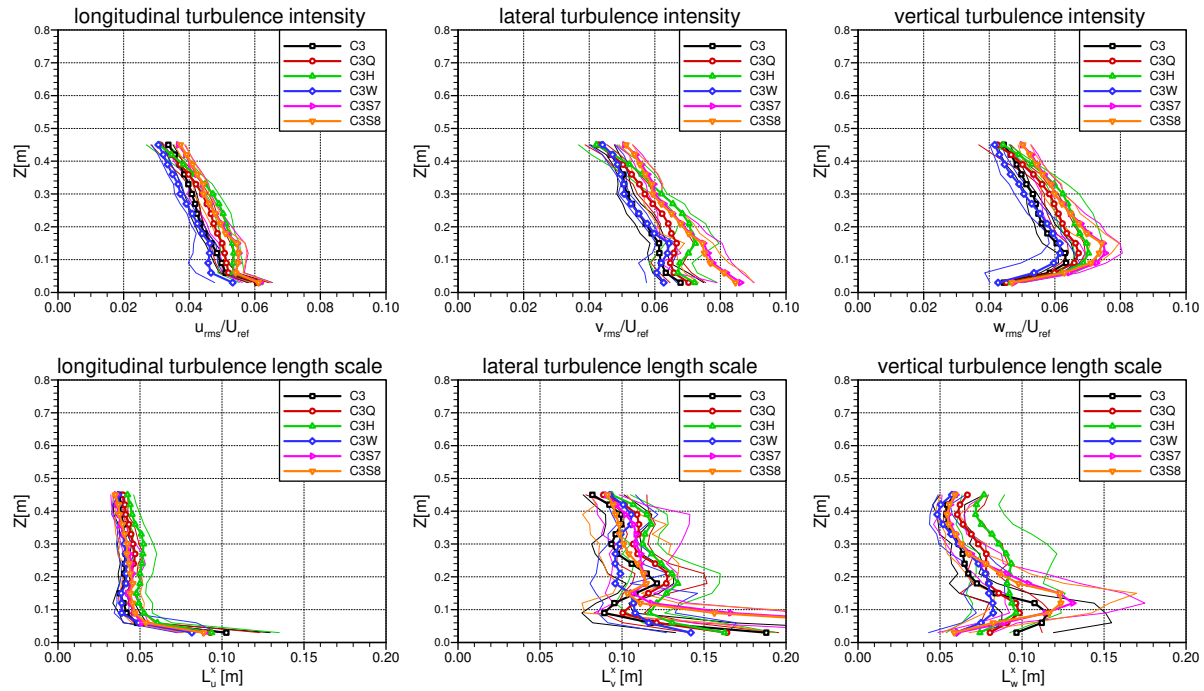


Figure 3.8: Influence of varying the C3 spire configuration on the vertical turbulence profiles

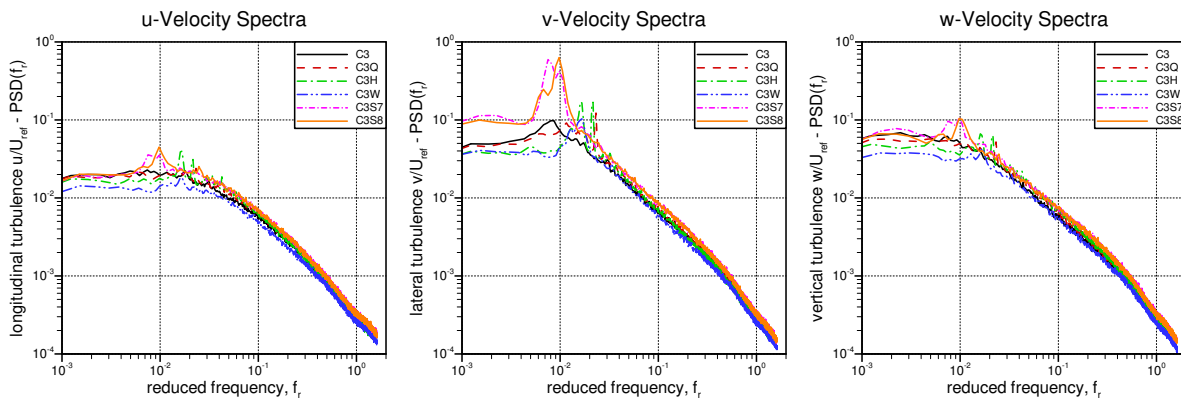


Figure 3.9: Influence of varying the C3 spire configuration on the wind spectra at $z = 0.06$ m

3.3.5 Influence of Changes in Small Spire Configuration

Variations in the C6 spire were also examined for sensitivity to changes in spacing, end effects, and combining it with a grid in the test section. The vertical profiles of turbulence characteristics and the wind spectra for these permutations are shown in Figures 3.10 and 3.11, respectively. The general observations are given as follows:

- There were no significant change in the magnitude of the turbulence intensities for the various permutations.
- Only the w length scales showed an influence with increased spacing lowering its vertical gradient.
- As with the C3 permutations in the last section, increased spire spacing influences the low-frequencies more than the high frequencies.
- Increasing the spire spacing amplifies a peak in the v spectra in the 0.02 to 0.03 reduced-frequency range.
- No significant influence was observed for the number of spires, indicating that any effects near the side walls do not influence the flow of interest near the centre, at least for the spacings evaluated here.
- The addition of a vertical-bar grid in the test section splits the flow characteristics into two distinct regions, one dominated by effects of the spires (below about 0.3 m) and one dominated by effects of the grid (above 0.3 m).

3.3.6 Comparison of Small Scale FTS Configurations

Figure 3.12 and 3.13 show a comparison of the range of turbulence conditions examined in the NRC 1.0 m \times 0.8 m Pilot Wind Tunnel test program. These conditions also represent the various conditions used to assess the sensitivity of HDV drag to turbulence, described in Section 4. All conditions measured in the current study were performed with the frame in the settling chamber, and therefore the smooth flow case for the HDV drag study, which was performed without the frame in the settling chamber, is not represented in the current data set. Some regions of the flow for the FRM case provide conditions similar to those of the smooth flow case. The locations with the lowest turbulence intensities, with values between 0.5% and 1.0% (between 0.15 m and 0.40 m from the floor) provide turbulence characteristics similar to what has been measured in the past under smooth flow conditions in the NRC 1.0 m \times 0.8 m Pilot Wind Tunnel. Of note is the similarity in turbulence intensity near the ground between the VB case and the C6Q case (for the longitudinal components) and the VB case and the C7F case (for the lateral and vertical components) but with distinctly different magnitudes of length scales, as reflected in the different shapes of the wind spectra. The VB spectra, compared to the C6Q and C7F spectra, show lower turbulence energy at low frequencies and higher energy at high frequencies, and are more pronounced for the v and w components. These similarities in turbulence intensities with differences in turbulence length scales will provide a comparison with which the influence of turbulence length scale can be evaluated.

Drag Reduction for HDVs - Progress Toward a Flow Treatment System - Year 2

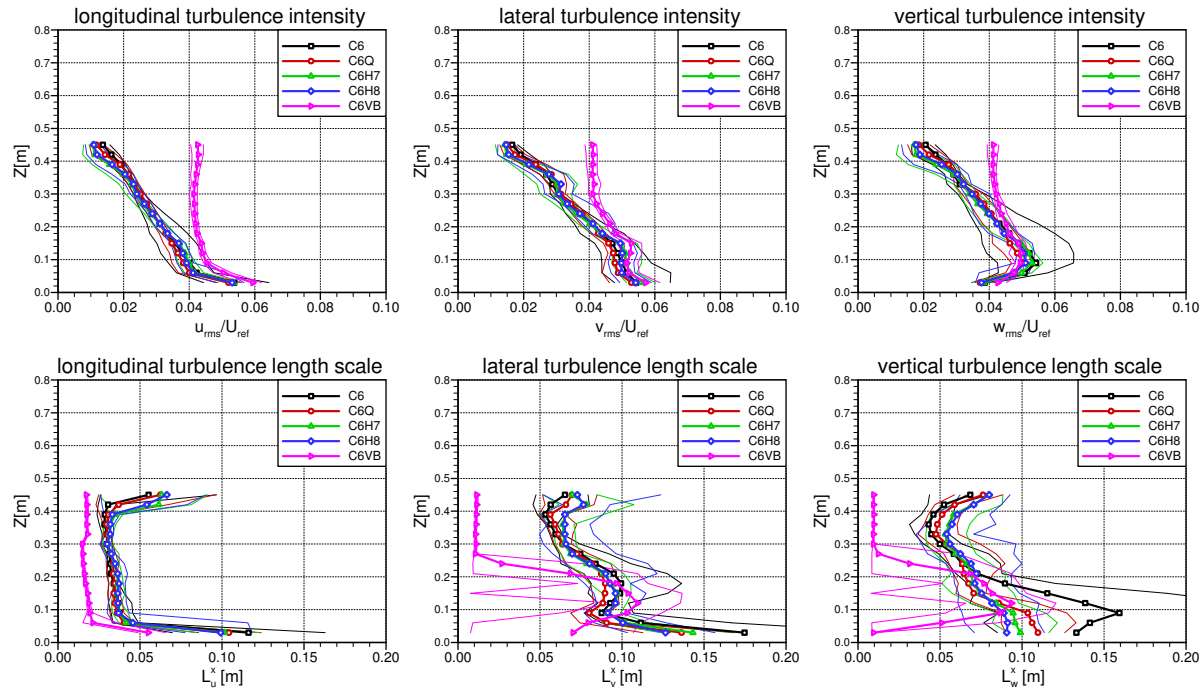


Figure 3.10: Influence of varying the C6 spire configuration on vertical turbulence profiles

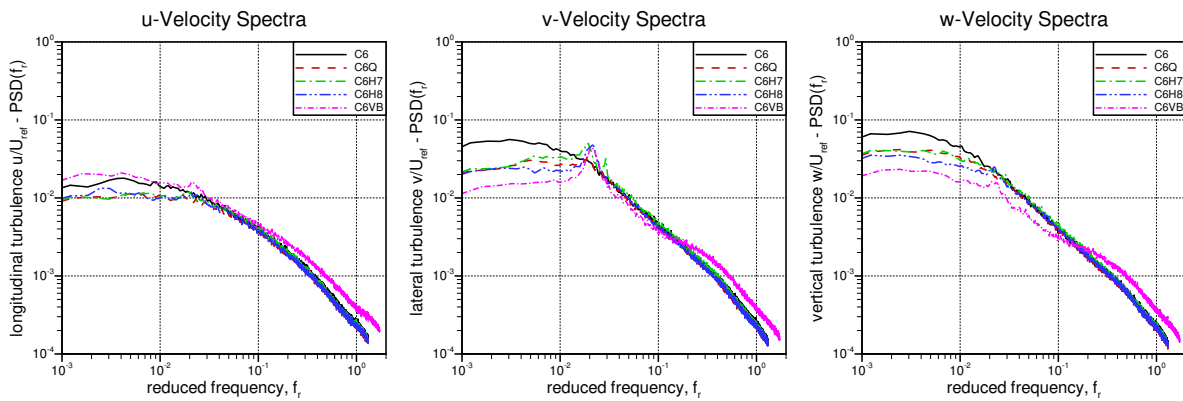


Figure 3.11: Influence of varying the C6 spire configuration on wind spectra at $z = 0.06$ m

Drag Reduction for HDVs - Progress Toward a Flow Treatment System - Year 2

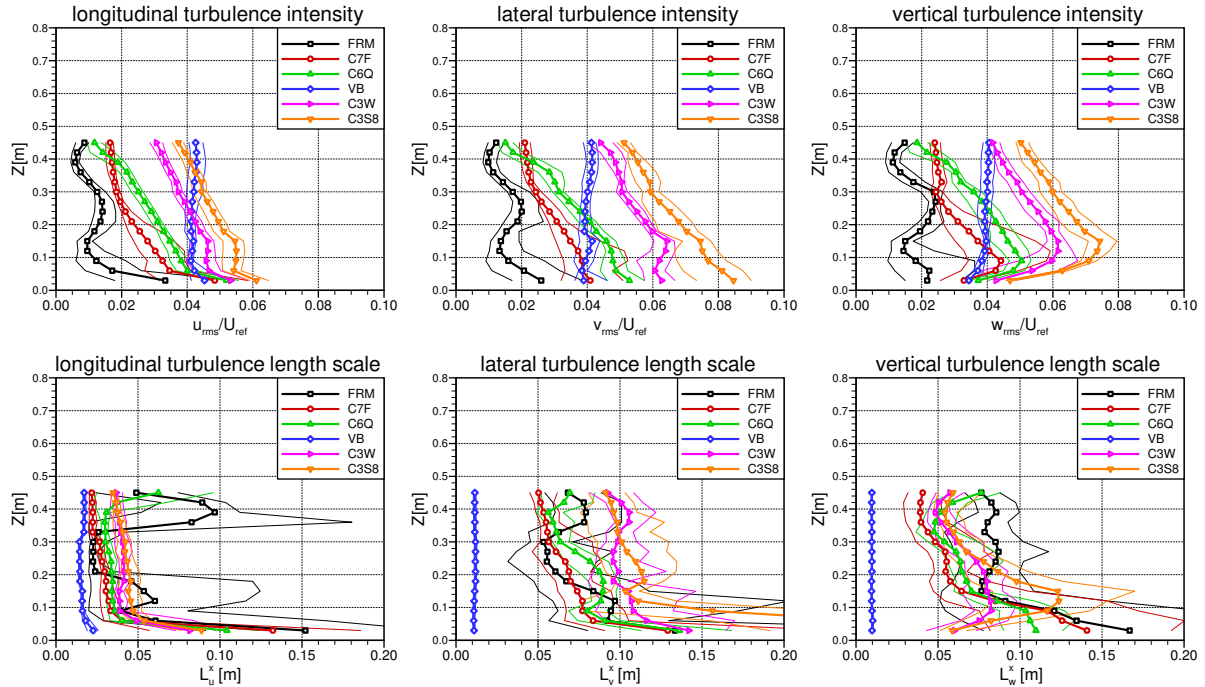


Figure 3.12: Comparison of the vertical turbulence profiles for concepts selected to evaluate HDV drag sensitivity

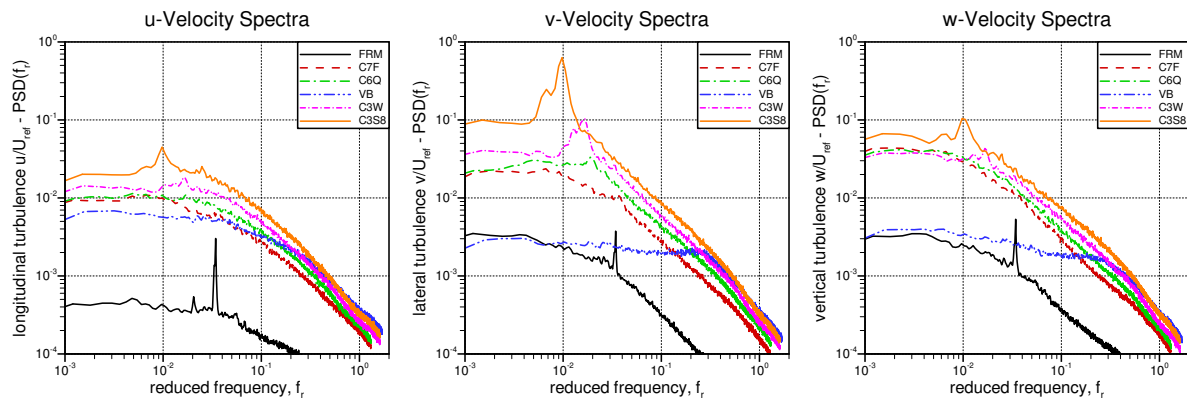


Figure 3.13: Comparison of the wind spectra at $z = 0.06$ m for concepts selected to evaluate HDV drag sensitivity

3.4 Selection of Candidate Concept and Comparison to Target Conditions

Of all the turbulence configuration examined in this study, the C6Q concept has been selected as the most appropriate candidate for replicating, in the wind tunnel, the wind characteristics experienced by vehicles on the road. The selection was based on a trade-off between matching turbulence intensities, length scale, and spectra for all three components of wind speed. Figure 3.14 shows the measured C6Q spectra compared to various conditions measured in the on-road turbulence study.

The target wind spectra from the on-road measurements represented the Moderate Terrain, Moderate Traffic, Moderate Winds (M-M-M) condition, for which the C6Q spectra when normalized appropriately provides a close match for reduced frequencies above 0.1 which for a full-sized vehicle traveling at 100 km/h represents approximately 3 Hz (10 m wavelength). Below a reduced frequency of 0.1, the C6Q configuration provides a good trade-off between matching the three wind-component spectra. For the longitudinal u component below a reduced frequency of 0.1, the C6Q configuration provides lower turbulence energy than the M-M-M condition but is still well within the band of spectra observed on the road. Similarly for the lateral v component below a reduced frequency of 0.1, the C6Q configuration provides higher turbulence energy than the M-M-M condition but is still within the band of spectra observed on the road. Only the vertical w component for the C6Q configuration falls outside the band of measurements observed on the road for the spectra below a reduced frequency of 0.1. For this component, the w turbulence energy is above the band of spectra observed on the road for reduced frequencies on the order of 0.01. This difference is predominantly due to an insufficient fetch of the wind tunnel for the vertical component of turbulence to be damped by the proximity of the ground.

Upon selection of the C6Q concept as the candidate for best representing on-road turbulence conditions, an additional set of Cobra probe measurements were performed in the NRC 1.0 m \times 0.8 m Pilot Wind Tunnel to measure the spatial correlations of the turbulence it produces. The results for the vertical and horizontal correlations are shown in Figures 3.15 and 3.16, respectively, compared to the on-road correlation measurements for various conditions. The C6Q correlation spacings have been scaled to represent full-scale road conditions. The u and v vertical correlations in Figure 3.15 are a good match to the road conditions, with the v component becoming negatively correlated for distances greater than 2 m (0.06 m in the wind tunnel). This negative correlation implies there are strong vortical/swirling structures in the flow aligned with the longitudinal direction. The vertical correlation of the w component is greater in the wind tunnel than what was observed on the road. This is again a result of insufficient fetch in the wind tunnel to damp the vertical fluctuations before they reach the test section.

The horizontal correlation measurements in Figure 3.16 also show good agreement between the C6Q and the on-road measurements, with the majority of the measurements falling within the spread of data measured on the road. The u component correlations are at the low extreme of the on-road data but still within the band of measurements. The v component correlations are well within the band of on-road measurements. The w component correlations are at the

Drag Reduction for HDVs - Progress Toward a Flow Treatment System - Year 2

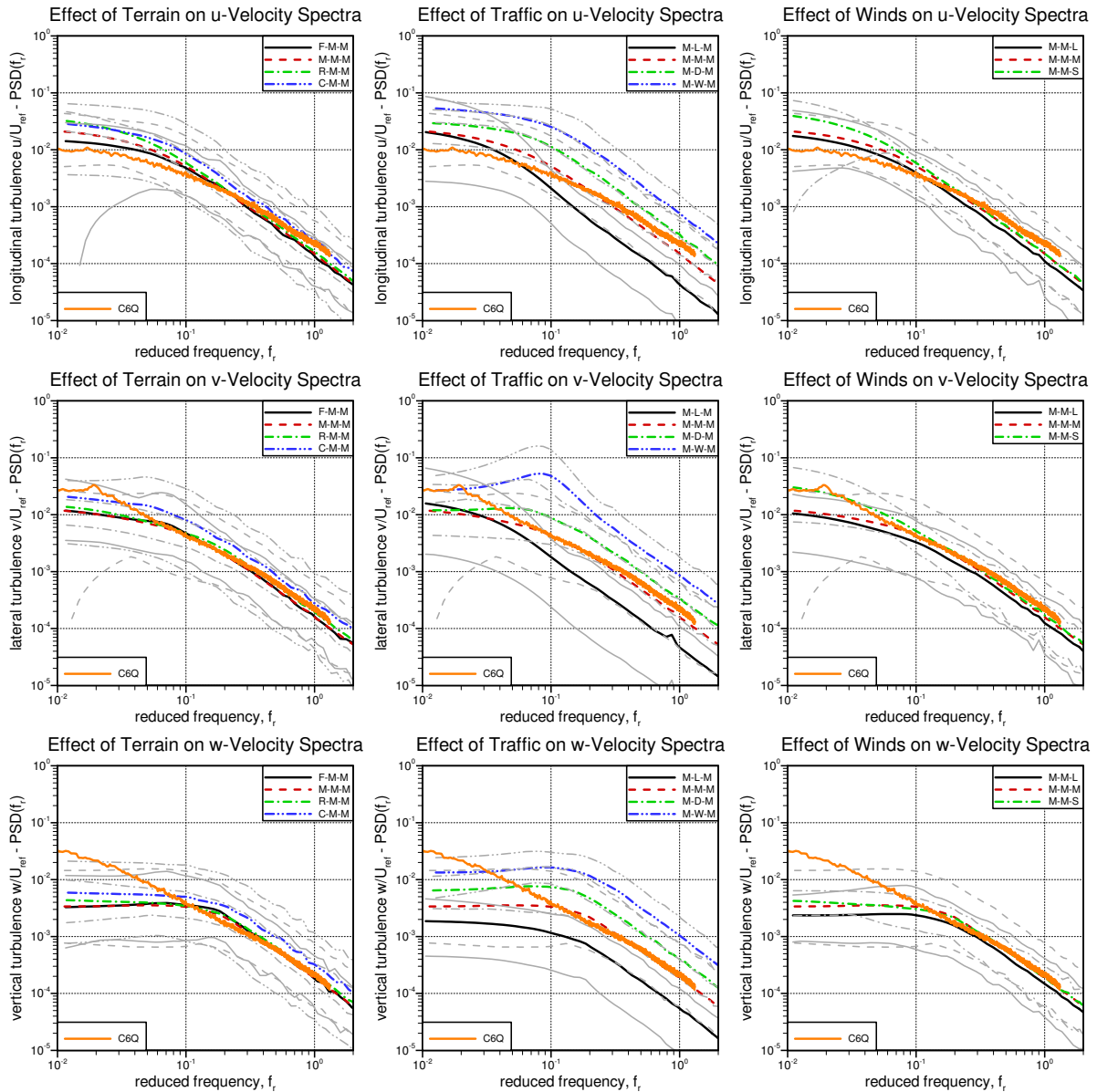


Figure 3.14: Comparison of candidate FTS concept (C6Q) with on-road wind spectra measurements

Drag Reduction for HDVs - Progress Toward a Flow Treatment System - Year 2

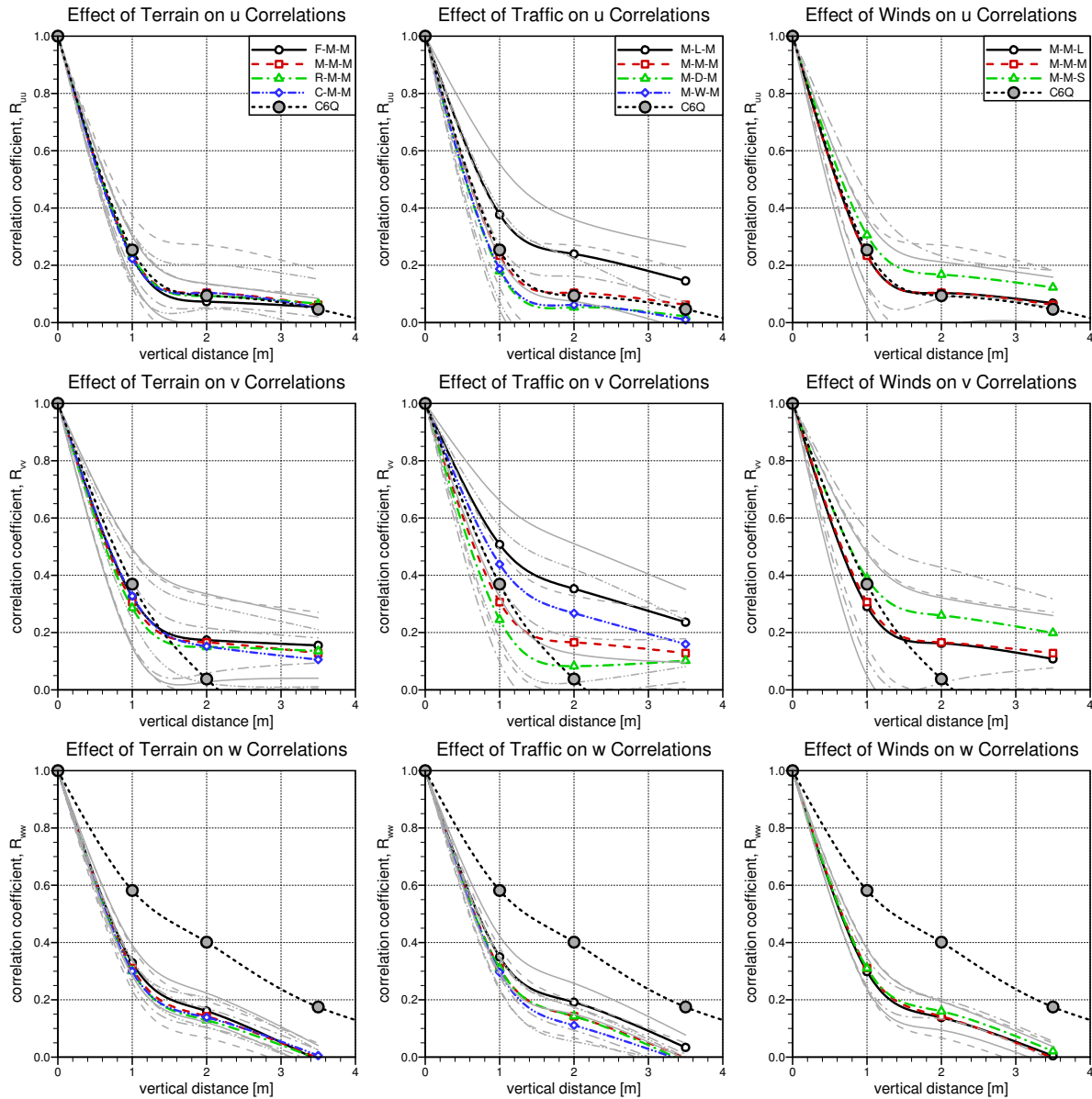


Figure 3.15: Comparison of candidate FTS concept (C6Q) with on-road vertical correlation measurements

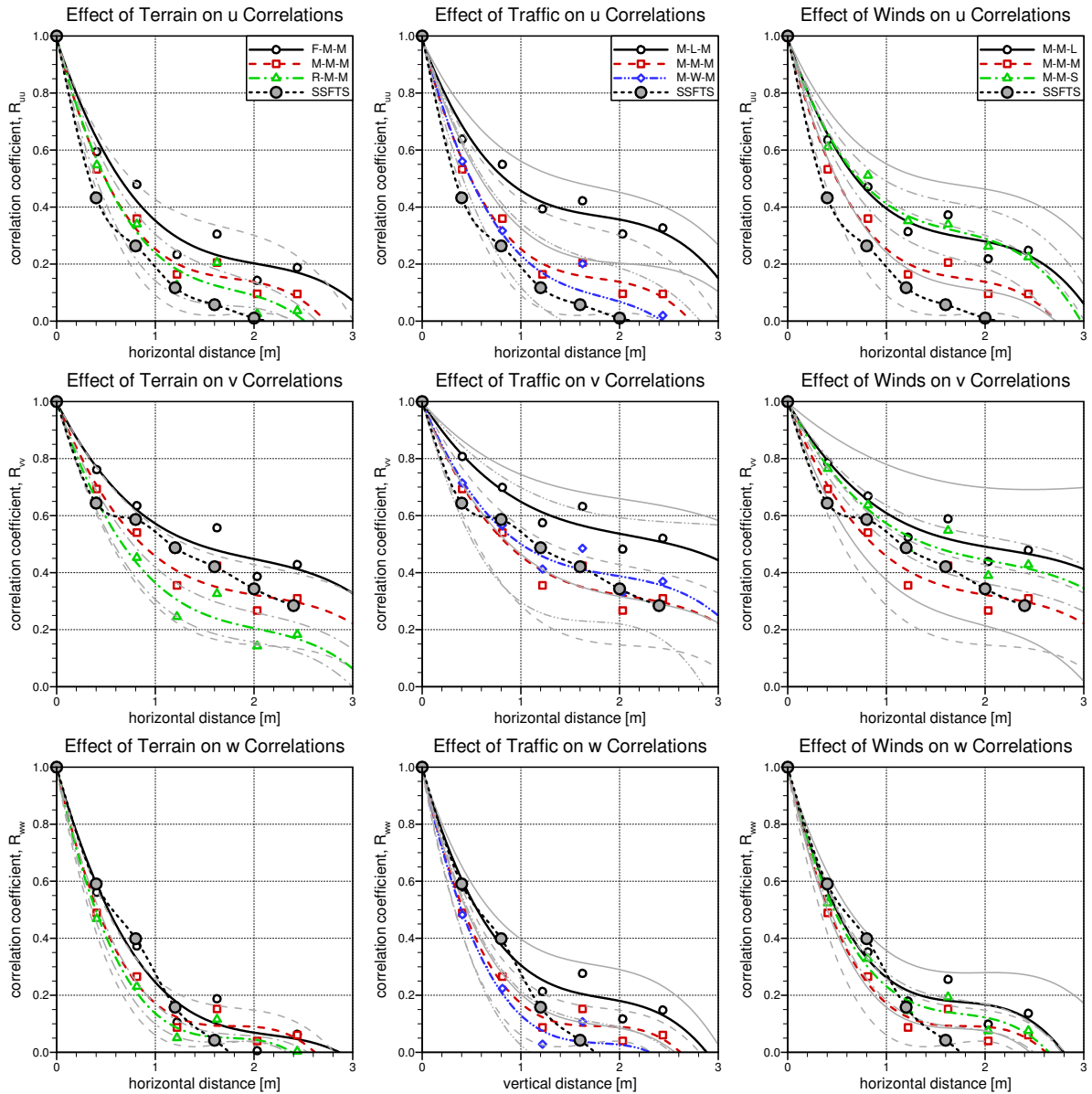


Figure 3.16: Comparison of candidate FTS concept (C6Q) with on-road horizontal correlation measurements

high extreme of the on-road data for the lower correlation lengths below 1 m, but still within the band of measurements. Some of the on-road horizontal correlation measurements for the w component showed small negative correlations, similar to the wind tunnel measurements but at greater correlation lengths, so the characteristics of the road-turbulence are well represented by the C6Q configuration.

The general turbulence characteristics of the C6Q spire configuration, both the intensities and length scale, are tabulated in Table 3.3 and compared to the target characteristics defined from the on-road measurements. As inferred from the discussion of the turbulence spectra, the v and w components show a higher turbulence intensity resulting from the higher energy content at low frequencies. Similarly, the differences in length scales are due to the differences in the shape of the wind spectra. Despite the specific component differences with the target spectra, the values of intensity and length scale are mostly within the range of conditions measured on the road. The only exception is the w length scales which were consistently below 1 m for the road measurements, yet are the highest of the three components measured in the wind tunnel.

Table 3.3: Comparison of C6Q turbulence characteristics to the target on-road condition (M-M: Moderate Terrain, Moderate Traffic, Moderate Winds)

Component	Turbulence Intensity, I		Turbulence Length Scale, L^x	
	Road	SSFTS	Road	SSFTS [†]
u	4.0 %	3.8 %	4.7 m	1.2 m
v	3.5 %	4.8 %	1.9 m	2.7 m
w	3.1 %	5.0 %	0.6 m	3.5 m

[†] full-scale equivalent

One consideration that is important for simulating appropriate turbulence in a wind tunnel is to characterize the longitudinal decay of the turbulence and its decay rate relative to the size of the model. Without a mechanism to continuously inject turbulence energy into the flow, the turbulence will decay with time, and hence in a convected flow will decay with distance. Figure 3.17 shows the laterally-averaged profiles of the C6Q turbulence measured at four longitudinal stations in the test section. The longitudinal spacing between locations A, B, C, and D is 0.34 m (11 m full scale), with the total distance between A and D being 1.02 m (34 m full scale). Location B refers to the plane at which the flow surveys for all of the turbulence configurations were performed. The longitudinal spacing between measurement planes is equivalent to approximately half the length of a 3% standard tractor-trailer combination (sleeper cab with a 53 ft trailer). The results show a negligible change in the u turbulence intensity over this distance, but a decay in the v and w intensities on the order of 1% intensity over the length of an HDV model. The length scales also show some change with longitudinal location with the v component showing the greatest decay of about 15% over the length of a 3% HDV model.

In addition to the turbulence intensities and length scales, vertical and horizontal correlation measurements were performed at two longitudinal locations (B and D) and these measurements are shown in Figures 3.18 and 3.19. Some differences are observed between the two

Drag Reduction for HDVs - Progress Toward a Flow Treatment System - Year 2

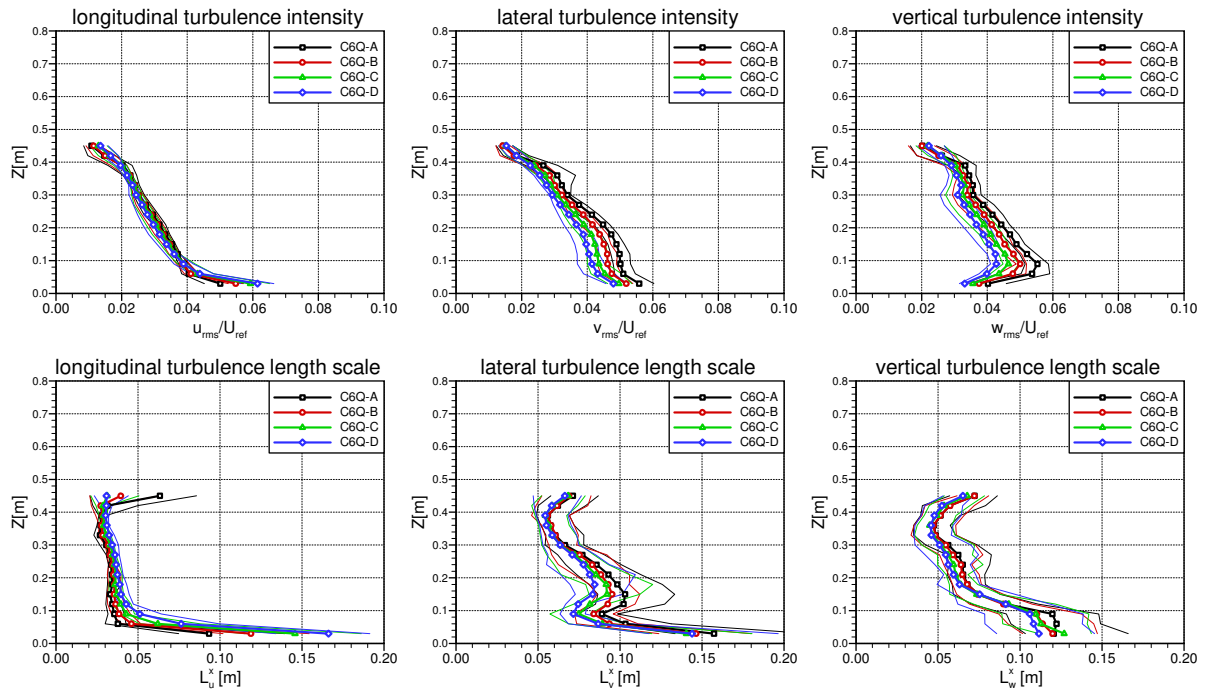


Figure 3.17: C6Q turbulence characteristics at different longitudinal locations

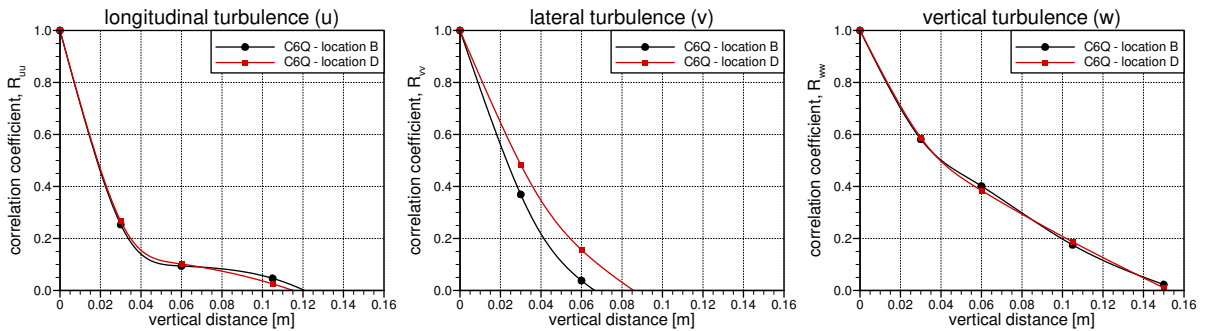


Figure 3.18: C6Q vertical correlation measurements at different longitudinal locations

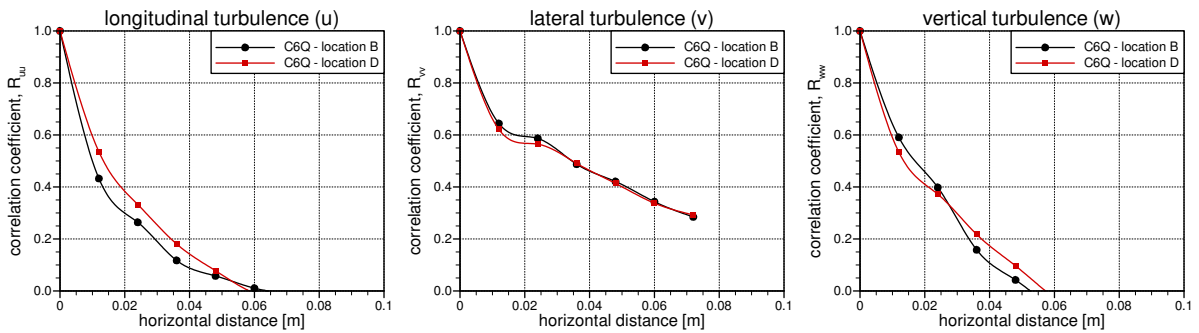


Figure 3.19: C6Q horizontal correlation measurements at different longitudinal locations

locations, such as an increase in correlation level with distance for the vertical v correlations and the horizontal u correlations, but these differences are not excessive. In general, the measurements show that the turbulence remains relatively consistent over the length of a representative 3% HDV model, which is representative of the 30% HDV model installed in the NRC 9 m Wind Tunnel.

3.5 Summary

As a starting point towards implementing a Flow Treatment System (FTS) in the NRC 9 m Wind Tunnel, several passive turbulence generation technologies were evaluated in the NRC 1.0 m \times 0.8 m Pilot Wind Tunnel for their ability to generate turbulence characteristics appropriate to represent the wind conditions that vehicles experience on the road. The test program allowed for the selection of a concept suitable for implementation in the NRC 9 m Wind Tunnel. The following summarizes the main findings of the detailed analysis of these results:

- Settling-chamber-mounted spires provided a better representation of on-road turbulence characteristics than test-section-mounted spire configurations. This results from a reduction in turbulence intensity of the wind through the wind-tunnel contraction while maintaining the large length scales associated with the large obstacles.
- Using only spires in the settling chamber (without any other turbulence generating device) was sufficient to obtain the desired wind spectrum (intensity of turbulence and length scales). It is sufficient to adjust the spire spacing and spire base-width to obtain the a target spectrum.
- Settling-chamber-mounted spires provided a negligible vertical gradient in the mean wind speed which is suitable for ground vehicle testing purposes.
- A benefit of mounting obstacles in the settling chamber is the low wind loads experienced by the structure in the lower-speed flow section. This will help with the structural design of a concept for the NRC 9 m Wind Tunnel.
- The C6Q configuration from the NRC 1.0 m \times 0.8 m Pilot Wind Tunnel test program was selected, as it provides wind spectra and spatial correlations that match well the on-road measurements.
- The longitudinal decay of the turbulence in the test section is sufficiently low that a scaled HDV model will experience nearly constant turbulence conditions along its length.

The selection of the C6Q configuration as the most appropriate was based in part on the study examining the sensitivity of HDV drag to turbulence, described in the next section of this report.

4. Sensitivity of HDV Drag to Turbulence

4.1 Problem Description

To select a Flow Treatment System (FTS) that will suitably represent the winds of importance for aerodynamic evaluations of HDVs and associated drag reduction technologies, the manner in which turbulence influences HDV aerodynamic performance must be understood. To do so, the third step towards the development of the FTS for the NRC 9 m Wind Tunnel is to examine how turbulence affects the mean and dynamic wind loads experienced by HDVs.

The most recent review of the influence of turbulence on ground-vehicle aerodynamics is that by Watkins and Cooper (2007), from which the following general conclusions were provided that are important for HDVs:

- Turbulence plays an important role for multi-body problems such as tractor-trailer combinations, especially for configurations that alter the flow at the interface between the two such as an air fairing. Optimum drag reduction geometries may be different whether optimized in smooth or turbulent flow.
- Previous work has shown differences in drag-reduction magnitude between wind tunnel and road data for technologies applied to HDVs, and some basic wind tunnel data shows that drag reductions are smaller in turbulent flows than smooth flows. Optimizations have shown different results when performed in smooth or turbulent flows. This implies that it may be more difficult to reduce drag of HDVs in realistic flow conditions.
- A quasi-steady method can be used to estimate the drag coefficient variation with wind angle in turbulent-flow based on results from smooth-flow tests. This method showed agreement for drag-coefficient reductions when considering the first generation of drag reduction technologies such as air fairings. The errors were similar to the magnitude of drag reductions observed with some of modern technologies to be evaluated in Phase 2 of the current project, and therefore the method is not suitable for the smaller decrements in drag expected in the current project.
- There may be a reduced influence of turbulence at high Reynolds numbers because any separated shear layers are generally less sensitive to turbulence at higher Reynolds numbers.
- Turbulence may influence the base pressure for vehicles with fixed separation points.
- There is no clear consensus on the effect of turbulence intensity versus length scale.

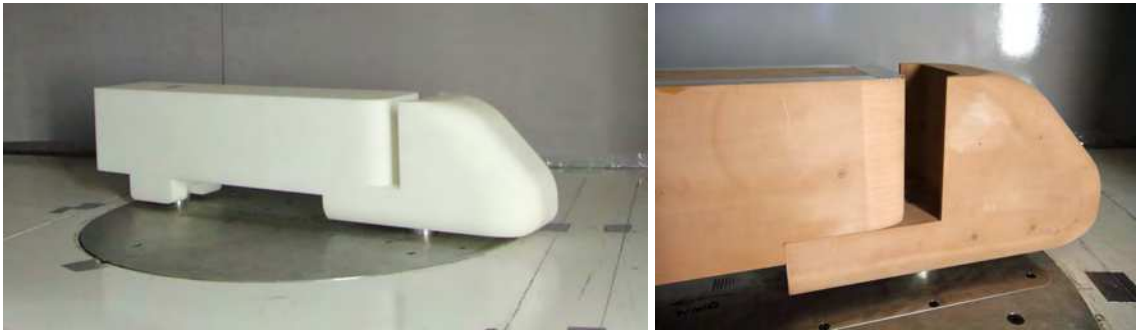


Figure 4.1: Simplified HDV models for drag-sensitivity measurements (left - lightweight foam model, right - Renshape pressure model)

As a follow-up to the small-scale FTS concept evaluation work described in the previous section, several of the FTS concepts were selected to evaluate their influence on the aerodynamic performance of a simple HDV model in the NRC 1.0 m \times 0.8 m Pilot Wind Tunnel.

Two small-scale HDV models were built and tested in the NRC 1.0 m \times 0.8 m Pilot Wind Tunnel with the selected FTS concepts, shown in Figure 4.1. One model is a lightweight model for use with a dynamic balance to evaluate the mean and dynamic drag loads experienced by an HDV in turbulent flow. The second model is instrumented with pressure taps over the surface of the model to evaluate the mean and dynamic pressures that affect the mean and dynamic wind loads. Details of the models and the considerations leading to their designs are described in the progress report for the first year of the project (McAuliffe *et al.*, 2013a).

4.2 Wind Tunnel Setup and Measurement Procedures

The measurements were performed in the NRC 1.0 m \times 0.8 m Pilot Wind Tunnel with the same closed test-section configuration used in the small-scale FTS concept evaluation study described in Section 3. The NRC 10-lb Cruciform Balance was used to measure the wind loads experienced by the lightweight HDV model, and a Scanivalve ZOC33 pressure scanner (± 2500 Pa range) was used for the measurements with the pressure model.

Two types of measurement runs were performed:

1. Speeds sweeps were performed to evaluate the Reynolds number sensitivity of the models, for wind speeds of 5 to 44 m/s in approximately 5 m/s increments. These sweeps were done predominantly at zero wind/yaw angle.
2. Two sets of yaw sweeps, each at a different wind speed, were performed to evaluate the effect of cross winds. The wind angles for these sweeps were 0° , $\pm 1^\circ$, $\pm 2.5^\circ$, $\pm 5^\circ$, $\pm 7.5^\circ$, $\pm 10^\circ$, $\pm 12.5^\circ$, and $\pm 15^\circ$. One set was performed at 27 m/s and the other at 44 m/s.

Light-weighting of one of the models was pursued to provide a high natural frequency of the model/balance system such that the dynamic loads of interest can be resolved without excitation of the system. Although the goal was to ensure the natural frequency associated with

the drag axis of the model was in excess of 100 Hz, the measured natural frequency was approximately 87 Hz. The model/balance system also had a lower stiffness associated with the lateral/rolling mode of approximately 57 Hz. For much of the test program, excitation of the lateral/rolling mode provided negligible influence on the drag axis of the system. However, when the lateral/rolling mode was excited by the vortex shedding phenomenon at the base of the model, a significant spectral peak was observed in the drag measurements. This occurred at wind speeds of approximately 35 m/s. To avoid any excitation of model/balance natural frequencies, the drag measurement signals were digitally low-pass filtered with a cut-off frequency of 40 Hz. For the two wind speeds of interest for the yaw-sweep measurements (27 m/s and 44 m/s) this cut-off frequency represents reduced frequencies based on model width of 0.20 and 0.12, respectively, and therefore any drag rms measurements do not capture vortex shedding-induced dynamic loads present above a reduced frequency of 0.2.

The basic aerodynamic performance of a ground vehicle is expressed by means of force and moment coefficients. For the current test program only the drag coefficient, representing the force along the axis of “motion” of the vehicle, is of interest and is defined as:

$$C_D = \frac{F_D}{Q_{ref} \cdot A_{ref}} \quad (4.1)$$

where F_D is the drag force, Q_{ref} is the reference dynamic pressure of the wind ($= 1/2\rho U_{ref}^2$), and A_{ref} is the reference area for the vehicle of interest, typically the frontal area. Although model drag force is the primary wind-load component of interest, the side force can be useful and is generally required for applying blockage corrections to the data. During the test program, a problem arose with the strain gauge for the balance side-force component, and most of the data do not have reliable side force measurements. As such, the measurements presented herein have not been corrected for blockage effects. For the measurements described in Section 7 related to the blockage-correction study, a different balance was used after consistent problems arose with the 10-lb cruciform balance.

Balance data were acquired during the test program at a sampling rate of 1250 Hz for 30 s at each condition. Based on the measured wind-tunnel and balance data, the following parameters were calculated for each of these 30 s sampling periods:

- Mean reference dynamic pressure and wind speed, defined by calibration of the wind-tunnel contraction using a pitot probe, for each turbulent conditions (Q_{ref} , U_{ref}),
- Time series of the drag coefficient ($C_D(t)$), using the time series of the drag force ($F_D(t)$) with the mean dynamic pressure (Q_{ref}),
- Mean drag coefficient (C_D), representing an average of the time series,
- Rms drag coefficient (C_{Drms}), representing the standard deviation of the time series,
- The drag coefficient spectrum ($PSD_{C_D}(f)$), defined by the power-spectral-density (PSD) distribution, of the time series.

The major contributor to error in the HDV load measurements was drift of the balance strain gauges due to changes in the ambient temperature within the balance structure. This temperature was influenced by the ambient room temperature (approximately 20°C) and the temper-

ature of the wind in the test section (anywhere between 15°C and 35°C). The wind from the test section could leak into the balance cavity through the openings surrounding the model support posts. Initial measurements showed repeatability errors for the drag coefficients on the order of $\Delta C_D \approx 0.02$ which is approximately 4% of the zero-yaw value. A procedure was developed to stabilize the temperature experienced by the balance during the measurements. This consisted of running the wind tunnel at the appropriate wind speed for five minutes, shutting down and performing the tare measurements with the balance at or near the appropriate temperature, then ramping the wind speed back up to the desired condition and subsequently performing the measurements. This procedure reduced the drag-coefficient repeatability to an order of 0.005 to 0.010 (1-2%). It was more difficult to control the test-section temperature for speeds sweeps, but greater care was taken to adjust the wind tunnel cooling system to stabilize the temperature throughout these measurement runs.

To provide a single measure of the aerodynamic performance of a ground vehicle, a wind-averaged-drag coefficient (C_{WAD}) can be defined that, for a given ground speed (U_g), accounts for an equal probability of experiencing terrestrial winds from all directions. The C_{WAD} makes use of the distribution of C_D with wind angle, combined with a single mean terrestrial wind speed (U_{avg}) that represents long-term averaged conditions experienced on the road. The procedure involves averaging the vector combination of ground speed and wind speed for an equal probability of experiencing the mean wind speed from all directions. The general equation for the wind-averaged-drag coefficient is:

$$C_{WAD}(U_g) = \frac{1}{2\pi} \int_0^{2\pi} C_D(\eta) \left[1 + \left(\frac{U_{avg}}{U_g} \right)^2 + 2 \left(\frac{U_{avg}}{U_g} \right) \cos \theta \right] d\theta \quad (4.2)$$

where

$$\eta = \tan^{-1} \left[\frac{(U_{avg}/U_g) \sin \theta}{1 + (U_{avg}/U_g) \cos \theta} \right] \quad (4.3)$$

For Canada and the United States, a typical mean terrestrial wind speed (U_{avg}) used for these calculations is 11 km/h (7 mph, *SAE Wind Tunnel Test Procedure for Trucks and Busses*, 2012).

In addition to measuring the mean and dynamic wind loads, which represent an integration of the force distributions over the entire surface of the model, measurements of the surface pressure were performed at 63 discrete locations over the HDV model. Figure 4.2 shows the locations of the pressure taps and the groupings of taps used for the presentation of data in this report. For presenting the pressure data later in the report, these groupings allow the data to be plotted based on the model-surface spacing distributions. This allows, for example, a pressure distribution over the model centreline to be plotted relative to the distance between taps, providing a visual representation of the pressure gradients over the model surface.

As with the balance measurements, the surface pressure measurements were acquired at a high sampling rate to analyze the dynamic response of the surface pressures to the different turbulence conditions. The pressure data was acquired at 500 Hz for 30 s at each condition. Mean, rms, and PSDs of the pressure measurements were calculated, but for the rms and PSD data to be representative of what is occurring at the surface of the model, the change in amplitude and phase response of the unsteady signals due to the length of the pressure tubing

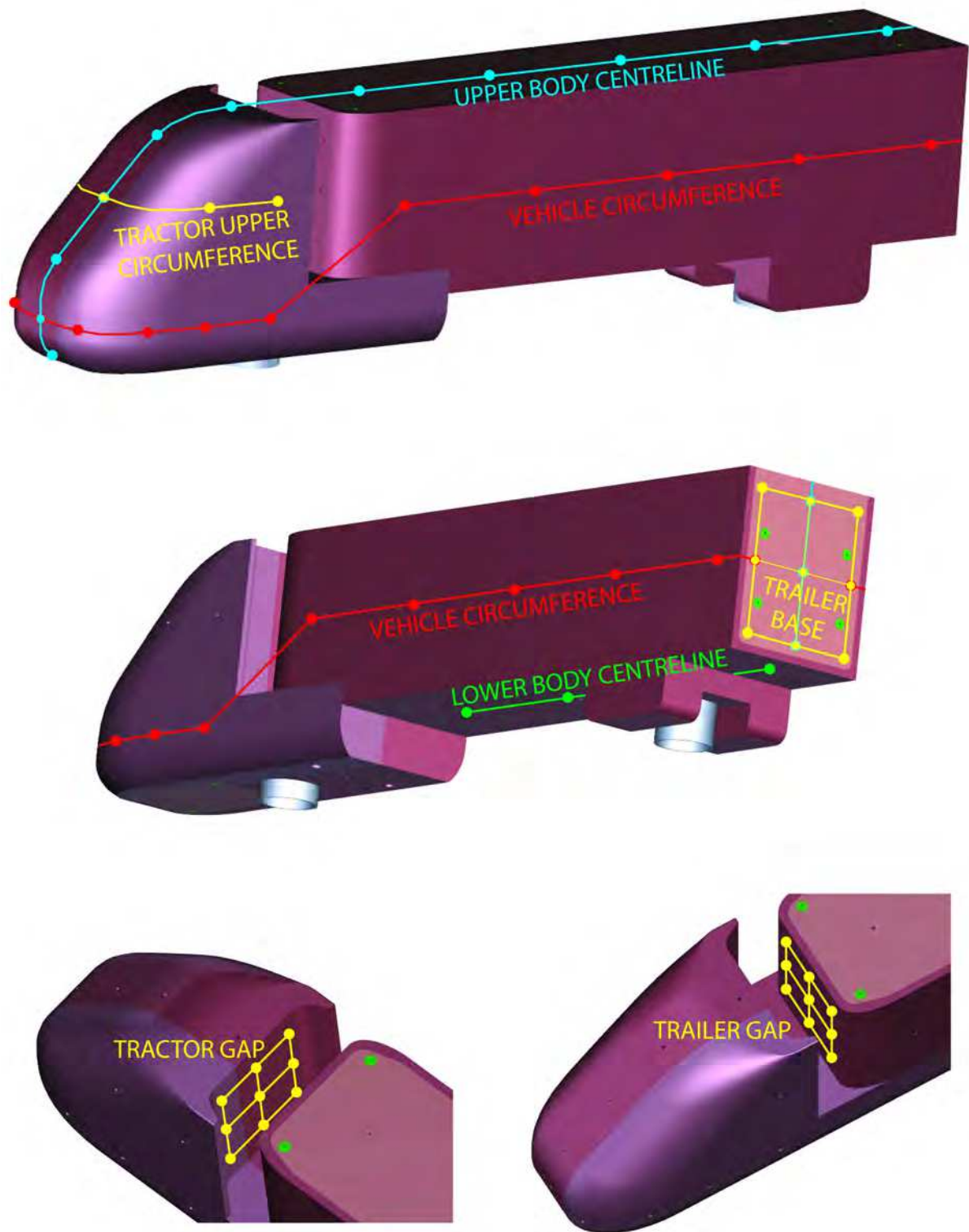


Figure 4.2: Pressure tap locations and groupings on HDV model

must be corrected. To do so, the pressure tubes/channels connecting each surface-pressure tap to the pressure scanners were calibrated for their frequency-response characteristics. The pressure channels were calibrated using a set of equipment consisting of the pressure scanner, a horn-driver/amplifier driven with white noise, a fast-response pressure sensor, and a spectrum analyzer. The fast-response pressure sensor measures the time-resolved pressure signal at the model surface, and the spectrum analyzer correlates it with the output from the pressure scanner to provide a transfer function ($G(f)$) for each pressure channel. To correct the measured pressure signals from the wind tunnel tests, the time-series of the signals were first converted to the frequency domain via a Fast Fourier Transform (FFT), and the mean-square spectral distribution of the corrected signal is calculated by dividing that quantity for the measured signal by the corresponding transfer function:

$$S_{P_{surface}}(f) = \frac{S_{P_{measured}}(f)}{G(f)} \quad (4.4)$$

The mean-square spectral distribution is then converted back to the time domain, providing the unsteady pressure signal at the surface of the model, from which the mean, rms, and PSDs were calculated. The pressures were also normalized to a pressure-coefficient form as follows:

$$C_p = \frac{P - P_{ref}}{Q_{ref}} \quad (4.5)$$

$$C_{Prms} = \frac{P_{rms}}{Q_{ref}} \quad (4.6)$$

where P_{ref} and Q_{ref} are the reference static and dynamic pressures in the test section, as defined through calibration of the test section with a pitot probe for each turbulence condition.

The HDV model loads and surface pressures were measured for the six flow conditions described in Section 3.3.6. The turbulence characteristics of these six flow conditions are provided in Table 4.1. The turbulence length scales in Table 4.1 are normalized by the width of the 5% model (0.13 m) to provide a measure of the scale of the turbulence to the vehicle size. A range in longitudinal turbulence intensities from below 1% to almost 6% is represented in this set of configurations, with the lateral and vertical turbulence intensities exceeding 7%.

Table 4.1: Turbulence intensities and length scales of configurations used to evaluate sensitivity of HDV drag to turbulence, measured 0.09 m from the ground

Config.	I_u [%]	I_v [%]	I_w [%]	L_u^x/W [-]	L_v^x/W [-]	L_w^x/W [-]
SMTH	0.6	1.0	1.1	0.75	0.61	0.66
C7F	3.2	3.8	4.4	0.27	0.59	0.90
C6Q	3.8	4.8	5.0	0.28	0.62	0.80
VB	4.1	3.9	3.8	0.12	0.09	0.08
C3W	4.6	6.2	6.0	0.30	0.83	0.63
C3S8	5.5	7.7	7.1	0.36	1.20	0.90

4.3 Wind Loads

The influence of turbulence and Reynolds number on the overall drag loads of the simplified HDV body is presented in Figure 4.3 which shows the variation in mean drag coefficient with wind speed. As expected for a bluff body of this shape, the drag coefficient shows strong sensitivity to Reynolds number at low speeds (below 20 m/s, $Re = 175,000$). As described in the year 1 progress report (McAuliffe *et al.*, 2013a), the front face of the model was designed with a reduced sensitivity to Reynolds-number within the range of wind speeds for the current study. The results in Figure 4.3 show a relatively flat variation at the higher speeds for all turbulence environments, including one case at a non-zero wind angle (C6Q at 7.5°), confirming this reduced sensitivity to Reynolds number. Above 20 m/s, the smooth-flow case at 0° wind angle compares well with the corresponding C7F, C6Q, and VB conditions. These differ from the C3W and C3S8 conditions at 0° wind angle that show up to 10% higher drag coefficients at the higher speeds.

Differences between turbulence conditions are further evaluated from yaw-sweep results at two different speeds, the data for which are shown in Figure 4.4. In general, the trends are the same for both speeds, but the differences between the two plots show a greater level of Reynolds number sensitivity at wind angles exceeding $\pm 7.5^\circ$, identified by the higher drag coefficients at 44 m/s at the extremes of the wind angle range. In both plots, the low-wind-angle range shows again the similarities between the smooth flow condition with the C7F, C6Q, and VB conditions. As turbulence intensity is increased, the drag coefficient at zero-wind-angle for the C3S8 condition is 10% greater than that for the smooth-flow condition. However, as the wind angle increases a convergence in the drag coefficient values appears in excess of about $\pm 10^\circ$ for all except the VB condition which consistently shows a lower drag coefficient at the higher angles. In regards to the 44 m/s speed sweeps, the lower values for

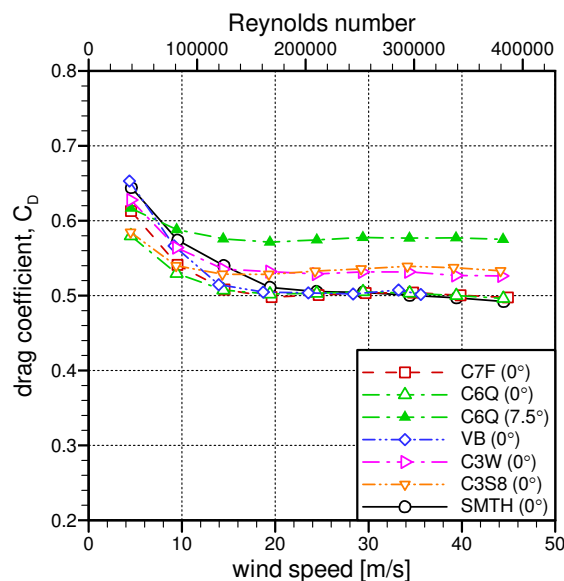


Figure 4.3: Influence of turbulence and Reynolds number on the mean drag coefficient

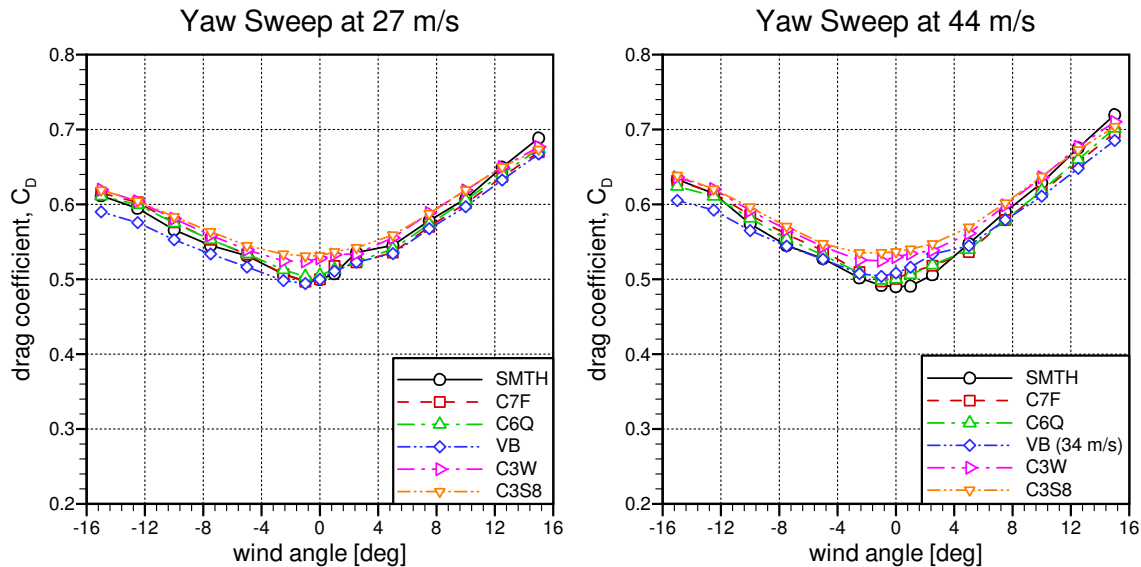


Figure 4.4: Influence of turbulence and wind angle on the mean drag coefficient

the VB condition can, to an extent, be attributed to the fact that it was performed at a lower wind speed (34 m/s) to avoid an excessively-loud flow-induced ringing of the vertical bars. Despite this, the trend of the VB configuration to exhibit lower drag at the higher wind angles is evident at 27 m/s as well.

In Figure 4.4, the drag-coefficient variations with wind angle are not symmetric about zero, as is generally expected for a laterally-symmetric model shape. Often, bodies operating in the critical Reynolds number regime (operating regime with strong sensitivity to Reynolds number) will behave in this manner due to slight differences in geometry that affect the boundary layer transition and separation characteristics in a slightly different manner over each side of the model. Some geometry differences were observed in the fabricated models that may provide a source of this asymmetry. Due to the machining process for which the models must be flipped in the machine and re-aligned, a slight lateral offset in the upper curved surface of the lightweight model from the lower surface was noted (<1 mm). Small steps in the surface geometry were sanded but this could lead to differences in the laminar-to-turbulent transition process of the flow due to differences in the local pressure gradients. Also, due to the retrofitting of the wind tunnel to accommodate a closed test section, the turntable is not exactly at the center of the test section (offset by approximately 1 cm), such that the nose of the models will be closer to the wall under positive wind angle conditions. It is conceivable that the slightly greater blockage near the nose at positive wind angles is a contributor to the higher drag under these conditions. In addition to the overall asymmetry of the drag coefficient at higher wind angles, a different asymmetry is observed at small positive wind angles. This asymmetry is affected by Reynolds number and turbulence condition. It is most evident at 44 m/s where the difference is distinct between the smooth flow, the C7F, the C6Q, and the VB conditions. The smooth flow condition shows a symmetric trend about zero but the others show a bump in the curve between 0° and 2.5°. At 27 m/s this bump is evident for all of

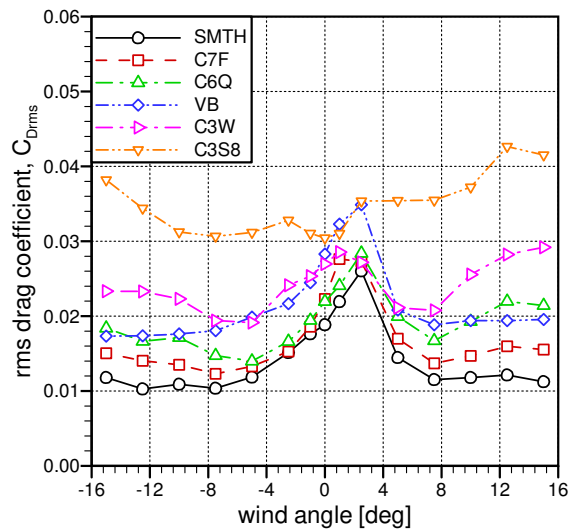


Figure 4.5: Influence of turbulence and wind angle on the drag coefficient for 44 m/s yaw-sweep cases (VB case at 34 m/s)

these turbulence conditions. After evaluating the results and repeating some measurements, the reason for this bump has been attributed to a combination of the large diameter cylindrical posts on which the model is supported combined with a slight cross-wind in the ground-floor boundary layer (evident in the flow measurements by the positive lateral wind speed near the ground in the flow mapping shown in Figure 3.2 and in the lateral wind angle profile of Figure 3.3).

The asymmetry at small positive wind angles is also evident in the rms drag coefficient measurements that are presented for the 44 m/s speed sweeps in Figure 4.5. All but the C3S8 condition show the peak rms values at 1° or 2.5° . Recall that these rms data represent the rms of the filtered signals and represent response frequencies below a reduced frequency of 0.13 (based on model width). Of particular note here is that the peak rms levels near zero wind angle are all of similar magnitude, but show distinct differences at higher wind angles (both positive and negative). This implies that the flow mechanism(s) which induce the drag fluctuations near 0° are predominantly influenced by the model and its shape, whereas the flow mechanism(s) which induce the drag fluctuations at higher wind angles (both positive and negative) are influenced predominantly by turbulence in the flow.

In the $\pm 5^\circ$ wind angle range in Figure 4.5, the VB case exhibits similar rms drag coefficient levels to those measured for the highest-turbulence conditions (C3W and C3S8). The difference between the VB and the C6Q condition (similar turbulence intensities with different length scales), indicates an influence of turbulence length scale on whatever flow mechanism(s) induce the drag fluctuations at low wind angles. At higher wind angles, the rms drag coefficient levels for these two turbulence conditions is similar, indicating less of a sensitivity to length scale under these wind-angle conditions.

In an attempt to identify the influence of any specific band of turbulence frequencies on the dynamic wind loads experienced by the HDV model, aerodynamic admittance calculations were performed to contrast the spectra of the dynamic drag response to a respective quasi-steady response based on the turbulent wind spectra. The analysis proved to be problematic due to the variation in which the wind spectra changes with height from the ground. This caused difficulty in selecting an appropriate spectra with which to contrast the dynamic drag response. Although these results are not shown here, some basic inferences were drawn from comparing the results based on different wind spectra. The intent of this analysis was to identify if there were specific bands of frequencies to which the dynamic drag loads show an amplified dynamic response. In general, and as expected, the highest intermittency values were at the lowest frequencies, below a reduced frequency of 0.01, with damped response at the higher reduced frequencies examined in the analysis. Reduced frequencies below 0.01 represent wavelengths greater than $10\times$ the model length and therefore the model drag response would be expected to be quasi-steady. The damped response at higher reduced frequencies is due to the size of the associated turbulent structures and their inability to produce a correlated change in surface pressures over the entire model. It should be noted that the frequency associated with vortex shedding from the base of the HDV model was above the filter cut-off used in processing the dynamic data, and therefore it was not possible through the aerodynamic admittance analysis to observe any amplified response due to vortex shedding. However, the PSDs of the non-filtered dynamic loads data showed negligible response of the drag component to the vortex shedding frequency, except near 44 m/s where a natural frequency of the model was excited by the vortex shedding phenomena. Some preliminary measurements showed that the side force, the yawing moment, and the rolling moment exhibit a dynamic response to the vortex shedding excitation, as inferred by some measurements performed at wind speeds below 44 m/s.

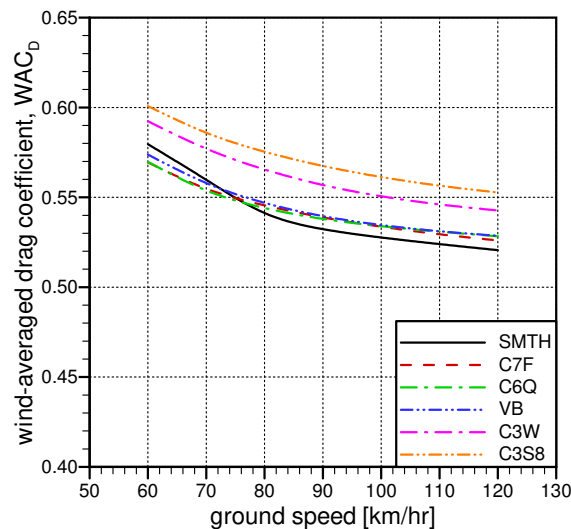


Figure 4.6: Influence of turbulence on the wind-averaged drag coefficient for a range of vehicle ground speeds

In returning to the mean drag coefficient results, a measure of the overall effect of a turbulence condition on the HDV model drag is the wind-average drag coefficient that represents an averaged value for a given road speed given a typical wind strength. For the different turbulent-wind conditions, the variation in wind-averaged drag coefficient for a range of vehicle ground speeds is shown in Figure 4.6. In general the wind-averaged drag coefficient decreases with increasing ground speed because for a given wind strength a pure cross wind of that strength will represent a lower wind angle, and hence less of the high-wind-angle high-drag conditions will be encountered over time. These data were calculated using the highest-speed yaw-sweep distributions for each turbulence condition. In general, for highway speeds above 80 km/h, the smooth-flow conditions provide the lowest wind-average drag coefficient, which then increases with increasing turbulence intensity. The three moderate turbulence conditions (C7F, C6Q, and VB) all show approximately the same wind-averaged-drag values. At 100 km/h ground speed, a 7% difference is observed in the wind-average drag between the smooth flow case ($I_u = 0.6\%$) and the C3S8 case ($I_u = 5.5\%$), indicating a non-negligible effect of turbulence on the long-term performance of an HDV.

The sources of the differences in drag coefficients, both mean and dynamic, between different turbulence conditions are examined in the next section.

4.4 Surface Pressures

HDVs are bluff bodies for which the largest proportion of the drag results from the pressure forces perpendicular to its surfaces, rather than the friction drag that acts parallel to its surfaces. As such, an examination of the changes in surface pressures over the HDV model resulting from different turbulent-flow environments can be used to identify the sources of these drag differences, and identify where sensitivities to turbulence arise.

Figure 4.7 show a sample of the surface pressure data measured under smooth-flow conditions at four different wind angles. Each subplot of the figure shows the variation in mean and rms pressure coefficients for a different region of the model. The locations of the pressure taps and the respective groupings were described in Section 4.2 and shown in Figure 4.2.

The current set of pressure data provides a wealth of information describing the flow field surrounding the HDV model. However, the intent of this section is to identify the influence of turbulence on the flow surrounding the HDV model and therefore only a cursory discussion of the general pressure field is described. The most significant findings regarding surface pressure analysis and specifically the effects of wind angle on the surface pressures for the smooth-flow conditions (Figure 4.7) are:

- The strongest pressure gradients over the HDV model are observed over the rounded front surfaces of the tractor model.
- The highest rms pressure coefficients are observed in regions with separated flows, including the gap region and the trailer base, at all wind angles. With increasing wind angle, strong pressure fluctuations become apparent for the downwind side of the vehicle, the under-body, and the upper-body.

Drag Reduction for HDVs - Progress Toward a Flow Treatment System - Year 2

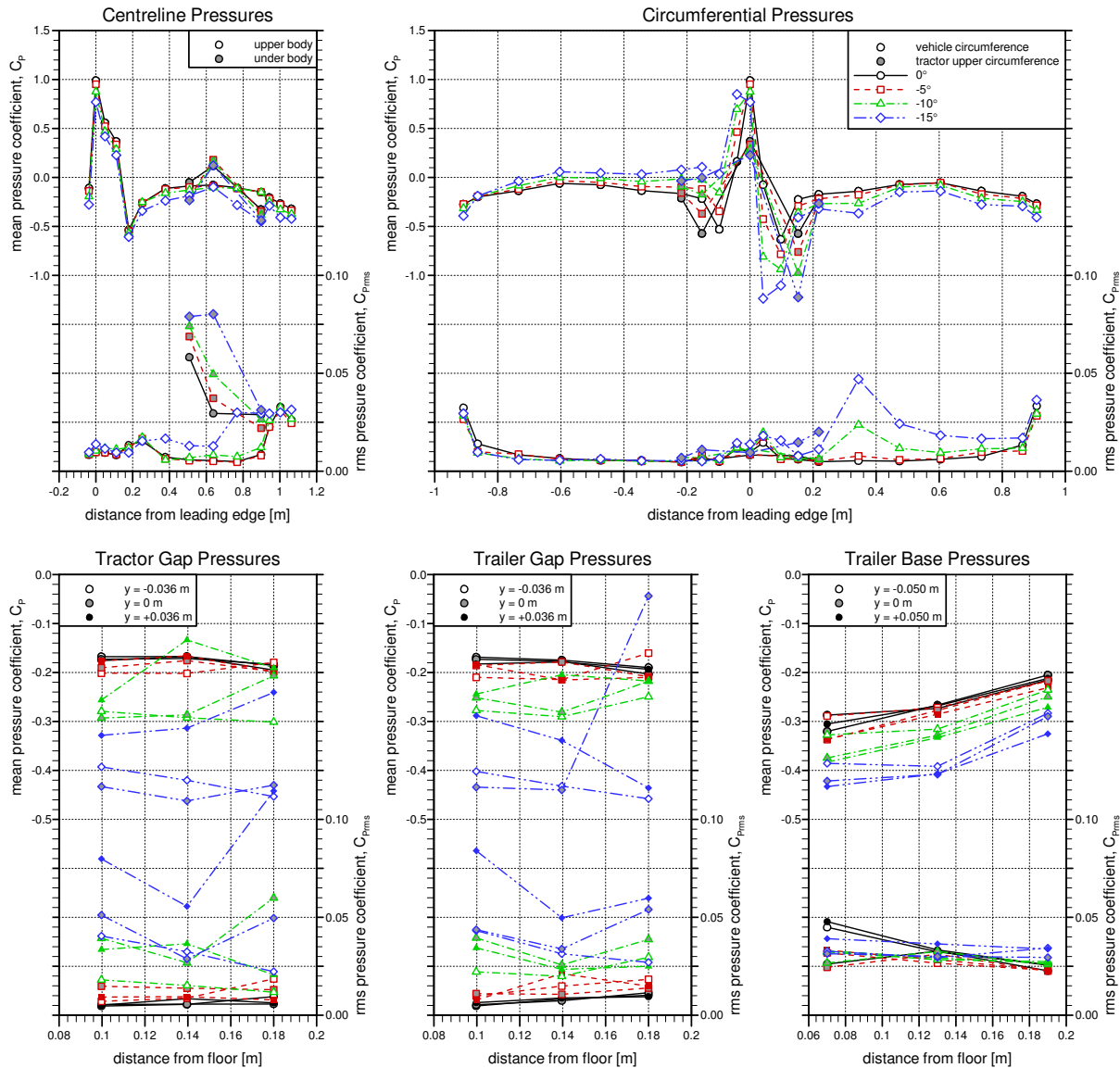


Figure 4.7: Influence of wind angle on HDV pressure distribution in smooth-flow conditions

- With increasing wind angle, the pressure differential across the tractor-trailer gap region drives more flow through the gap, which subsequently caused the flow to emerge on the downwind side of the gap to induce a flow separation over the trailer side surface indicated by the high pressure fluctuations on the downwind side of the trailer.
- The trailer base region shows decreased mean pressure with increasing wind angle, that contributes to a greater front-to-back pressure difference across the HDV model, leading to a higher drag coefficient.
- The base pressures show the lowest influence of wind angle on the pressures fluctua-

tions. As will be shown later, the base pressure fluctuations are influenced by the vortex shedding phenomenon in the wake structure that is not influenced in a significant manner by the operating conditions.

To identify the effects of turbulence on the surface pressures over the HDV model, pressure data is shown in Figures 4.8 and 4.9 for wind angles of 0° and -10° , respectively. Instead of showing the absolute mean pressure coefficients, these plots show the difference in mean pressure coefficient from the equivalent smooth-flow condition. They also show the rms pressure coefficients for all conditions including smooth flow. To prevent clutter in the plots, only three turbulence conditions are compared to the smooth-flow results, those being the C6Q, the VB, and the C3W conditions. However, any trends noted with regards to the effect of turbulence are also consistent with the results of the C7F and C3S8 conditions.

In general, it appears that the regions on the HDV model that show the greatest influence from turbulence on the mean pressures, are the same locations that show the largest magnitude, and variations thereof, in pressure fluctuations. This implies that the turbulence in the wind affects the net pressures that contribute to the vehicle drag. This is most prominently observed in the *Centreline Pressures* and *Circumferential Pressures* plots, for both wind angles, over the front surfaces of the HDV model. Here, differences in the mean pressure coefficients in excess of 0.05 (meaning in excess of 5% of the dynamic pressure of the wind) are observed. The magnitudes of the differences are not proportional in any noticeable manner with turbulence level, and therefore it appears that just the presence of elevated turbulence has a measurable influence on the surface pressures. To put into context the potential significance of such a change in surface pressure, a consistent 0.05 change in pressure coefficient over one particular drag-influencing surface (front of tractor or base of trailer) would result in a 10% change to the model drag coefficient. These pressure differences are not uniform over an entire surface and therefore the effects are not as significant as 10%, but the potential for large differences in the drag associated with particular surfaces or components is evident.

The influence of turbulence on the surface pressures is much more evident for the -10° wind angle case than the 0° case. Under such a cross-wind condition, differences in mean pressures between smooth and turbulent winds become apparent over the upper aft surface of the trailer and in the gap region between the tractor and trailer. These greater differences in mean pressures are also associated with greater differences in pressure fluctuations. In contrast, the influence of turbulence on the base pressures is similar for both wind angles.

Of interest in the pressure data are some distinct differences between the C6Q and VB cases that have similar turbulence intensity magnitudes but largely different length scales and wind spectra. Despite the similar magnitudes in turbulence intensity, the magnitude of pressure fluctuations is generally higher over the model for the C6Q condition. In the *Circumferential Pressures* plots, the strongest pressure fluctuations for the smaller length scale condition (VB) is observed at the centre port on the front face of the tractor. In contrast, the large length scale condition (C6Q), and similarly the smooth-flow and C3W conditions, have the strongest pressure fluctuations at the pressure taps on the front corners adjacent to the centre tap. This effect was further investigated by examining the simultaneous changes in surface pressure fluctuations over the HDV model surface (not shown here), from which it was evident that the larger length scale conditions show an antisymmetric pattern of pressure fluctuations (strong

Drag Reduction for HDVs - Progress Toward a Flow Treatment System - Year 2

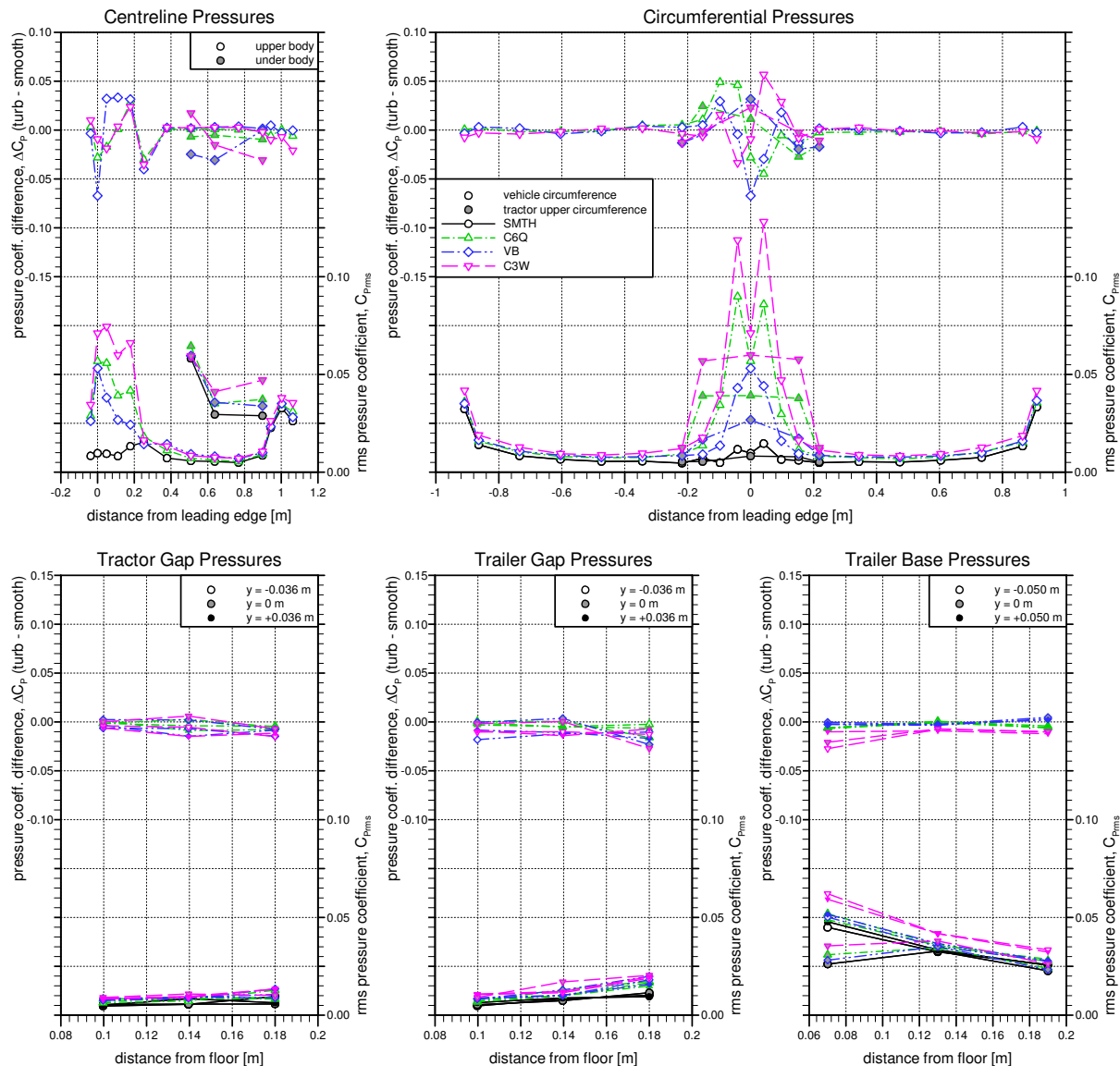


Figure 4.8: Influence of turbulence HDV pressure distribution at 0° wind angle

negative correlation) about the model centreline that appeared to represent a change in the wind angle from side-to-side. Conversely, the smaller length scale condition showed much lower level of correlation about the centreline resulting from the smaller scales of the turbulent structures. The difference in length scale also appears to influence the magnitude of mean pressures over some regions of the HDV model. For example, the aft roof pressures show much greater sensitivity to the larger-scale turbulence than the smaller-scale turbulence.

As noted above, turbulence influences some surfaces of the HDV model more than others. To identify better the influence of turbulence on the model surface pressures, the spectra of pressure fluctuations provide further evidence of the differences, or lack thereof. Figure 4.10 shows

Drag Reduction for HDVs - Progress Toward a Flow Treatment System - Year 2

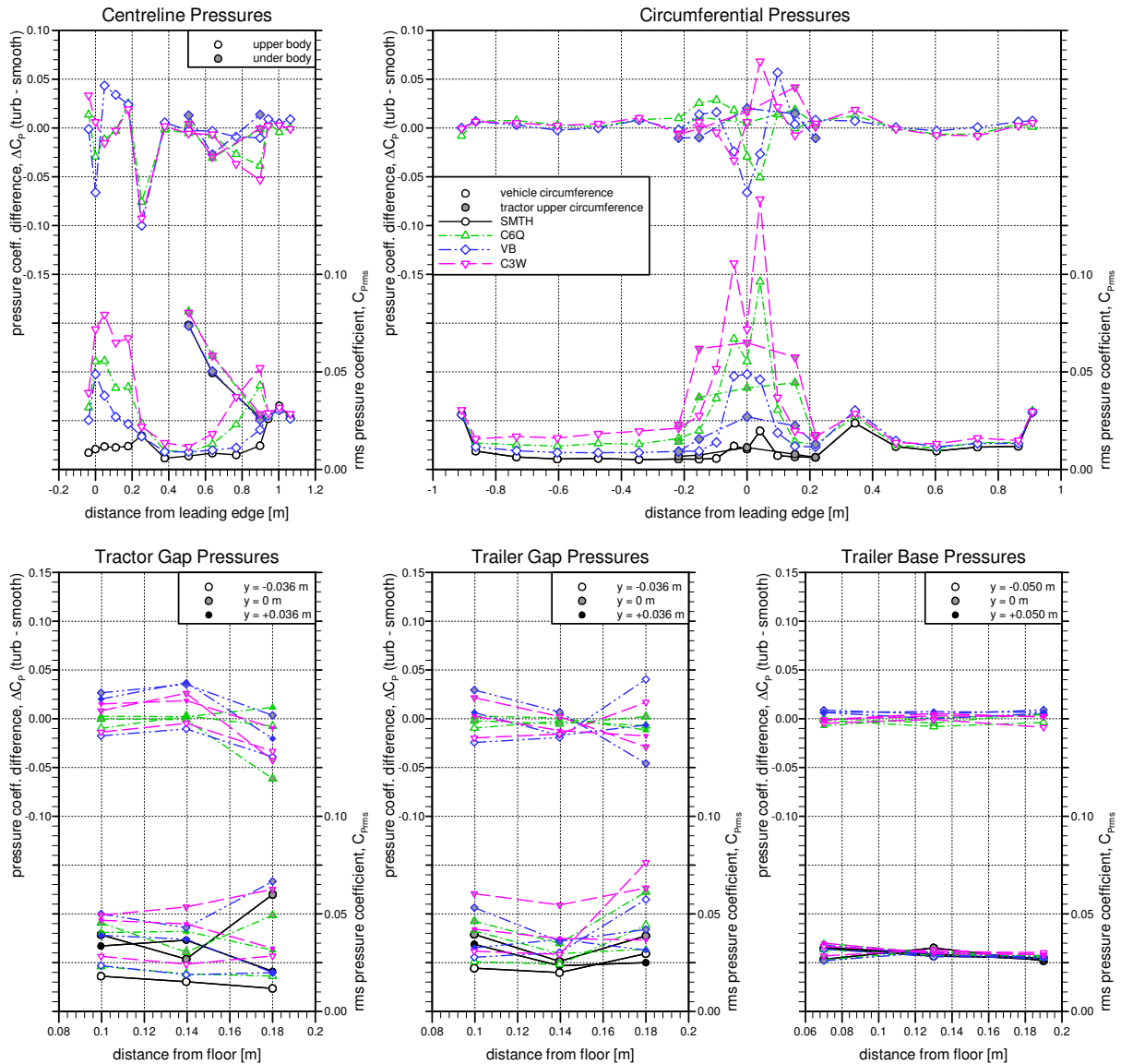


Figure 4.9: Influence of turbulence HDV pressure distribution at -10° wind angle

the pressure spectra measured at four pressure taps, for wind angles of 0° and -10°, under the smooth-flow, C6Q, VB and C3W turbulence conditions. It is to be noted that a distinct peak in the C3W pressure spectra at a reduced frequency of about 0.07 is often observed and it is a result of a strong peak in the wind spectra for this conditions, not a result of a model-induced flow mechanism.

At the front corner of the model (upper row of plots in Figure 4.10), where the greatest pressure fluctuations were observed for the C6Q and C3W conditions, the pressure-coefficient spectra show distinct differences between the four wind conditions. This is also apparent at both wind angles. As identified from the rms levels, the smooth-flow condition shows the lowest fluc-

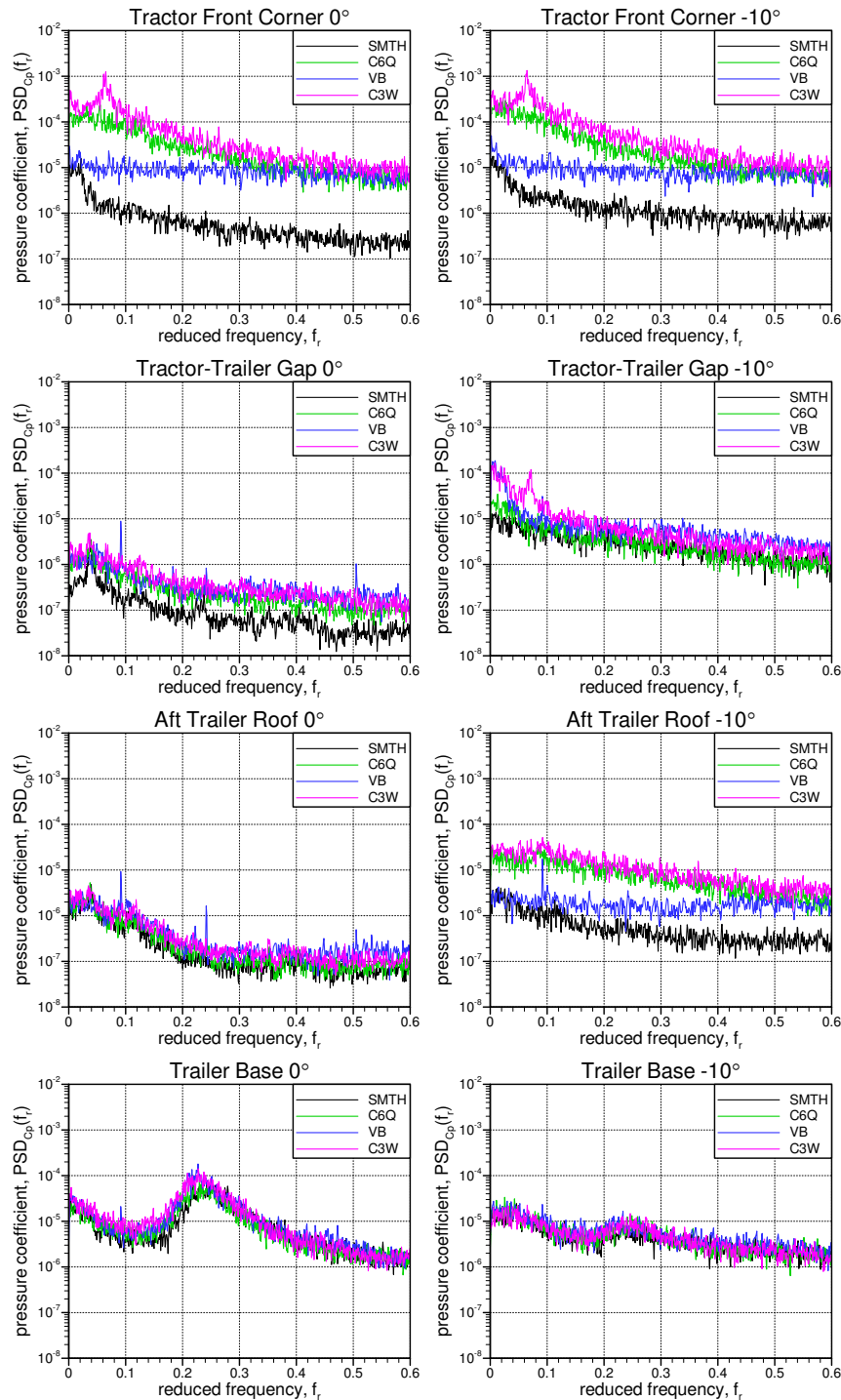


Figure 4.10: Surface-pressure spectra at four locations, for 0° and -10° wind angles, under the smooth-flow, C6Q, VB and C3W conditions

tuation energy, followed by the VB case, then the C6Q case, and with the C3W case showing the greatest energy level. In general the energy in the pressure fluctuations is highest for the lowest frequencies. Of particular interest is the difference between the C6Q and VB conditions which have similar turbulence intensities but the C6Q condition has a greater proportion of the turbulence energy at low frequencies. This is similar to what was observed in the wind spectra measurements for these two cases (compared in Figure 3.13), particularly the v and w component spectra, for which the VB case shows a much flatter distribution over the low frequency range than the C6Q case. This implies that the surface pressure fluctuations are more susceptible to large-scale/low-frequency turbulence.

In the gap region (second row of plots in Figure 4.10), the pressure spectra show similar trends for all turbulence conditions. At 0° wind angle, the three turbulent-flow conditions show similar energy content. At -10° wind angle, the VB and C3W conditions show higher energy at reduced frequencies below 0.05. Here, the VB condition exhibits higher pressure fluctuations than the C6Q case, unlike the exterior front surface described in the preceding paragraph that show much greater energy from the C6Q condition.

The aft-trailer-roof spectra (third row of plots in Figure 4.10) shows the greatest difference between the two wind angle conditions. At 0° wind angle, the spectra are all similar with low energy across the distribution. At the higher wind angle of -10° , the differences between the wind conditions are similar to what was observed on the front face of the HDV model, implying that the flow over this surface at higher wind angles is influenced more by the freestream winds than the upstream components of the HDV model.

The pressure spectra at the base of the model show the smallest influence of the freestream turbulence condition. The spectra are nearly indistinguishable in this region and are dominated by the turbulence in the wake structure. A peak in the spectra is observed at a reduced frequency between 0.20 and 0.25 which is associated with a vortex shedding phenomenon in the wake. This range of frequencies corroborates what was identified for the vortex shedding frequency behind a 10% scale HDV model in a sister project under the eTV II program (McAuliffe, 2013c). The strength of the vortex shedding is attenuated with increased wind angle, as identified by the difference between the 0° and -10° spectra.

Different freestream turbulence environments influence the flow over the HDV model differently. From the measurements presented here, larger-length-scale turbulence on the order of the width of the model appears to have a greater influence on mean and dynamic surface pressures than turbulence of much smaller scale.

4.5 Summary

The results in this section of the report have demonstrated some effects of turbulent wind conditions on a simplified but representative HDV model. To summarize the results, the following general conclusions have been drawn:

- Turbulence intensity has an influence on the mean drag coefficient of the HDV model, particularly at low wind angles ($\pm 5^\circ$ range) where a 10% difference in zero-wind-angle

drag coefficient was observed for the range of turbulence conditions examined.

- A 7% increase in wind-averaged-drag coefficient (for 100 km/h ground speed) was observed between the smooth-flow condition and the highest-turbulence condition (C3S8) that has a longitudinal turbulence intensity of approximately 6%.
- For conditions that most represent on-road turbulence conditions (C6Q), a moderate increase in wind-averaged-drag coefficient was observed (2%) over the smooth flow conditions.
- Mean and dynamic surface pressures are influenced by freestream turbulence, such that the surfaces of the model with the greatest differences in rms pressure are the same regions that show the greatest differences in mean pressures.

Although the wind load measurements don't show a significant difference in the mean wind loads, and hence mean drag coefficient, of the HDV model for moderate levels of turbulence (C7F, C6Q, and VB conditions) relative to smooth-flow conditions, the pressure measurements (mean, rms, and spectra) show some distinct differences over various regions of the HDV model. The manner in which mean surface pressures are influenced by turbulence, more so over some regions of the model than others, implies that differences in drag-reduction from various technologies may also be influenced by turbulence, even for the moderate turbulence levels that are most commonly experienced on the road. The regions for which the performance of drag reduction technologies will likely be influenced by turbulence, based on the surface pressure measurements presented here, are:

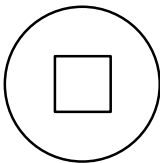
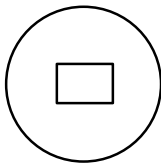
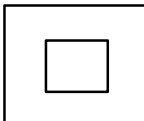
- the tractor-trailer gap region;
- changes to the shape of the trailer upper body; and
- the trailer under-body region.

5. Intermediate Scale Verification of the Flow Treatment System Concept

5.1 Problem Description

Based on the on-road measurements of Section 2, the small-scale FTS development work in Section 3, and the HDV-drag sensitivity-to-turbulence study in Section 4, a concept for the large-scale FTS was selected. The small-scale C6Q concept was found to be most appropriate for application with the 30%-scale HDV model being built for the NRC 9 m Wind Tunnel. One concern for scaling the selected concept based on measurements in the NRC 1.0 m \times 0.8 m Pilot Wind Tunnel, which has a rectangular settling chamber, is the ability to achieve lateral uniformity of the wind characteristics in the test section of the NRC 9 m Wind Tunnel, which has a circular settling chamber. Achieving such uniformity for a circular-to-rectangular shaped contraction between the settling chamber and the test section is not a trivial task when considering a flow condition with height-varying turbulence properties. To mitigate the risk associated with this scaling issue, an intermediate-scale demonstration was performed in the NRC 2 m \times 3 m Wind Tunnel which has a more-suitable circular-to-rectangular contraction shape. The differences in the shapes and sizes of the three wind-tunnel contractions are shown in Figure 5.1. In addition to the shape differences, the contraction ratio (settling-chamber-area to test-section-area) of the NRC 9 m Wind Tunnel is greater than that of the NRC 1.0 m \times 0.8 m Pilot Wind Tunnel (6.0 versus 3.6). The NRC 2 m \times 3 m Wind Tunnel has a contraction ratio of 8.5, and therefore will provide a way of evaluating any influences of contraction ratio on the

Figure 5.1: Dimensions of the settling chamber and test section with the contraction ratio for three NRC Wind Tunnels

	NRC 9m x 9m wt	NRC 2m x 3m wt	NRC Pilot wt
			
Settling Chamber	Round, 25m diameter	Round, 7.5m diameter	Rectangular, 1.6m x 1.8m
Test Section	Square, 9.1m x 9.1m	Rectangular, 1.9m x 2.7m	Rectangular, 0.8m x 1.0m
Contraction ratio	6	8.5	3.6

turbulence properties in the test section.

One of the requirements was for the FTS to be deployed or removed in a time period no longer than five hours in the NRC 9 m Wind Tunnel, to avoid excessive costs during a test program. Turbulence generation using large obstacles such as spires is generally implemented using solid structures to withstand the wind loads. Installation of a large solid structure in the NRC 9 m Wind Tunnel would not conform to the quick installation/removal requirement. The lower wind speeds in the settling chamber compared to the test section provides the benefit that the wind loads will be significantly lower than what the model would experience, and therefore a simpler and lightweight installation is feasible.

An added consideration for the quick installation/removal requirement is to minimize the number of spires in the settling chamber. Results from the small-scale concept study in Section 3 showed that the spires can have increased spacing without significantly affecting the flow properties in the test section. The intermediate-scale demonstration in the NRC 2 m \times 3 m Wind Tunnel was also used as a means to evaluate the smallest number of spires possible for the full-scale FTS in the settling chamber of the NRC 9 m Wind Tunnel.

5.2 Approach

In order to generate the turbulence characteristics required in the test section of the NRC 2 m \times 3 m Wind Tunnel, it was necessary to use large obstacles that create the appropriate intensity and size of turbulence structures in proportion with the size of a typical model of HDV. The initial configuration of the intermediate-scale FTS (ISFTS) was based, in part, on the C6Q configuration for the small-scale FTS (SSFTS) measurements presented in Section 3. However, several changes to the concept were implemented for quick-installation/teardown considerations. This included a change to the planform shape (wedge-shaped instead of flat), and increased spacing to minimize the number of spires required. The setup in the NRC 2 m \times 3 m Wind Tunnel was designed to allow changes to the base width of the spires and changes to the spacing. A description of the concept, its design, and the various configurations, is provided in the next section (Section 5.3).

Measurements of the wind velocity in the test section were performed using four Cobra probes. These probes can measure the instantaneous three wind velocity components of the flow. A survey of the flow characteristics was performed using a vertical traverse on which the four Cobra probes were mounted (see Figure 5.2). Vertical profile measurements were done at 5 cm from the floor to 1 m high by increments of 10 cm (from 10 cm to 100 cm) and for 12 lateral positions. Three lateral positions of the traverse rig allowed coverage of these 12 positions (see Figure 5.3). With the optimized FTS configuration, additional measurements were performed at upstream and downstream locations. The three longitudinal positions of the Cobra probes were defined to evaluate the change in turbulence characteristics along the test section (see Figure 5.3). Measurements with different horizontal and vertical spacing between the four probes were carried out at two longitudinal locations to evaluate the spatial correlations of the turbulence (see Figure 5.4).

5.3 Design

THIS SECTION REDACTED



Figure 5.2: Left: Downstream view of the vertical traverse for measurements at the centre of the test section with the 4 Cobra probes mounted on a horizontal bar and spaced by 15 cm. Right: Side view of the vertical traverse during wind on measurements

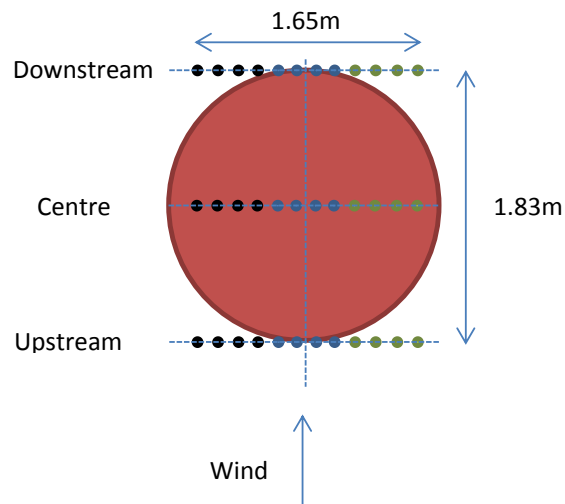


Figure 5.3: Sketch of the top view of the test section with the 12 lateral positions and the 3 longitudinal positions where wind measurements were performed using Cobra probes. Black: Vertical traverse mounted on the left side of the test section, Blue: Vertical traverse mounted in the centre of the test section and, Green: Vertical traverse mounted on the right side of the test section

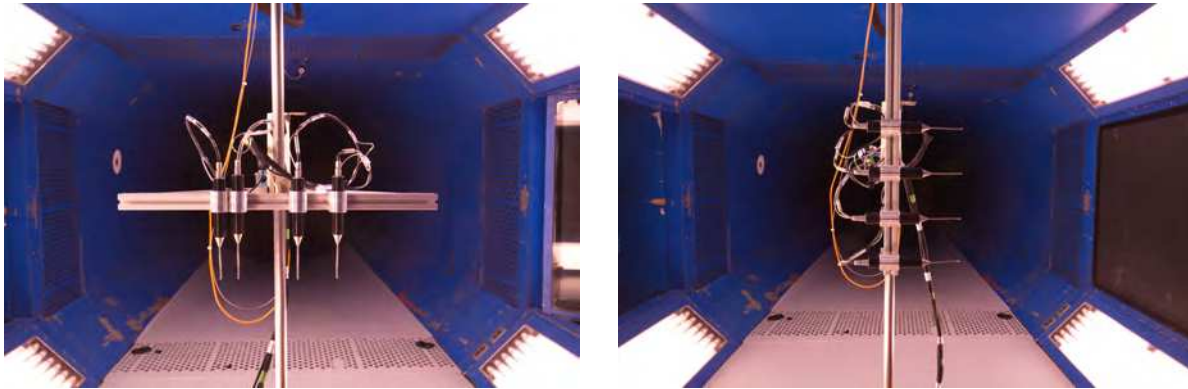


Figure 5.4: Left: Cobra probes mounted on the bar for the horizontal spatial correlation. Right: Cobra probes mounted on the bar for the vertical spatial correlation

5.4 Results

The Cobra probe data was processed in the same manner as the Small-Scale FTS (SSFTS) measurements from the NRC 1.0 m \times 0.8 m Pilot Wind Tunnel (presented in Section 3). Flow characteristics are defined by the three components of wind speed (longitudinal- u , lateral- v , and vertical- w), their associated turbulence intensities (I_u , I_v , and I_w), the turbulence length scales (L_u^x , L_v^x and L_w^x), the spectra of the wind speed components ($PSD_{u,v,w}$), the vertical and the horizontal cross-correlation distributions of the three components (R_{uu} , R_{vv} , and R_{ww}). A reference length (L_{ref}) of 0.075 m was used for scaling the turbulence characteristics measured in the NRC 2 m \times 3 m Wind Tunnel, to allow comparison to the SSFTS measurements ($L_{ref} = 0.03$ m) and the on-road measurements ($L_{ref} = 1.0$ m).

The first analysis is related to the spectra of the 3 components of the flow as measured centred longitudinally in the test section and, taking the mean value of 12 lateral positions, covering the area between -0.825m to 0.825m from each side of the centre. Figure 5.5 shows the results obtained with the 6-spire configuration (the baseline configuration) compared to the small-scale C6Q configuration results from the SSFTS study, and the on-road measurement for different levels of traffic density. It is clear that the ISFTS designed for the NRC 2 m \times 3 m Wind Tunnel provided similar turbulence characteristics than the concept developed for the NRC 1.0 m \times 0.8 m Pilot Wind Tunnel, confirming the design methodology used. The comparison with the on-road turbulence measurements is as good as what was observed for the SSFTS. The major difference between the ISFTS and SSFTS spectra are at the lowest frequencies, where the ISFTS shows lower turbulence energy for the u component and higher energy for the v and w components. This is likely a result of the greater contraction ratio of the NRC 2 m \times 3 m Wind Tunnel compared to the NRC 1.0 m \times 0.8 m Pilot Wind Tunnel (8.5 versus 3.6). It is expected that this effect will be of lower magnitude for the NRC 9 m Wind Tunnel which has a contraction ratio of 6.

The second analysis is related to the number of spires and the lateral uniformity of the flow in the test section. Figures 5.6 and 5.7 show the results for the 6-spire and 5-spire configurations, respectively. The data are presented so that the results for longitudinal, lateral and vertical

wind component are in the first, second and third column. The first row represents the mean wind speed, the second row shows the intensity of turbulence and the third row provides the turbulence length scales.

In examining Figures 5.6 and 5.7, one is looking for as much lateral uniformity as possible to ensure that an HDV model installed in the test section will experience similar turbulent-flow conditions across its width, even at high yaw angles. The 5-spire configuration shows a much greater level on non-uniformity than the 6-spire configuration, particularly for the lateral and vertical components. It should be noted that there was no discernible difference in the laterally-averaged wind spectra between the 5 spire and 6 spire configurations. Based on the similarity of the ISFTS wind spectra to the SSFTS and to the on-road measurements, and the results of the lateral uniformity analysis, the 6 spire configuration was chosen as the most appropriate from which the design of the large-scale FTS system for the NRC 9 m Wind Tunnel could be developed.

Although the 5-spire configuration shows a greater level of lateral non-uniformity, the 6-spire configuration does not provide perfectly-uniform conditions. To assess better the magnitude of the non-uniformity, the sources of the non-uniformities, and their potential implications, two sets of plots are provided in Figures 5.8 and 5.9. Figures 5.8 shows vertical profiles of the laterally-averaged flow characteristics (lines with markers) with their associated minimum and maximum values (lines without markers with associated colours). Figure 5.9 contrasts the lateral distributions of the flow properties at 0.2 m from the test-section floor for several sets of measurements. In addition to the 6-spire and 5-spire configurations at the centre of the turntable, a repeat of the 6-spire centre data is shown, along with the data sets measured upwind and downwind. All data sets show similar profiles averaged laterally in Figure 5.8, the 5-spire and the downwind configurations showing the greatest spread, represented by the largest difference between minimum and maximum values.

The middle column of Figure 5.9 compares the lateral variation in the mean wind character-

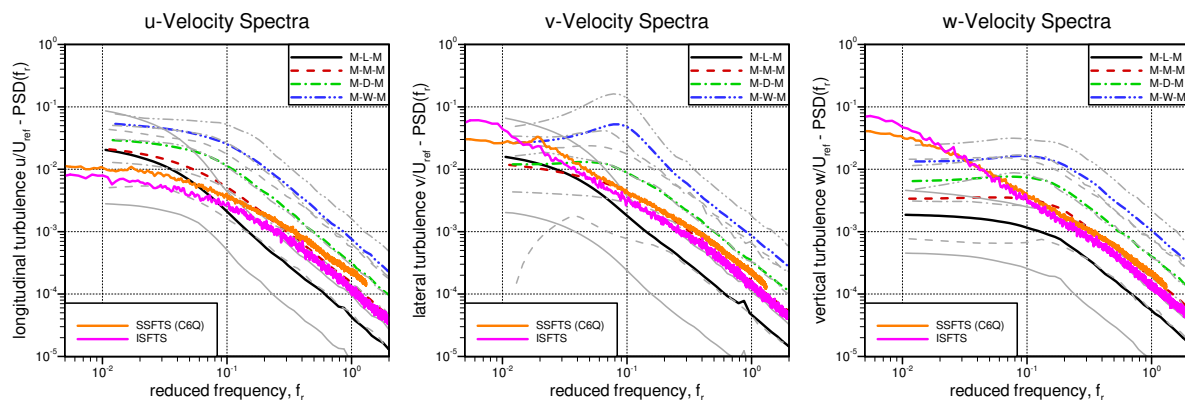


Figure 5.5: Spectrum of the longitudinal, lateral and vertical wind components for configurations tested in the NRC 2 m × 3 m Wind Tunnel (ISFTS) compared with results from NRC 1.0 m × 0.8 m Pilot Wind Tunnel (SSFTS) and on-road measurements

Drag Reduction for HDVs - Progress Toward a Flow Treatment System - Year 2

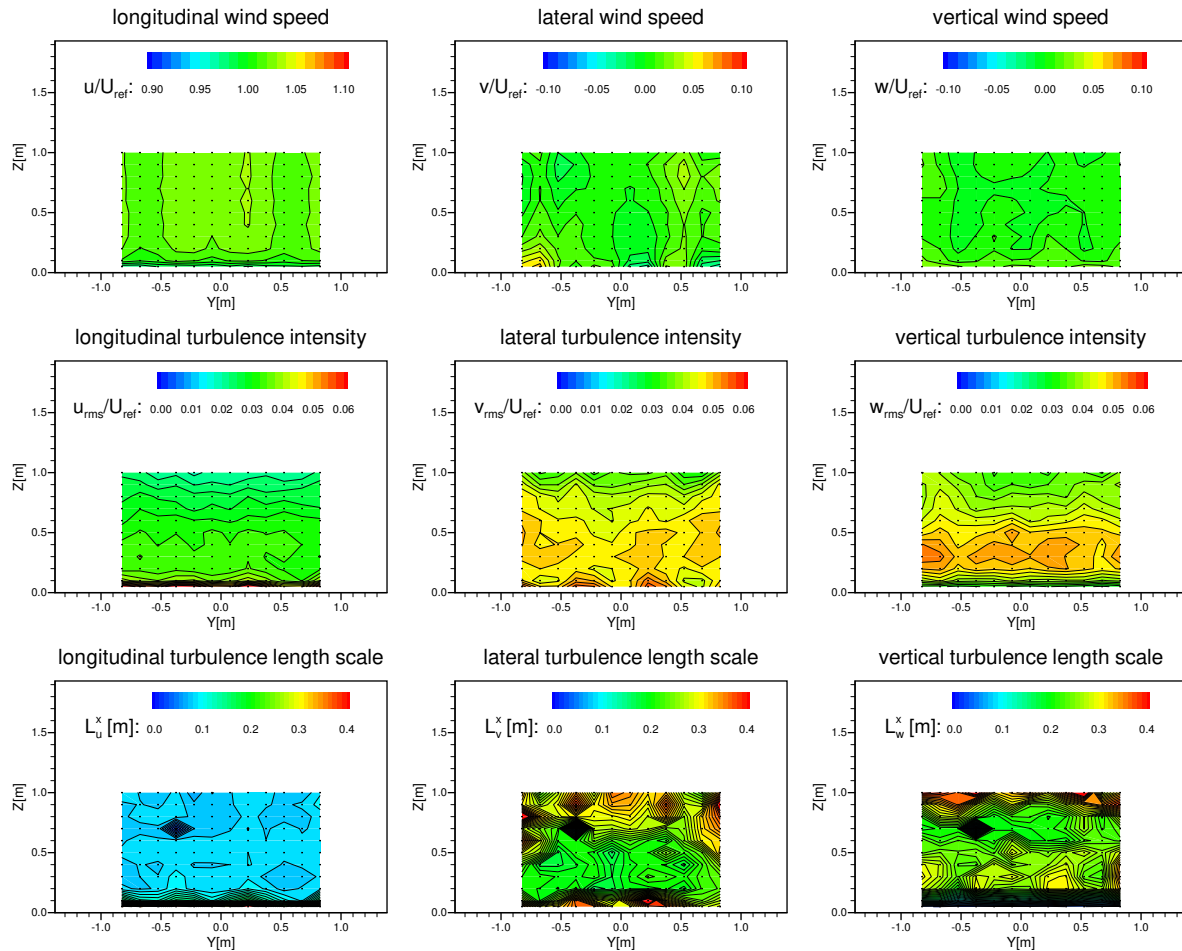


Figure 5.6: Mean wind-speed ratio, turbulence intensity and turbulence length scales for the longitudinal, lateral and vertical wind components for the configuration using 6 spires

istics (top), the turbulence intensities (middle) and the turbulence length scales (bottom) for the 6-spire and 5-spire configurations. In general, and as previously described, the 6-spire configuration provides lower variation in the wind characteristics laterally across the test section. The turbulence properties of the longitudinal wind component (u) does not show much lateral variation. The turbulence properties of the lateral and vertical components (v and w) show greater lateral variation that reflects the patterns of the settling chamber spires, with either a high or low peak at centreline whether there is a spire (5-spire configuration) or gap (6-spire configuration) at the centre of the settling chamber. However, the mean wind speed and lateral wind angle exhibit the same pattern for the 6-spire and 5-spire configurations. This has been attributed to the wooden-panel floor structure to which the spires were mounted in the wind tunnel.

To characterize fully the flow in the test section, further measurements were collected for the

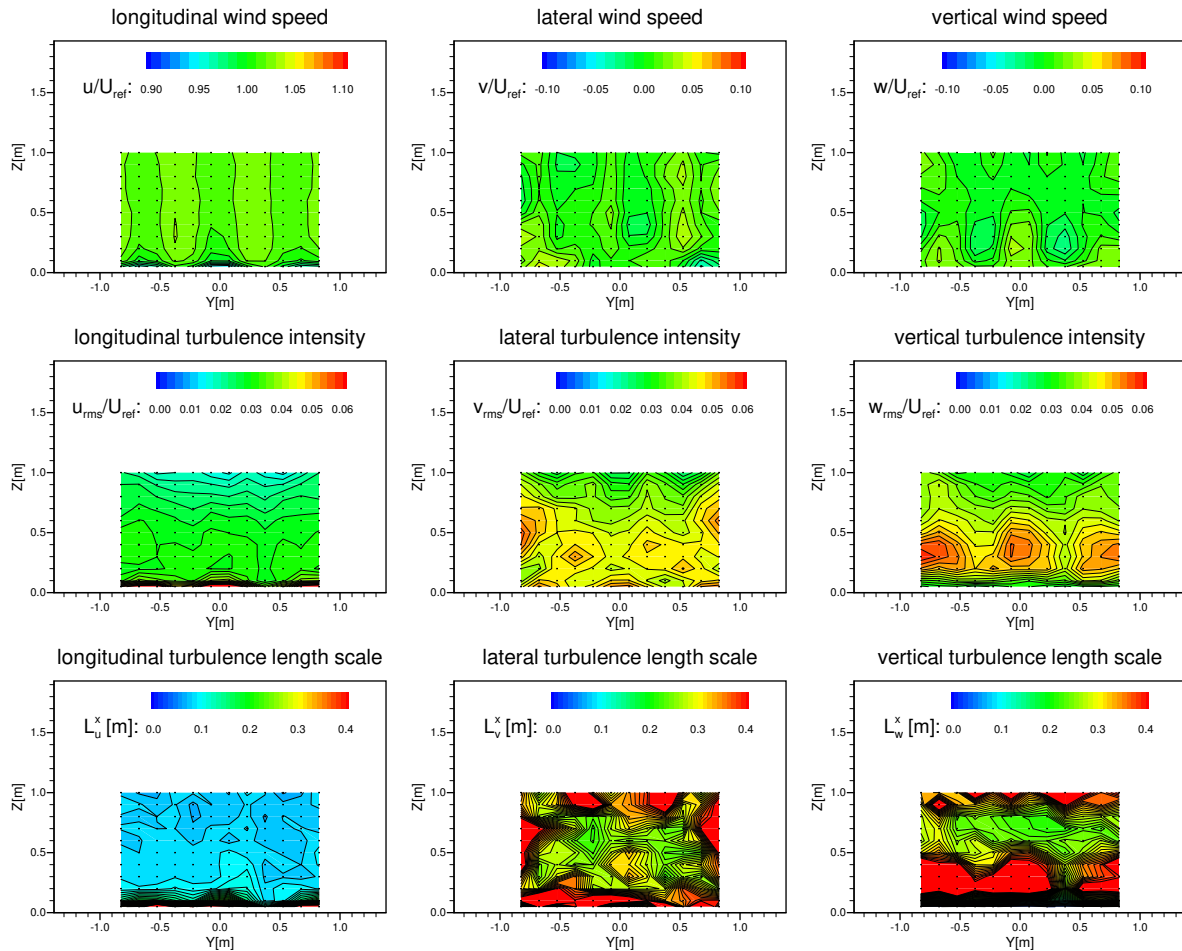


Figure 5.7: Mean wind-speed ratio, turbulence intensity and turbulence length scales for the longitudinal, lateral and vertical wind components for the configuration using 5 spires

6-spire configuration. A repeat case was performed to evaluate the capacity of the spire system to reproduce the same flow condition in the test section. The repeat was performed after re-installing the 6-spire arrangement, after the 5-spire configuration was deemed inadequate. Measurements were also performed at two different longitudinal positions of the vertical traverse to see the impact on the mean flow characteristics. The upstream and downstream positions were located 0.92 m from the centre of the turntable. These three additional cases are also shown in Figure 5.8 and 5.9 contrasted against the baseline 6-spire centre-plane measurements. The data shows first that the results associated with the repeat of measurement case compares well with the first set of measurements done at the same longitudinal location. However, some differences can be observed for the measurements done at the upstream and downstream positions. It is primarily the lateral and vertical wind components that show a variation compared with the measurements done at the turntable centre. In general, the mean value of turbulence

Drag Reduction for HDVs - Progress Toward a Flow Treatment System - Year 2

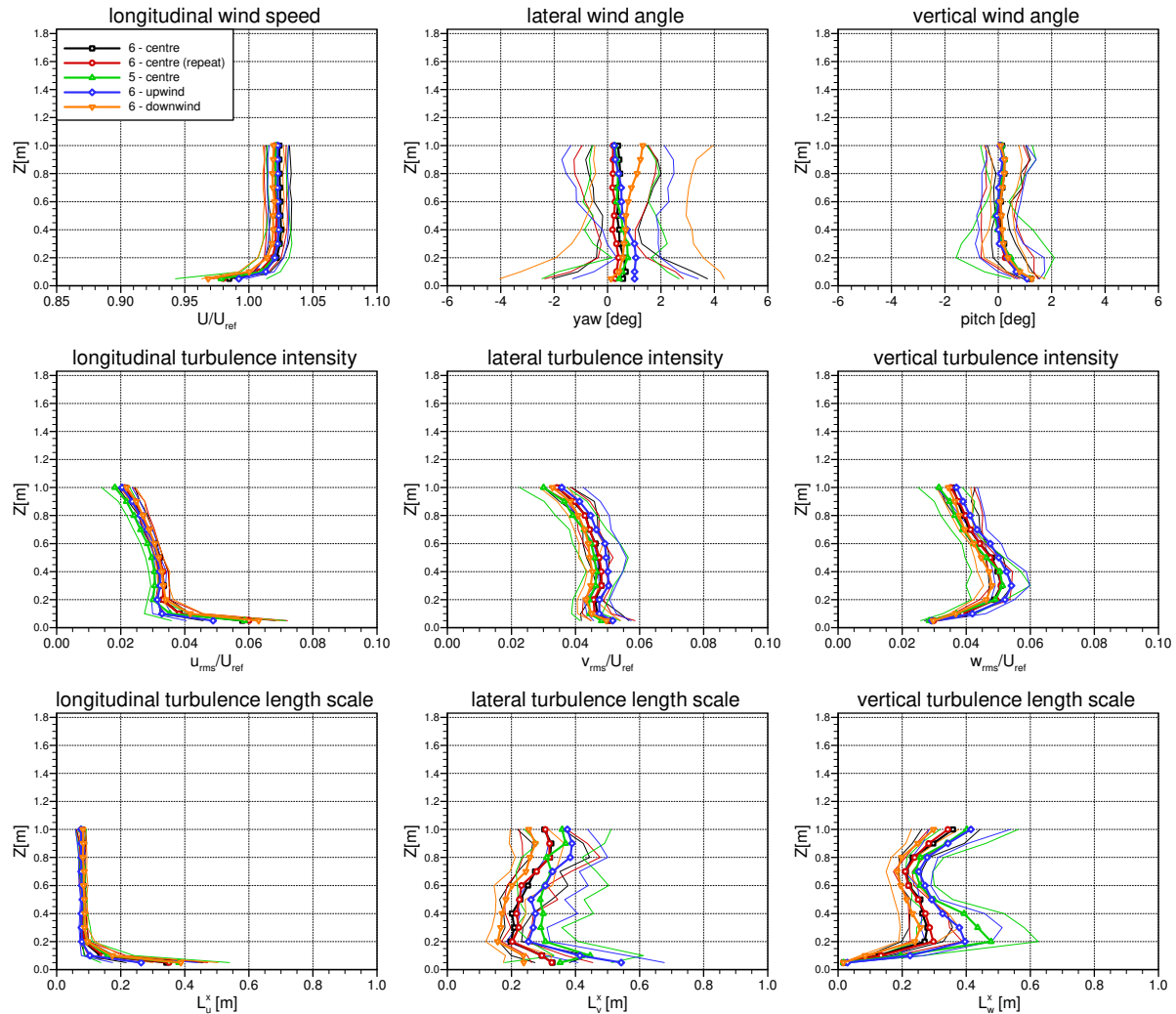


Figure 5.8: Mean value of the 12 lateral positions for the wind ratio, turbulence intensity and turbulence length scales to characterize the 6-spire configuration

intensities and turbulence length scales were higher upstream and lower downstream, similar to what was observed for the SSFTS measurements. The downwind location also shows a greater level of non-uniformity in the flow characteristics. Table 5.1 presents a comparison of the mean values of the turbulence intensity and turbulence length scales as measured 0.2m above the floor for the different configurations tested.

Finally, measurements of the vertical and horizontal spatial correlations of the turbulence were performed at two longitudinal locations. The vertical and horizontal correlation distributions measured at the turntable centre are shown in Figures 5.10 and 5.11, respectively, compared to the SSFTS and sample on-road measurements. A good comparison is observed between the SSFTS and ISFTS data, providing further confidence that the full-scale FTS will deliver

Drag Reduction for HDVs - Progress Toward a Flow Treatment System - Year 2

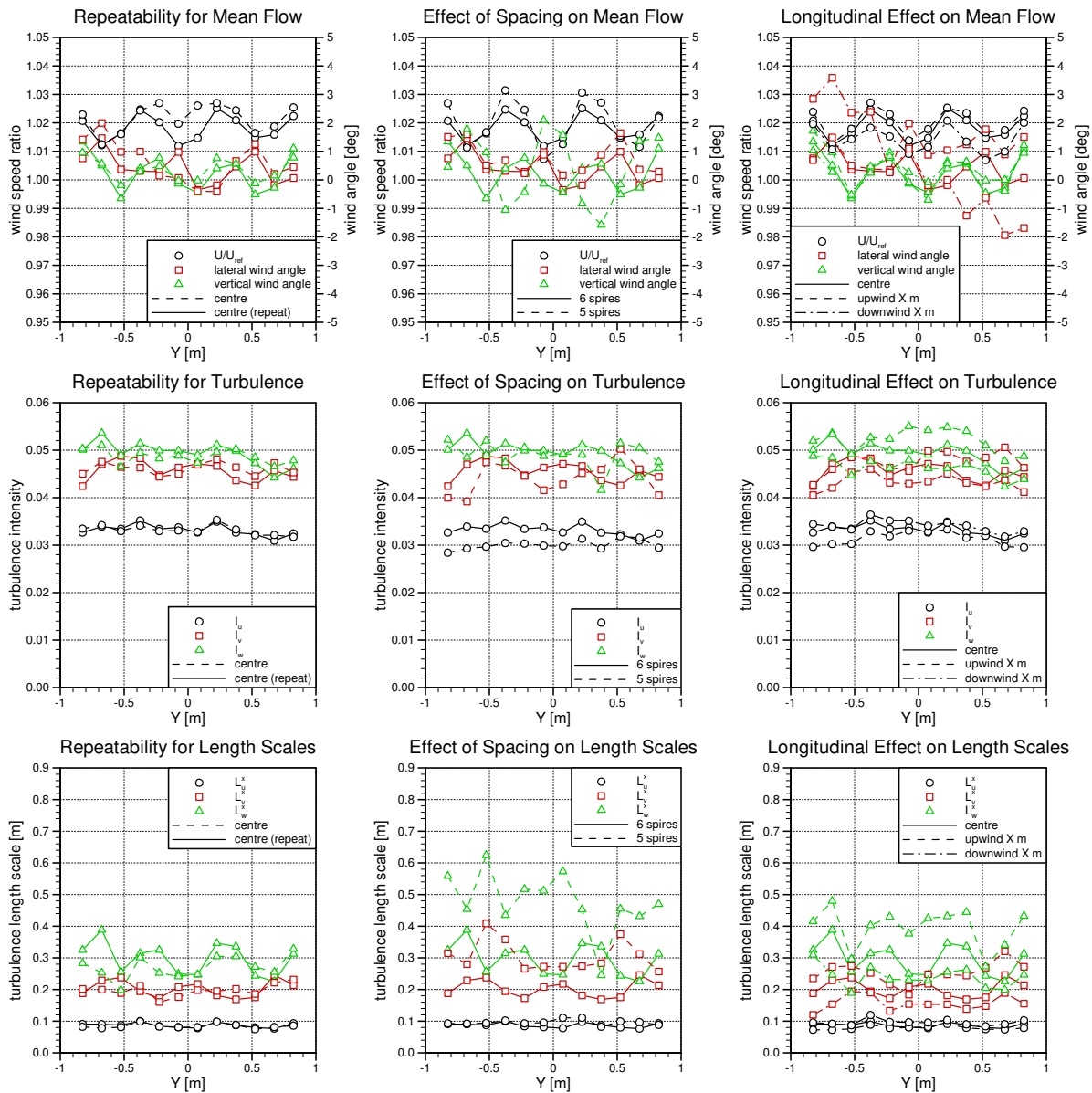


Figure 5.9: Lateral distributions of flow, ISFTS Measurements

representative on-road turbulence conditions. Correlation distributions at the downstream longitudinal location showed, although not presented here, the same trends as what was observed for the C6Q configuration during the SSFTS measurements. Some slight changes in the correlation magnitudes were observed with longitudinal distance, but not by any significant magnitude.

Table 5.2 compares the turbulence characteristics measured in the ISFTS demonstration compared to the SSFTS selected concept and the Moderate Terrain, Moderate Traffic, Moderate

Table 5.1: Mean lateral values of the 3-component of turbulence intensity and length scales at 20 cm from the floor for the cases with 6 spires and 5 spires.

	I_u (%)	I_v (%)	I_w (%)	L_u^x (m)	L_v^x (m)	L_w^x (m)
6 spires centre	3.3	4.6	4.8	0.08	0.20	0.27
5 spires centre	3.0	4.4	4.9	0.10	0.31	0.48
6 spires repeat	3.3	4.5	4.9	0.09	0.20	0.30
6 spires upstream	3.1	4.8	5.2	0.08	0.25	0.40
6 spires downstream	3.4	4.3	4.6	0.10	0.16	0.24

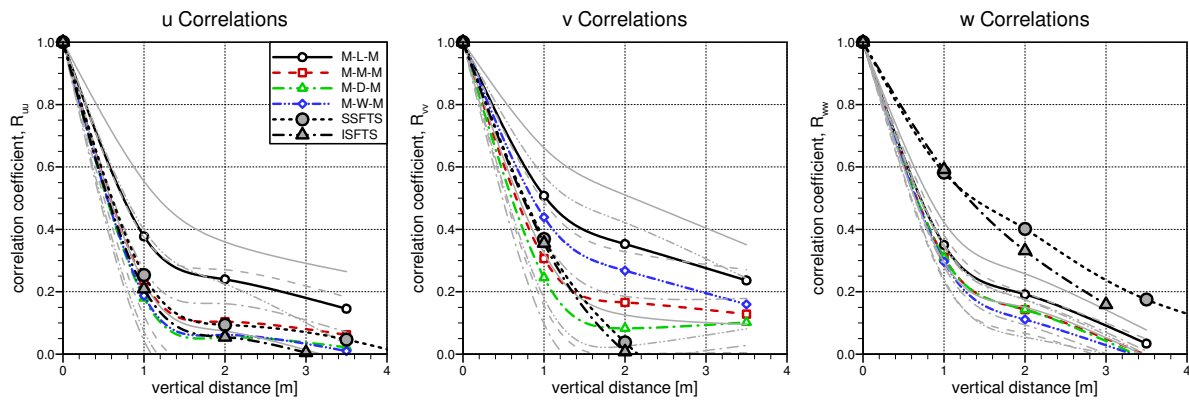
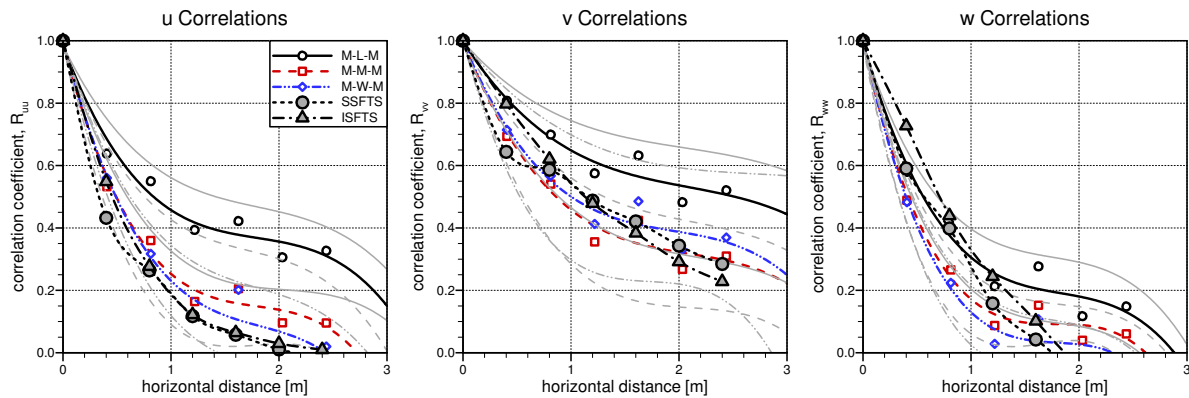
**Figure 5.10:** Vertical spatial correlation as measured at the center of the test section for the 3-wind components**Figure 5.11:** Horizontal spatial correlation as measured at the center of the test section for the 3-wind components

Table 5.2: Comparison of SSFTS and ISFTS turbulence characteristics with the target on-road condition (M-M-M: Moderate Terrain, Moderate Traffic, Moderate Winds)

Component	Turbulence Intensity, I			Turbulence Length Scale, L^x		
	Road	SSFTS	ISFTS	Road	SSFTS [†]	ISFTS [†]
u	4.0 %	3.8 %	3.3%	4.7 m	1.2 m	1.2 m
v	3.5 %	4.8 %	4.5%	1.9 m	2.7 m	2.7 m
w	3.1 %	5.0 %	4.9%	0.6 m	3.5 m	4.0 m

[†] full-scale equivalent

Winds target condition selected from the on-road measurements. As with the SSFTS results, the v and w components of the ISFTS configuration show a higher turbulence intensity resulting from the higher energy content at low frequencies, and vertical turbulence length scales are larger than those observed on the road due to insufficient fetch for the vertical fluctuations to be damped by the proximity of the floor.

5.5 Summary

Based on the comparison of the results obtained in the NRC 1.0 m × 0.8 m Pilot Wind Tunnel and the NRC 2 m × 3 m Wind Tunnel for similar FTS configurations, it appears that the geometry of the settling chamber and the test section does not have a significant influence on the turbulence characteristics measured in the test section. The contraction ratio appears to have a small influence on the ratio of the longitudinal turbulence intensity (I_u) to the lateral and longitudinal values (I_v and I_w), with a lower I_u for a greater contraction ratio. The shapes of the wind spectra at high frequencies were not influenced, however the contraction ratio does impact the low frequency range of the spectra for all three wind components. The contraction affects the elongation of the larger-scale turbulence structures as they are confined into a smaller area. The added strain on the flow as it accelerated through the contraction influences the longitudinal turbulence differently than the lateral and vertical turbulence. Important conclusions from this intermediate-scale demonstration of the FTS concept are:

- The design process used to scale the small-scale concept in the NRC 1.0 m × 0.8 m Pilot Wind Tunnel to the intermediate-scale concept in the NRC 2 m × 3 m Wind Tunnel was validated based on the study of the baseline 6-spire concept;
- A minimum of 6 spires are required to ensure adequate flow uniformity;
- The manner in which the spires are mounted to the floor may influence the uniformity of flow in the test section, and therefore care must be taken to minimize any support structures between spires.

6. Design of the Full-Scale Flow Treatment System

THIS SECTION REDACTED

7. Blockage Corrections for HDVs

7.1 Problem Description

One of the arguments for using scale models, rather than full-scale vehicles, to test the aerodynamic performance of heavy vehicles is the influence of the closed walls of the wind-tunnel test section on the aerodynamic performance of a body in the wind tunnel. The confinement of the air due to the walls causes an effective increase in wind speed as seen by the vehicle that cannot be measured directly during a test. Blockage corrections are used to adjust the measurements to represent non-confined conditions. Many blockage correction techniques are available; however most are calibrated for bodies that are not representative of HDVs. A small number of these techniques have been used with some success for HDV-type bodies, but recent evidence from correlations between wind tunnel and track measurements shows that there is still work to be done to optimize blockage corrections for HDV shapes (Tanguay, 2011). Also, there is no direct evidence to suggest these techniques behave the same way under smooth-flow conditions (for which they have been developed) as they do for the representative turbulent flows to be generated by the FTS. The use of current methods for the 30%-scale HDV tests with the FTS in the NRC 9 m Wind Tunnel will introduce uncertainty in the drag measurements, particularly at higher cross-wind angles where the flow blockage is higher and the drag of the model in the test section can be double the head-on wind case.

SAE SP-1176 (1996) provides a detailed description of the flow mechanisms associated with blockage for ground vehicles, and compares the most common blockage corrections used for ground-vehicle testing at the time, including the Thom-Herriot method, which is evaluated here. SAE SP-1176 (1996) also describes the Maskell II method, which is a precursor to the Maskell III method evaluated here. In recent years, Cooper re-implemented Maskell II into a form that uses solid blockage as well, namely Maskell III (Cooper *et al.*, 1999) which has become a standard at the NRC 9 m Wind Tunnel based on good agreement between half-scale and full-scale measurements of the same HDV configuration (Leuschen and Mebarki, 2012). A recent comparison of surface-pressure measurements on a full-sized HDV tested in the NRC 9 m Wind Tunnel and on a track as part of a coast-down campaign showed disagreement between the track results and the Maskell III corrected data in the wind tunnel. The Thom-Herriot method provided a better comparison of these surface pressures, which has led to its evaluation along with the Maskell III method in the current evaluation study.

The two blockage corrections evaluated herein provide two parameters for correcting the wind tunnel measurement data. These consist of a dynamic pressure correction (Q_c/Q_u), which accounts for the speed-up effect around the model, and the wake-increment drag correction (ΔC_{Dwi}), which accounts for the effects of the blockage on the base pressures that influence

the measured drag coefficient. Corrections are performed in wind-tunnel-axis coordinates and then rotated back to body-axis coordinates. The correction to the wind-tunnel-axis drag coefficient is defined as:

$$C_D = \frac{C_{Du} + \Delta C_{Dwi}}{Q_c / Q_u} \quad (7.1)$$

and the correction to surface pressure coefficients is

$$C_p = 1 - \frac{1 - C_{pu}}{Q_c / Q_u}. \quad (7.2)$$

In addition to correcting the model loads and pressures, the side forces influence the effective wind angle as seen by the model. Using a standard method described by Barlow *et al.* (1999), the wind angle was corrected based on the side-force measurements. This is common practice with correction methods used in the NRC 9 m Wind Tunnel.

7.2 Setup

The blockage-correction-evaluation tests were performed in the NRC 1.0 m × 0.8 m Pilot Wind Tunnel using a similar setup as that for evaluating the sensitivity of HDV drag to turbulence, described in Section 4. The 5% Renshape pressure model from that study was used for both wind load and pressure measurements in the current study. In addition, four other models were built with the same shape but at different scales. Versions representing 3%, 7.5% and 10% scale were built with pressure taps in the same relative locations. The four models are shown in Figure 7.1.

For this study, the NRC 50-lb cruciform balance was used for all measurements, replacing the NRC 10-lb cruciform balance due to the higher loads expected from the larger models. For the two largest model sizes, the support-post locations (relative to the 5% model) extended beyond the useful boundaries of the turntable and therefore inboard post locations were added. To accommodate the different post locations for the small versus large models, dummy posts were installed on each model (protruding from the bottom of the model to within a millimeter of the floor) such that all models would have an identical shape. In addition to ensuring the model geometry was identical, it was desired to ensure the flow experienced by the four models was similar. To account for the floor boundary layer and its possible influence, upstream boundary layer trips were used for the 5%, 7.5% and 10% models to provide a near constant ratio of the floor boundary-layer displacement-thickness to the underbody height. To eliminate any influence of Reynolds number, wind-angle-sweep measurements for each model were performed at different wind speeds such that the Reynolds number was approximately 220,000, based on model width, at zero wind angle for all the models.

The blockage correction measurements were performed in three flow configurations, representing the smooth-flow, the C6Q and the C3W configurations studied in earlier phases of the work (see Sections 3 and 4). These configurations provided longitudinal freestream turbulence intensities (I_u) of 0.6%, 3.8% and 4.6%, respectively.

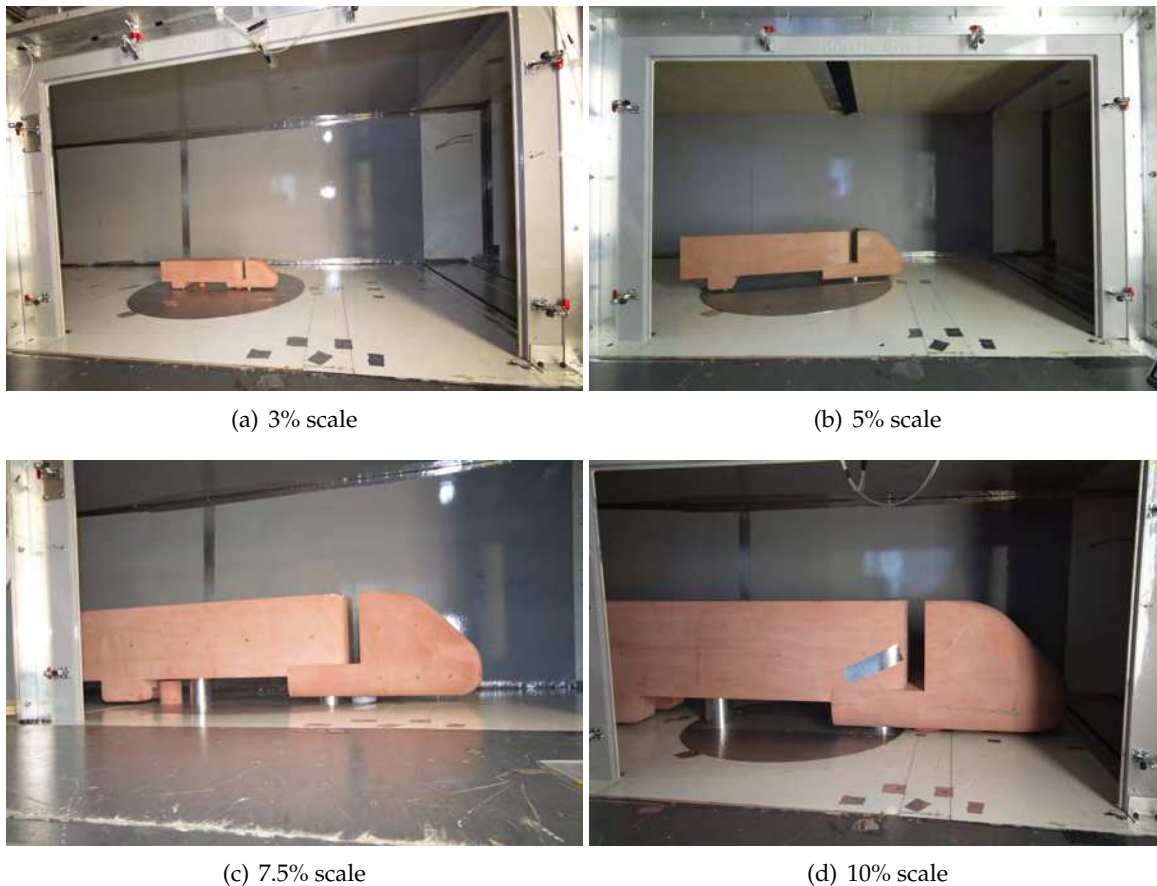


Figure 7.1: Simplified HDV models for the blockage-correction study

7.3 Results

As described in Section 4.3 with regards to the 5% unsteady load and surface-pressure tests, an asymmetry in the drag coefficient distributions with wind angle were present for small positive wind angles. The same observations were made with the other three model sizes in the current study, which has been attributed to the lateral asymmetry in test section flow characteristics (represented in mean wind-speed plots of Figure 3.2 on Page 39). Therefore, only negative wind angle results are presented here.

Figure 7.2 presents the corrected and uncorrected yaw sweep measurements for the four models, under the three turbulence conditions. Uncorrected measurements are shown in the top row with the Maskell III and Thom-Herriot corrected data sets in the middle and bottom rows, respectively. The three columns represent the three levels of turbulence. Within each plot, the drag-coefficient distributions of the four model scales are shown in wind-tunnel-axis (solid markers) and body-axis coordinates (open markers). The uncorrected data shows increasing measured drag coefficients with increasing model size, for both coordinate systems. Similar uncorrected results are observed for all three turbulence configurations. The Maskell III re-

Drag Reduction for HDVs - Progress Toward a Flow Treatment System - Year 2

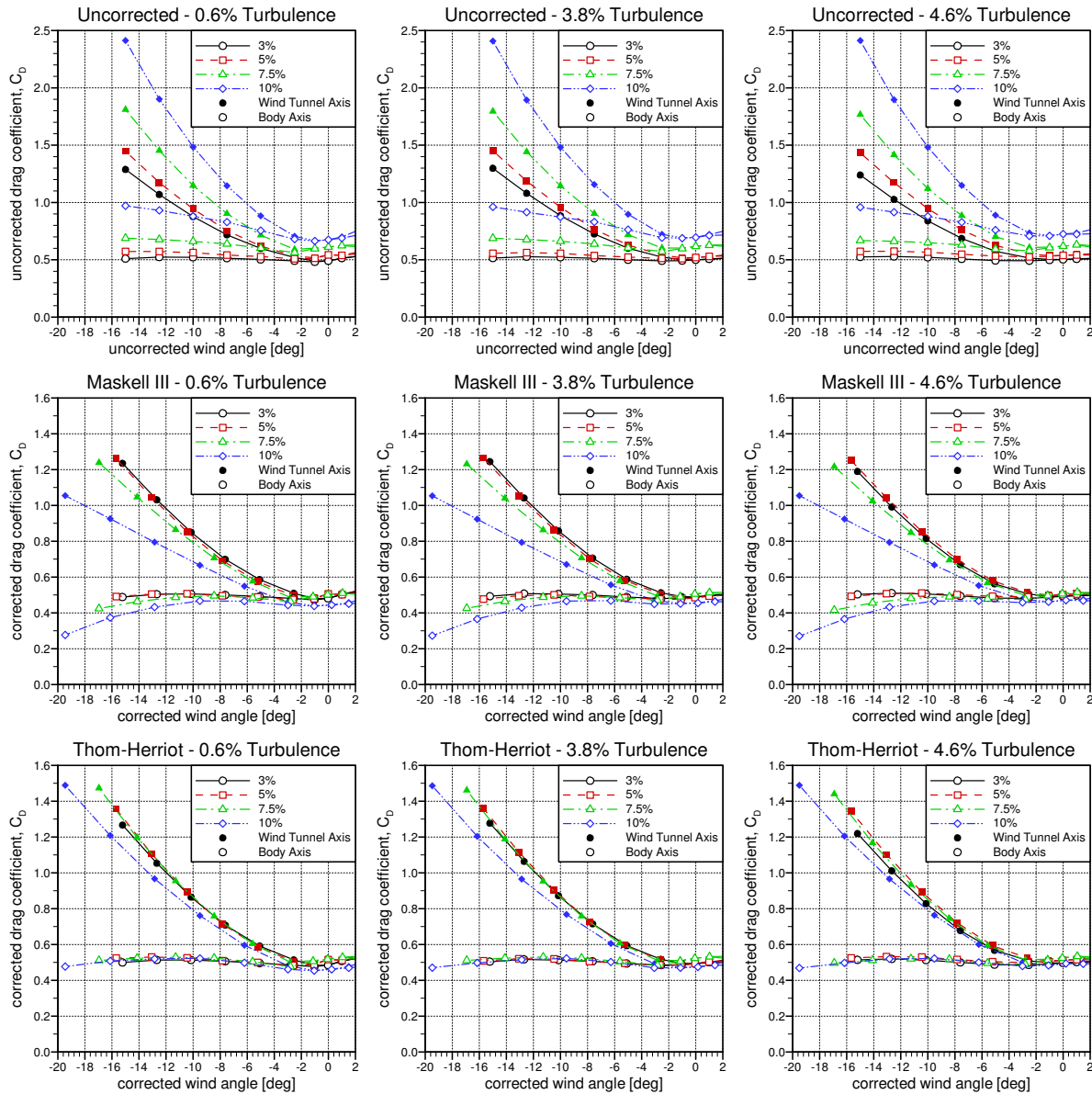


Figure 7.2: Comparison of blockage-corrections: body axis (open markers) and wind-tunnel axis (solid markers) drag coefficient distributions with wind angle for three turbulence levels (left column - 0.6%, middle column - 3.8%, right column - 4.6%) uncorrected (top row) and corrected with Maskell III method (middle row), and Thom-Herriot method (bottom row)

sults in the middle row show an over-correction of the drag coefficient data for the 10% model over the entire wind angle range, represented by lower corrected drag coefficients. Reasonable agreement in the Maskell III corrected results are observed for the three smallest models up to a wind angle of about -10° , beyond which the 7.5% model shows increasing overcorrection. The Thom-Herriot corrected results in the bottom row show excellent agreement in the body-axis drag coefficient data over the full wind angle range. The wind-tunnel-axis results for the 10% model show slight overcorrection, however the body-axis data is of most importance for an evaluation of the vehicle drag.

To evaluate better the correction magnitude of the two techniques and how well they correct the drag coefficient data, Figure 7.3 shows for three wind angles the variation of body-axis drag coefficient with blockage level as represented by model scale. Again, the three columns represent the three turbulence conditions. The upper row shows results at -1° wind angle, with the middle and bottom rows showing the data for -5° and -10° wind angles, respectively. At the small wind angle of -1° , the highest blockage level shows an overcorrection for both the Maskell III and Thom-Herriot methods. However, at the higher wind angles, the Thom-Herriot method shows agreement within a ΔC_D of approximately 0.015. The discrepancies at the smaller wind angle condition is attributed more to the drag-coefficient asymmetries near zero wind angle that have been observed with most of the models. The Maskell III method shows increasing overcorrection with blockage level, indicated by the decreasing corrected drag coefficients. Similar results are observed under all three turbulence conditions.

The centreline pressure coefficient distributions for the four models are shown for two conditions in Figure 7.4. The centreline pressure tap locations were shown previously in Figure 4.2 on Page 61. One condition represents low turbulence and low wind angle (left column) and the other represents high turbulence and high wind angle (right column). Again the uncorrected, Maskell III-corrected and Thom-Herriot-corrected data are shown in the top, middle, and bottom rows, respectively. Both conditions shows the same trends, that the Maskell III method overcorrects the pressure coefficients and that the Thom-Herriot method provides good agreement for the corrected data.

As one last step towards evaluating the difference between the two blockage correction techniques, the variations with blockage level of the dynamic pressure correction and of the wake-increment drag correction are shown in Figure 7.5 for the low turbulence configuration at -5° . It is observed that the Maskell III method has a higher dynamic pressure correction and lower wake-increment drag correction than the Thom-Herriot method. This trade-off between the two is the reason for the close agreement in corrected drag coefficients between the two methods, at least for the three smaller models, while the Maskell III method shows a strong overcorrection of the model pressure coefficients which rely on only one of the correction parameters.

Drag Reduction for HDVs - Progress Toward a Flow Treatment System - Year 2

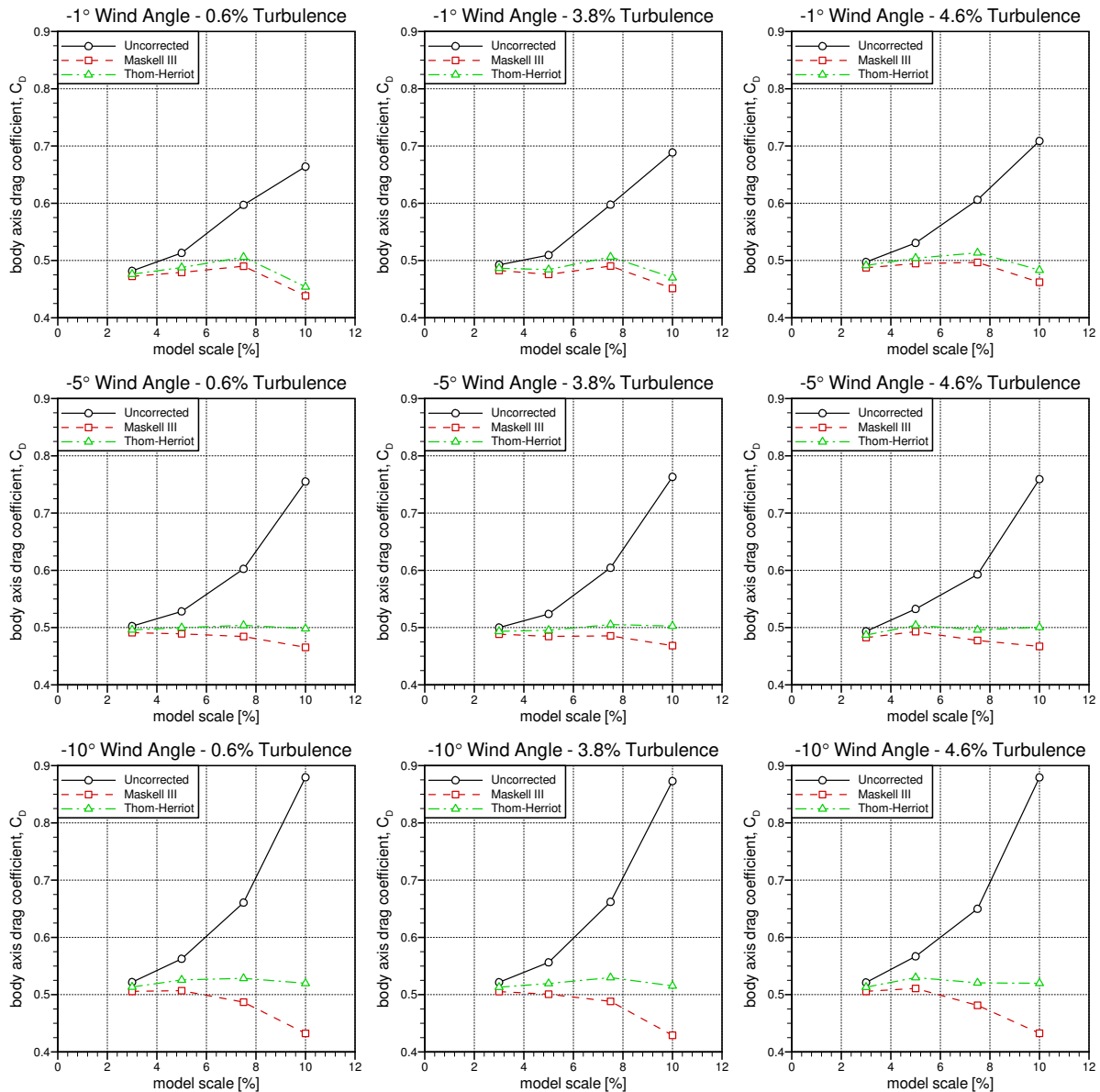


Figure 7.3: Comparison of blockage-corrections: body-axis drag coefficient distributions with model scale for three turbulence levels (left column - 0.6%, middle column - 3.8%, right column - 4.6%) and three wind angles (-1° - top row, -5° - middle row, -10° - bottom row)

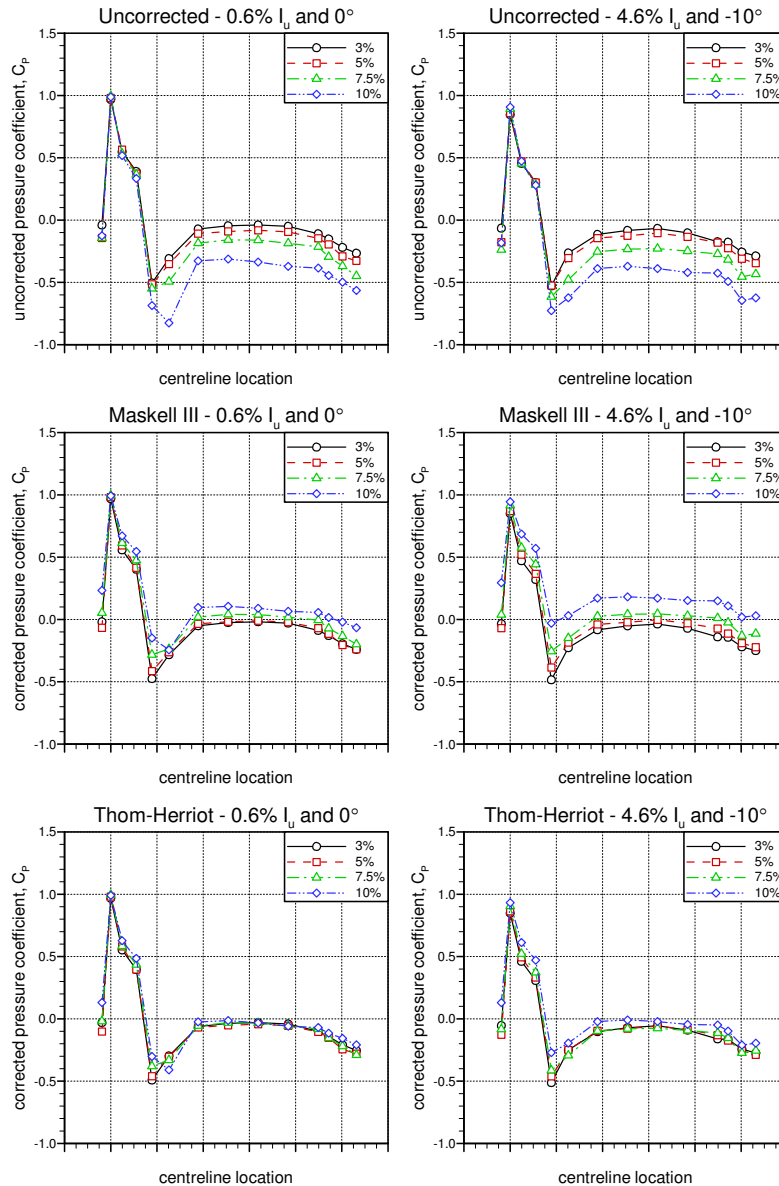


Figure 7.4: Comparison of blockage-corrections: centreline pressure coefficient distributions for two conditions (0.6% turbulence at 0° wind angle - left column, and 4.6% turbulence at -10° wind angle - right column) uncorrected (top row) and corrected with Maskell III method (middle row), and Thom-Herriot method (bottom row)

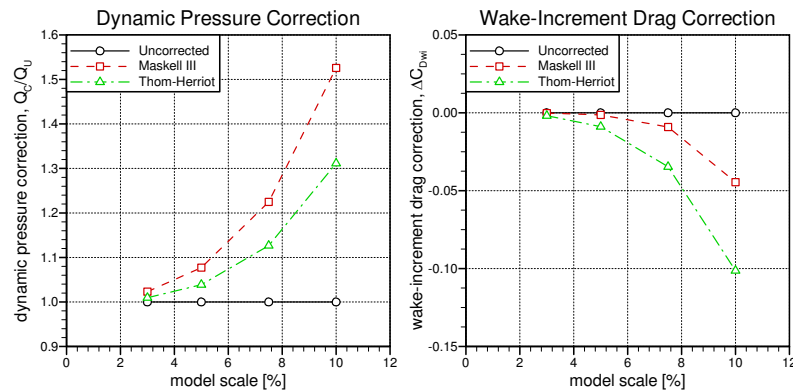


Figure 7.5: Comparison of blockage-corrections: dynamic pressure and wake-increment drag-coefficient corrections for the Maskell III and Thom-Herriot methods (0.6% turbulence at -5° wind angle)

7.4 Summary

Two blockage correction methods, the Maskell III and the Thom-Herriot methods, have been evaluated for their ability to correct adequately the wind load and pressure data from a set of four simplified HDV models of different scales tested in the NRC $1.0 \text{ m} \times 0.8 \text{ m}$ Pilot Wind Tunnel. The Maskell III and Thom-Herriot methods have been used previously at NRC to correct wind-tunnel data for HDV models. Results of the analysis showed that the Thom-Herriot method provides a reliable correction for all but the largest model. Despite some disagreement using this method with the largest model (13% physical blockage) at high wind angles ($>10^\circ$ degrees) for the surface pressures, the drag coefficients were corrected reliably well at the higher wind angles using the Thom-Herriot method, particularly at wind angles below 10° , which are most representative of those encountered at highway speeds on the road. No influence of turbulence was observed on the ability of the method to correct adequately the wind load and pressure data. Therefore, the Thom-Herriot method has been selected for use with the 30%-scale HDV model with the FTS in the NRC 9 m Wind Tunnel.

8. Conclusions and Future Work

Through its ecoTECHNOLOGY for Vehicle II program, Transport Canada has commissioned a project to investigate the aerodynamic improvements possible with current and emerging drag reduction technologies for heavy-duty vehicles (HDVs), with the intent of guiding future implementation of such technologies for Canada's transportation industry. The project will consist of wind-tunnel testing of a scale-model HDV with various drag reduction technologies.

This report described progress towards the development of a Flow Treatment System (FTS) that will provide representative wind conditions in the wind tunnel as is experienced by vehicles on the road (Phase 1 - Stream A). Six major tasks were performed in year two of the project:

1. Analysis of the on-road turbulence measurements and the selection of target wind spectra;
2. Analysis of the small-scale FTS concept measurements and the selection of a suitable concept for the FTS;
3. Analysis of the 5% scale HDV model measurements to identify the sensitivity of HDV drag to turbulence;
4. Demonstration of the FTS concept at intermediate scale in the NRC 2 m \times 3 m Wind Tunnel;
5. Design of the full-scale FTS for installation in the NRC 9 m Wind Tunnel; and
6. Selection of a blockage correction suitable for HDV-shaped bodies.

In the third year of the project, fabrication and commissioning of the full-scale FTS will be completed, leading to its use with the 30% scale HDV in the NRC 9 m Wind Tunnel.

References

- Barlow, J. B., Rae, W. H. and Pope, A. (1999), *Low-Speed Wind Tunnel Testing*, 3rd ed., Wiley-Interscience.
- Bearman, P. and Morel, T. (1983), "Effect of Freestream Turbulence on the Flow Around Bluff Bodies," *Progress in Aerospace Sciences*, **20**, pp. 97–123.
- Cooper, K. R., Mercker, E. and Wiedemann, L. (1999), "Improved Blockage Corrections for Bluff Bodies in Closed and Open Wind Tunnels," *10th International Conference on Wind Effects on Buildings and Structures*, Sweden.
- ESDU (2001), "Characteristics of Atmospheric Turbulence Near the Ground Part II: Single Point Data For Strong Winds (Neutral Atmosphere)," ESDU Data Item No. 85020, *Engineering Sciences Data Unit*.
- Leuschen, J. and Mebarki, Y. (2012), "Examination of the Maskell III Blockage Correction Technique for Full Scale Testing in the NRC 9-Meter Wind Tunnel," *SAE Int. J. Commer. Veh.*, **5**, pp. 640–649.
- McAuliffe, B. R. (2013c), "Aerodynamic Safety Implications of a Passenger Vehicle Travelling in the Wake of a Boat-Tail Equipped HDV," NRC Report No. LTR-AL-2013-0014, *National Research Council Canada*.
- McAuliffe, B. R. (2014b), "Aerodynamic Testing of Drag Reduction Technologies for HDVs: Progress Toward the Design of a Scale-Model HDV for Wind Tunnel Testing (Year 2)," NRC Report No. LTR-AL-2014-0015, *National Research Council Canada*.
- McAuliffe, B. R., Desouza, F. and Leuschen, J. (2013a), "Aerodynamic Testing of Drag Reduction Technologies for HDVs: Progress Towards the Development of a Flow Treatment System," NRC Report No. LTR-AL-2013-0020, *National Research Council Canada*.
- National Academy of Sciences (2010), "Technologies and Approaches to Reducing the Fuel Consumption of Medium- and Heavy-Duty Vehicles," , *The National Academic Press*.
- Patten, J., McAuliffe, B. R., Mayda, W. and Tanguay, B. (2012), "Review of Aerodynamic Drag Reduction Devices for Heavy Trucks and Buses," No. CSTT-HVC-TR-205, *National Research Council Canada*.
- SAE SP-1176 (1996), "Closed-Test-Section Wind Tunnel Blockage Corrections for Road Vehicles," SAE Special Publication No. SP-1176, *SAE International*.
- SAE Wind Tunnel Test Procedure for Trucks and Busses (2012), "SAE Wind Tunnel Test Procedure for Trucks and Busses," 2012.

Drag Reduction for HDVs - Progress Toward a Flow Treatment System - Year 2

- Tanguay, B. (2011), "Aerodynamic Experiments on Two Tractor-Trailer Combinations at the Arizona Proving Ground," NRC Report No. LTR-AL-2011-0077, *National Research Council Canada*.
- Watkins, S. and Cooper, K. R. (2007), "The Unsteady Wind Environment of Road Vehicle, Part Two: Effects on Vehicle Development and Simulation of Turbulence," SAE Paper No. 2007-01-1237.
- Wordley, S. J. and Saunders, J. W. (2009), "On-Road Turbulence: Part 2," SAE Paper No. 09B-0045.